The EUMETSAT Satellite Application Facility on Land Surface Analysis (LSA SAF)

Validation Report (VR)

Land Surface Albedo

PRODUCTS: LSA-01 (MDAL), LSA-02 (MTAL), LSA-03 (ETAL)

The EUMETSAT
Network of
Satellite Application
Facilities

LSA SAF
Land Surface Analysis

DOCUMENT SIGNATURE TABLE

	Name	Date	Signature
Prepared by :	**Météo-France / CNRM**	**15/02/2012**	
Approved by :	**Land SAF Project Manager**	**15/02/2012**	

DOCUMENTATION CHANGE RECORD

Issue / Revision	Date	Description:
Version II/2012	**15/02/2012**	Version to be presented to ORR-Close-out

DISTRIBUTION LIST

Internal Consortium Distribution		
Organisation	**Name**	**No. Copies**
IM	Pedro Viterbo	
IM	Luís Pessanha	
IM	Isabel Trigo	
IDL	Carlos da Camara	
IM	Isabel Monteiro	
IM	Sandra Coelho	
IM	Carla Barroso	
IM	Pedro Diegues	
IM	Teresa Calado	
IM	Benvinda Barbosa	
IM	Ana Veloso	
IMK	Folke-S. Olesen	
IMK	Frank Goettsche	
IMK	Ewa Kabsch	
MF	Jean-Louis Roujean	
MF	Olivier Hautecoeur	
MF	Dominique Carrer	
RMI	Françoise Meulenberghs	
RMI	Arboleda Alirio	
RMI	Nicolas Ghilain	
FMI	Niilo Siljamo	
UV	Joaquin Melia	
UV	F. Javier García Haro	
UV/EOLAB	Fernando Camacho	
UV	Aleixander Verger	

External Distribution		
Organisation	**Name**	**No. Copies**
EUMETSAT	Frédéric Gasiglia	
EUMETSAT	Dominique Faucher	
EUMETSAT	Lorenzo Sarlo	
EUMETSAT	Lothar Schueller	
EDISOFT	Teresa Cardoso	
EDISOFT	Carlos Vicente	
EDISOFT	Cleber Balan	
SKYSOFT	Rui Alves	
SKYSOFT	João Canário	

Steering Group Distribution		
Nominated by:	**Name**	**No. Copies**
IM	**Carlos Direitinho Tavares**	
EUMETSAT	**Lorenzo Sarlo**	
EUMETSAT	**François Montagner**	
STG/AFG (USAM)	**Luigi de Leonibus**	
MF	**François Bouyssel**	
RMI	**Piet Termonia**	
FMI	**Carl Fortelius**	

Executive Summary

A daily surface albedo named MDAL is generated on an operational basis since February 2005 for the European region and since July 2005 for the whole Meteosat disk. Another surface albedo product, so-called MTAL, is generated from MDAL every 10 days, thereby being formulated as 'climatologic'. A regular generation of surface albedo from AVHRR/MetOp, ETAL, is scheduled to begin in 2013 for covering the whole globe. The main algorithm for AL derivation for both sensors relies first on the implementation of a knowledge Bi-directional Reflectance Distribution Function (BRDF) product, so far being internal. The approach herein is based on the use of a semi-empirical BRDF kernel model, claiming that the mathematical description of the reflectance anisotropy properties can be equivalent to a sum of a limited series of angular kernels, each of them describing a different light scattering process.

The present document reports the first and also most recent results of validation that were obtained for the LSA SAF AL products. The comparison is carried on for 3 levels of products: satellite-based, ground truth, and output of NWP models. In the case of MDAL and also MTAL, the a priori satellite product of reference is MODIS albedo product because it offers long-term perspectives. However, some data comparisons with POLDER sensor are shown from 2010 because the instrumental design of POLDER makes it suitable for albedo estimates. Ground observations taken at the first LSA SAF in situ station in Evora (Southern Portugal) and in Carpentras (south west of France) yield the in situ reference. In addition the BSRN station of Toravere (Estonia) and two stations located in western Africa complete the independent database. Finally, we consider forecast albedo from ECMWF. MDAL data are compared with the 16-days MODIS albedo product, MOD43B3, for Europe and North Africa boxes over a period of 17 months right after the onset of the production in 2005. For both continents, results show a good correspondence for the near infrared and the total broadband ranges, but also at that time an overestimation of the visible broadband albedo with respect to the MODIS product. However, it is worth emphasizing that the standard deviation relative to the mean albedo value is clearly reduced over Africa compared to those over Europe and values of albedo are usually larger than over Europe (0.27 of mean value for MSG VIS-DH albedo over North Africa against 0.08 over Europe and the 161 MODIS period).

Statistical results (bias and standard deviation) between the Land-SAF and MODIS broadband albedos reveal that during the period June 2005 to April 2006, the absolute bias for the visible broadband albedo is around 1%. Possible sources of discrepancies are angular sampling, reflectance model, narrow to broadband conversion, but more likely difference in aerosol correction. Note this latter has been further explored with time in considering more recently data sets for the year 2010. During the early era of production, results of comparison of MDAL against in situ observations collected for three contrasted African sites of AMMA (African Monsoon Multidisciplinary Analysis) project are deemed dependable. In general, Land-SAF product overestimates slightly the albedo with respect to the ground measurements, likely because in situ sensor sampled more vegetation. Therefore, it still remains the question of representativeness of the local ground measurements for the coarse scale SEVIRI pixel footprint size. However, a remarkable correspondence was obtained for the more heterogeneous site of Niamey (Niger). General conclusion from a comparison with AMMA sites is the ability to MDAL to capture aerosol and rainfall events.

The evaluation of MTAL was also performed right after the production started in 2009. A comparison of MDAL and MTAL broadband albedo products is carried for 2009 over two confident sites located in Namibia (Gobabeb) and Estonia (Toravere). The main conclusion is that MTAL offers more time steadiness, thereby better answering specific requirements addressed by climate users community for instance.

The analysis of time series of the aerosol optical thickness, that are available from the AERONET project, sustains the existence of a correlation between surface albedo estimates and the aerosol optical depth (AOD). This suggests that aerosols are responsible for a part of the (spurious) temporal variability remaining in the time series. These variations tend to be smoothed out by the temporal composition scheme. However, a potential bias remains if the averaged AOD does not correspond to the climatologic value specified. Thus, there exists clearly a gain in generating MDAL product in removing properly aerosol signal.

For such, an experimental MDAL product is performed for 6 months of the year 2010 in using the AOD at 550 nm issued from the MACC-II project (www.gmes-atmosphere.eu). This latter initiative disseminates in near-real conditions some atmospheric products based on a transport model for atmospheric particles with dedicated identification of sources and sinks. MACC forecast of AOD the closest (within 6 hours) to the slot is the value retained. Note that an continental type is still further considered for time being. First results are presented in this document. The conclusion is that there are slight differences in the results between both approaches (aerosol correction by climatologic data, versus use of MACC). Although these differences are more significant for the broadband correction. Hence, the MACC-based corrected albedo for aerosol is believed to be useful and will supersede the actual operational MDAL and MTAL products in the near future. In the meantime, these experimental products are referred as MDALMC and MTALMC for which first elements of their validation are shown in this document.

Table of Contents

1   Introduction

A well-established approach for operational albedo determination is based on semi-empirical BRDF kernel models which have received a great deal of attention and effort from the optical remote sensing community for the last decade (Roujean et al., 1992; Barnsley et al., 1994; Wanner et al., 1995; Strahler, 1994; Hu et al., 1997). The approach claims that the mathematical description of the reflectance properties can be split into a number of kernels, which describe the dominant light scattering processes. The physical arguments to sustain the analytical theory are that it yields a separation between geometric and volumetric effects interpreted as a transposition of scaling effects, a separation between the soil and vegetation, or the conjunction between thin and thick optical media (Lucht and Roujean, 2000). The use of kernel-based models is widely accepted because they yield an understandable solution to the complex problem of mixed BRDF products. For a number of space-borne sensors forming the quintessence of the new generation of multi-angular systems the kernel-based approach was adopted for the development of albedo products.

The SEVIRI-based surface albedo (AL) is currently generated on an operational basis from SEVIRI/Meteosat. The SEVIRI-based AL is a pre-operational product, available to users in near-real time (via EUMETCast) or offline (via ftp). User requests regarding AL are summarised in Table 1; further details may be found in the most recent version of the Product Requirements Document (PRD). Acronyms are as follows: MSG Daily Surface Albedo (MDAL), MSG Daily 10-day Surface Albedo (MTAL), EPS Surface Albedo (ETAL),

Table 1 Product Requirements for AL, in terms of area coverage, resolution and accuracy.

Product Name	Product Identifier	Coverage	Resolution		Accuracy		
			Temporal	Spatial	Threshold	Target	Optimal
MDAL (AL SEVIRI)	LSA-01	MSG disk	1 day	MSG pixel resolution	20%	AL>0.15: 20% AL<0.15: 0.03	7.5%
MTAL (AL SEVIRI)	LSA-02	MSG disk	10-day	MSG pixel resolution	10%	AL>0.15: 10% AL<0.15: 0.015	5%
ETAL (AL AVHRR)	LSA-03	Global	10-day	0.01°x 0.01°	10%	AL>0.15: 10% AL<0.15: 0.015	5%

2 Surface Albedo – SEVIRI

2.1 Albedo Product Images

The product comprises various broadband and spectral albedo variants. Example images are shown in Figure 1 and Figure 2. The product files of the four continental zones have been combined to generate these full disk images. Figure 3 shows an example of the uncertainty estimate delivered for each of the albedo variants. The uncertainty estimate is calculated by propagating estimates for the non-correlated (random) part of the input data errors through the model inversion (see the Product User Manual, section 2.11, p35). The figure also shows the quality (or processing) flag including information about the land/water mask, the processed regions and potential snow cover.
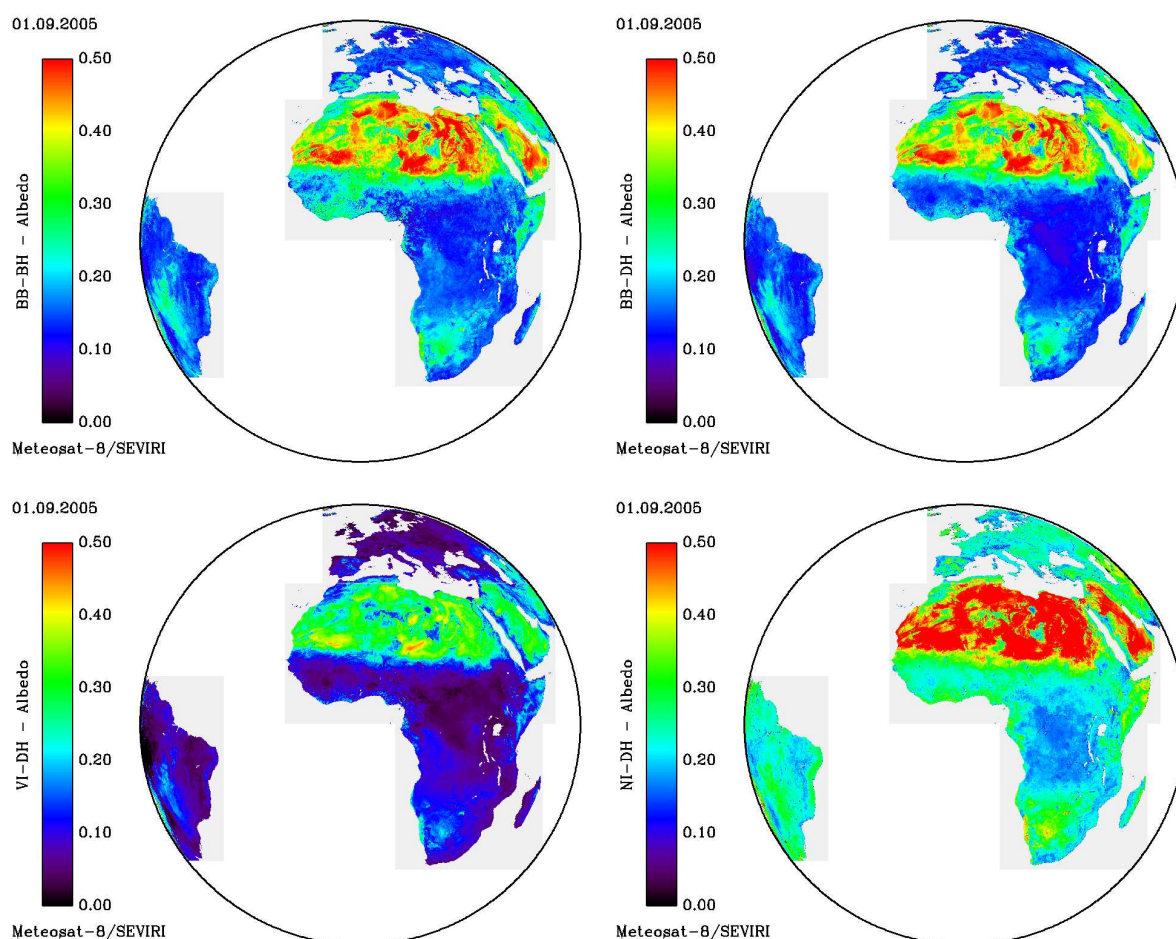
Figure 1: Broadband albedo product images for the 1st of September 2005. Top Left: Total short-wave bi-hemispherical. Top Right: Total shortwave directional-hemispherical. Bottom Left: Visible directional-hemispherical. Bottom Right: Near Infrared directional-hemispherical.
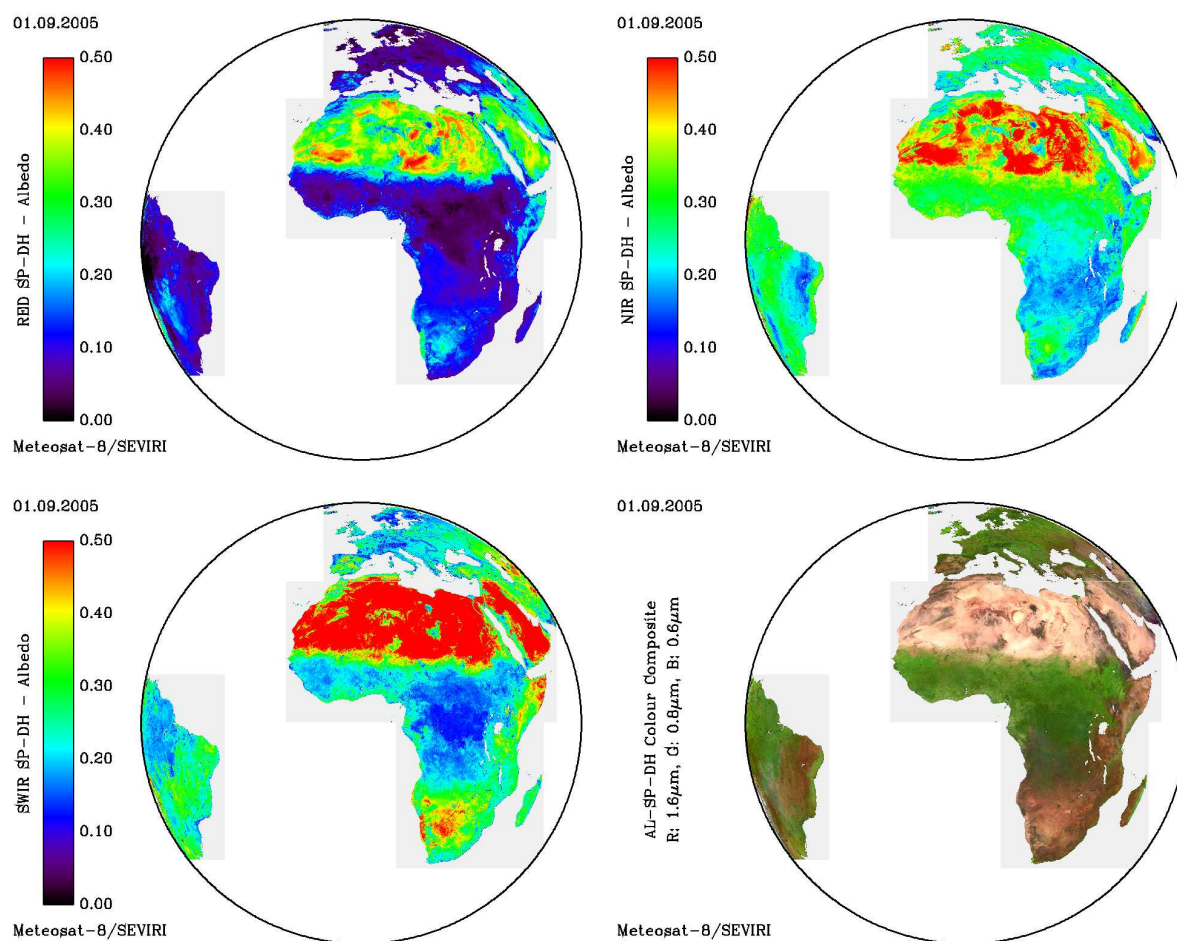
Figure 2: Spectral (directional-hemispherical) albedo product images for the 1st of September 2005. Top Left: Red Channel (0.6µm). Top Right: Near Infrared Channel (0.8µm). Bottom Left: Short-wave Infrared Channel (1.6µm). Bottom Right: Colour composite of the three spectral albedo images.
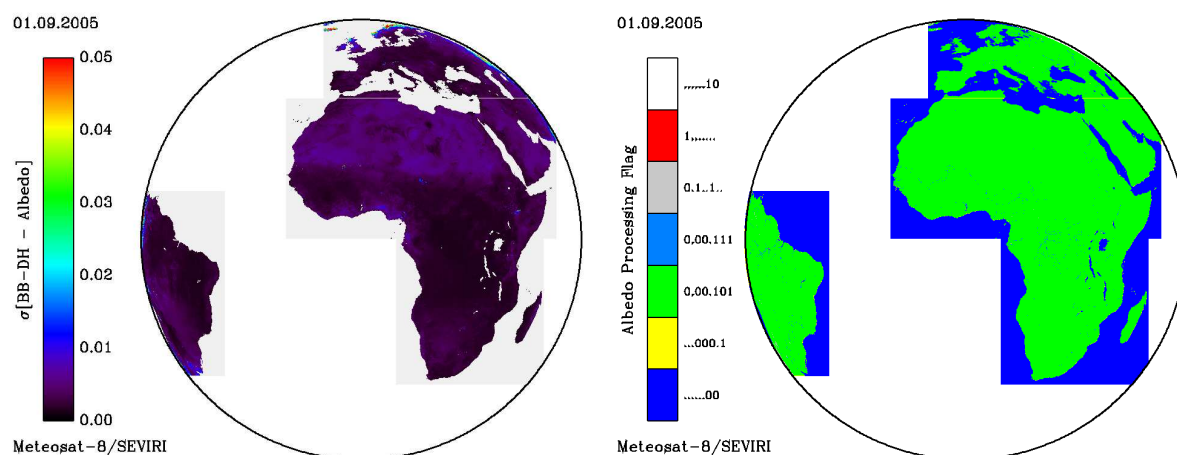

Figure 3: Example for the uncertainty estimate (total broadband directional-hemispherical) and the quality (or processing) flag provided for the 1st of September 2005. (Unprocessed lines at the bottom of the continental windows visible for Europe in this representation were caused by a problem in the utilisation of the cloud mask software, which has been solved in the meantime.)

2.2 Albedo Time Series for Selected Pixels

For a selection of sites Figure 4 shows time series of the obtained spectral and broadband albedo estimates. Most of the sites were chosen according to the location of ground validation stations and have been used before in the project for illustration purposes. The locations "Lago di Garda" and "Marktoberdorf" were added in order to show results for water and snow, respectively. A list of the site coordinates is given in the table 2 below.
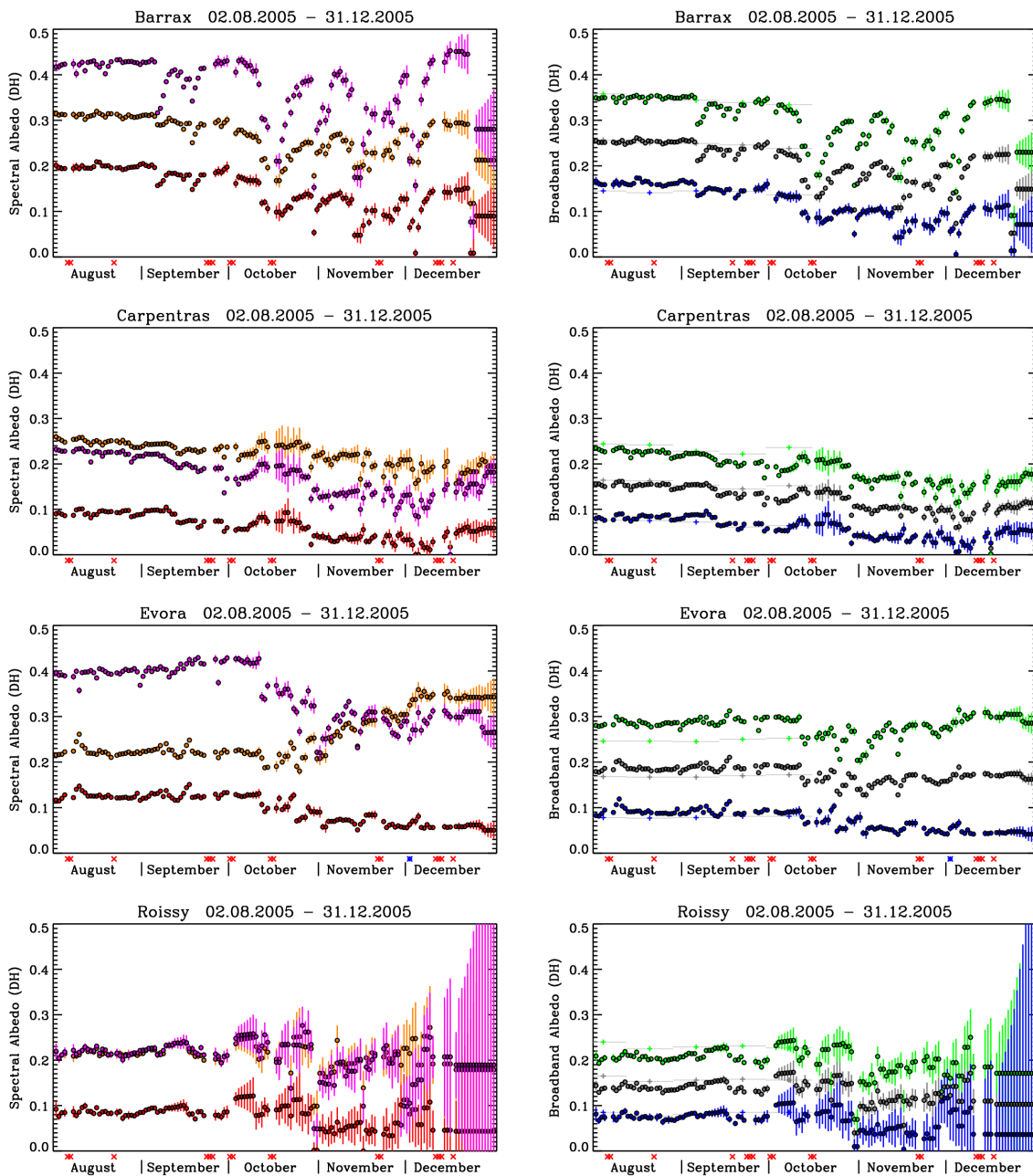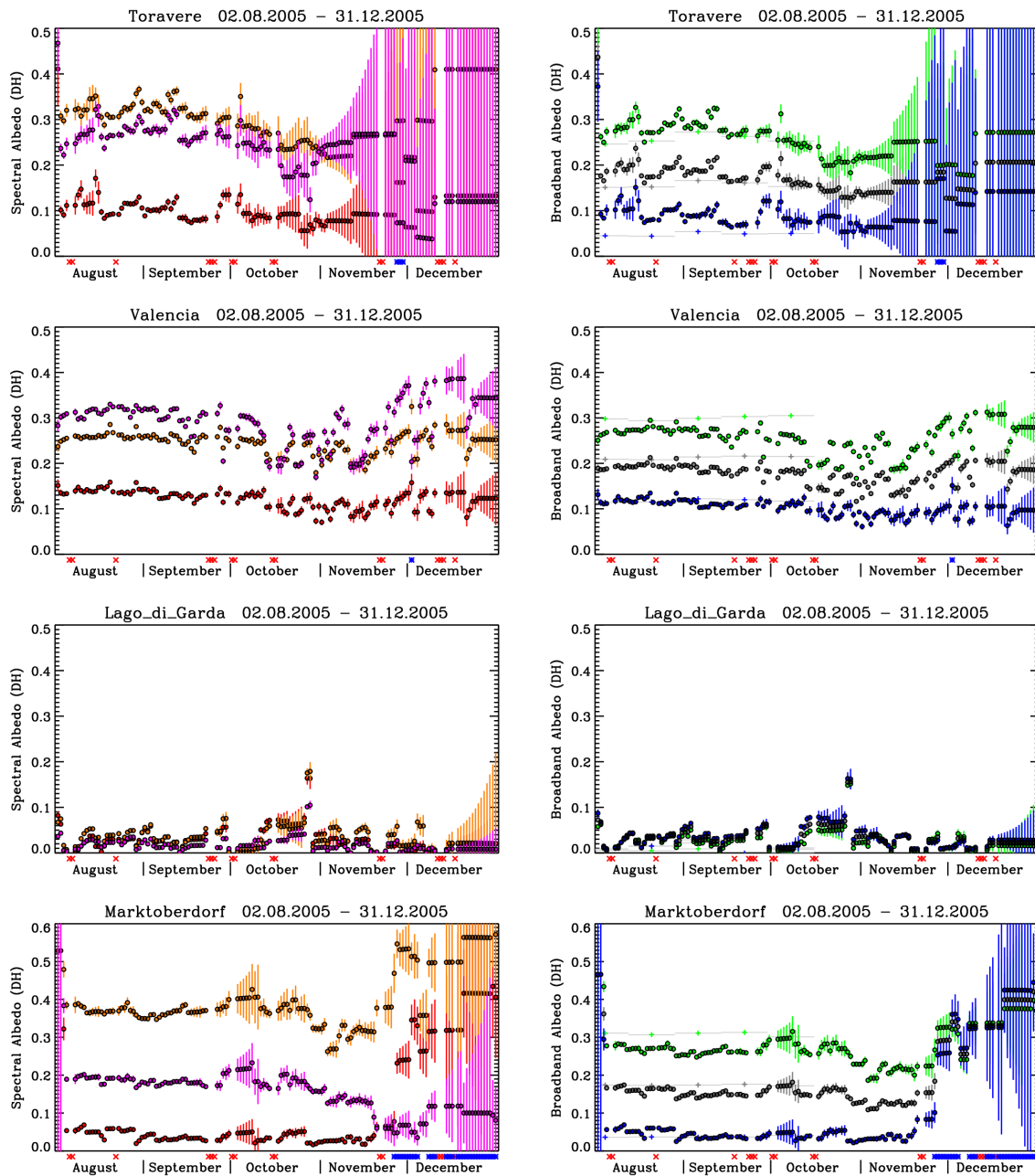
Figure 4: Time series of spectral (left) and broadband (right) directional-hemispherical albedo estimates for the pixels corresponding to the location of the corresponding sites. For spectral albedo red, orange, and magenta dots, respectively, correspond to the 0.6μm, 0.8μm, and 1.6μm SEVIRI channels. For broadband albedo the colours grey, blue, and green, respectively, correspond to the total short-wave range, to the visible, and to the near infrared. The vertical bars indicate the respective uncertainty estimates. (For low values they may be entirely covered by the dot symbol.) For broadband albedo until the beginning of October the plots also include MODIS estimates marked by crosses with "temporal error bars". A red cross on the time axis indicates that no product file was generated by the operational system for the respective day. The blue star indicates that the pixel was flagged as snow covered in the quality information. (The snow information is reported from the cloud mask to the albedo product files.)

The EUMETSAT
Network of
Satellite Application
Facilities

LSA SAF
Land Surface Analysis

Table 2: List of sites considered for illustrating the albedo product time series.

Site	Latitude	Longitude	Column	Line	Zone
Barrax	39.04	-2.08	250	532	Euro
Carpentras	44.083	5.059	436	414	Euro
Roissy	49.015	2.535	366	311	Euro
Evora	38.539	-8.000	085	546	Euro
Toravere	58.26	26.47	764	174	Euro
Valencia	39.57	-1.28	273	519	Euro
Lago di Garda	45.57	10.61	568	384	Euro
Marktoberdorf	47.78	10.62	557	338	Euro

The beginning of the period shown in the figure corresponds to the implementation of the algorithm version AL2 v5.0 in the operational system. During the months August and September 2005 the temporal coherence of the result is acceptable. However, from October rather large variations on small time scales become important. There are a number of reasons for the deterioration of the product quality:

- clouds become more frequent and are not efficiently enough eliminated. (The ideas that have already been implemented or are envisaged in order to attack this problem is reported in section 2.3.)

- a large number of slots and hence observations were lost due to instability problems in the operational system, in particular in October

- low solar elevation constitutes a principal problem for the albedo determination over (Northern) Europe for this time of the year, especially with observations from geostationary satellites. The resulting difficulties in model inversion are quantified by the delivered uncertainty estimates (Figure 3).

2.3 Residual cloud decontamination and cloud shadow elimination

2.3.1 Principle

Up to version AL2 v5.0, the albedo algorithm considers all observations declared as cloud-free by the cloud mask software, to say the CMa product from NowCasting SAF. However, it was found that some cloud contaminated pixels still remain, which may have led to spurious variability on short time scales in the resulting albedo estimates (cf. Figure 4). Therefore, a more 'agressive' technique to filter cloudy pixels has been implemented. It consists to discard a pixel plus two other pixels corresponding to slot before and after, when the cloud mask of the NWC-SAF is judged dubious.

Moreover, clouds make shadows on cloud clear surfaces what causes no legitimate variations of albedo. A simple principle of decontamination is now used (ref figure 5). The decontamination is function of azimuth position of the sun and eliminates just some pixels (not all), which are near a cloudy pixel.
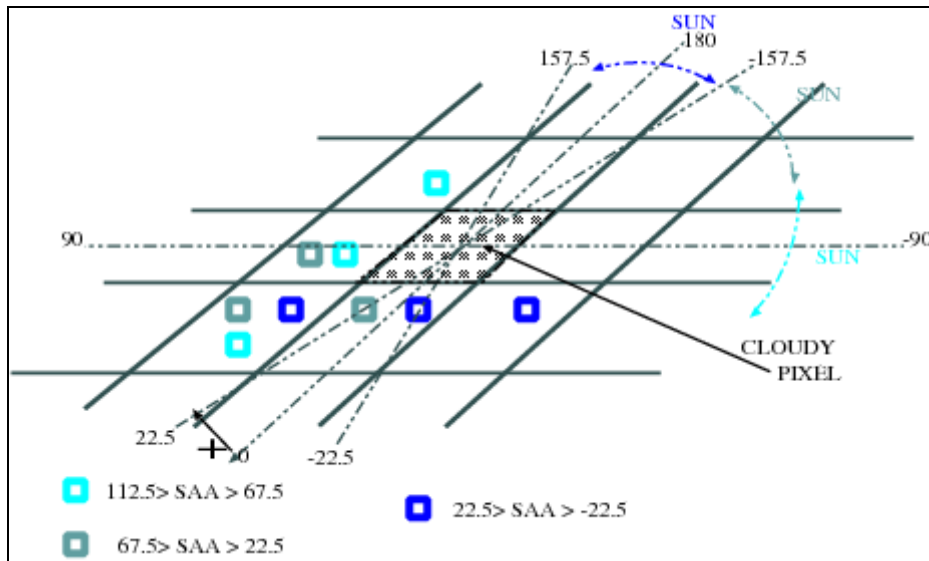
Figure 5: Sketch of the technique applied for the removal of cloud-contamined pixels as a function of the solar geometry. Three examples are given here to discard nearest neighbour pixels (blue squares) relative to a cloudy pixel, according to the solar azimuthal position.

Then, in version AL2 v5.1 the following improvements have been implemented:

1. A bad quality flag in the cloud mask product (CMa product from NowCasting SAF) serves to discard pixels even marked as clear.

2. Further pixels are then eliminated due to cloud shadowing.

3. Further pixels are eliminated from observations directly acquired before or after a cloudy slot.

Worthy to mention that owing to the 15 minutes repeat cycle of MSG/SEVIRI a large number of slots are available. Thus, adopting a conservative approach for discarding some of them does not seriously compromise the information content available for generating the albedo product.

2.3.2   Results

2.3.2.1   Top Of Canopy (TOC) reflectance

Figure 6 displays the impact of th new algorithm for cloud decontamination based on the quality flag information from NWC-SAF. In fact, even more pixels are eliminated prior to the BRDF model inversion, provided they belong to a slot before and after cloudy slots.
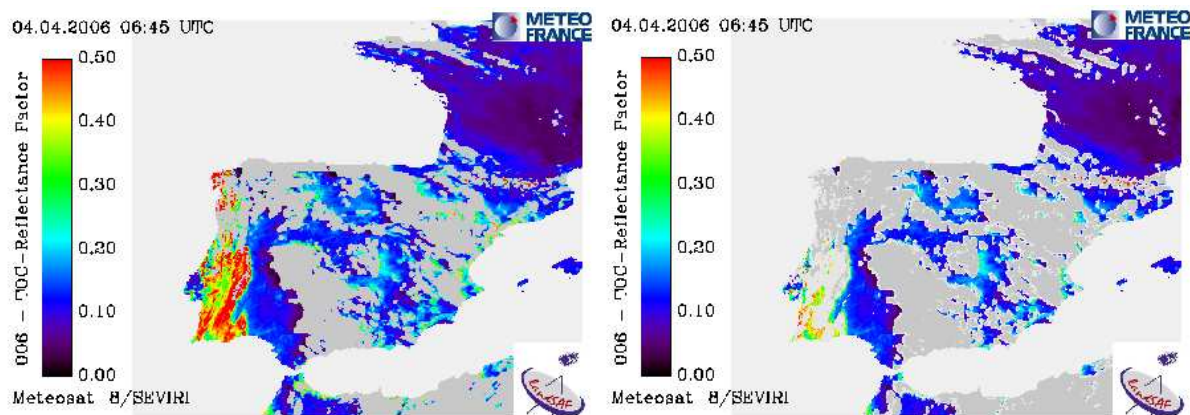

Figure 6: Top Of Canopy reflectance (AL1 code output) used by the BRDF inversion algorithm, the 20060404 at 06:45UTC; Left : before the implementation of AL1 v6.1.3 algorithm – Right : after the implementation of AL1 v6.1.3 algorithm.

2.3.2.2   Albedo

Figure 7 depicts reprocessed results for the time series shown before in Figure 4. The temporal coherence of the time series is improved. Nevertheless the origin of the remaining variability should be investigated more thoroughly. Due to the reduced number of used observations the uncertainty estimate is increased. The algorithm version AL2 v5.1 was implemented in the operational system on 14 December 2005. Note that the elimination of observations flagged with bad cloud mask quality is only effective in the re-processing from October 13 onwards, when the atmospheric correction code in the operational system, which propagates the cloud mask information was updated to version AL1 v6.1.3.
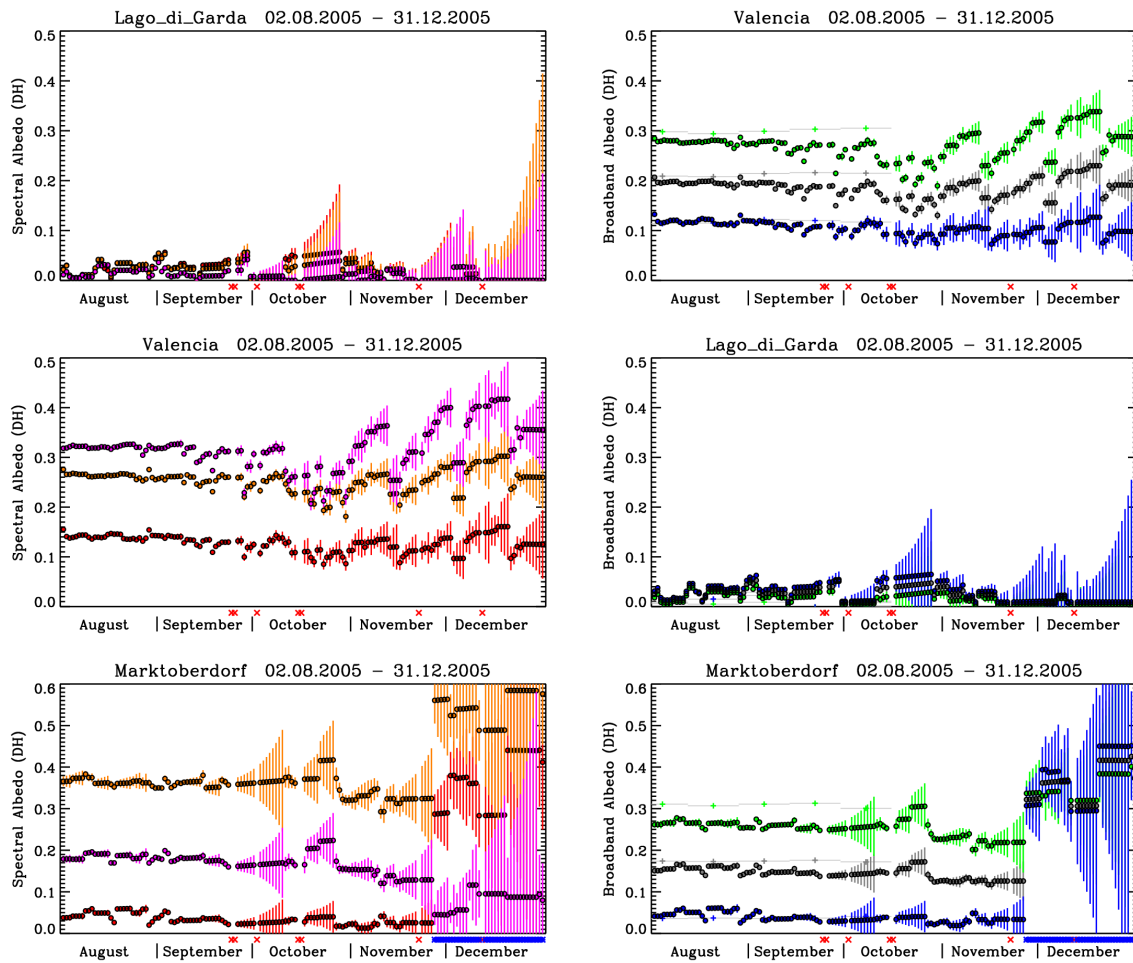
The EUMETSAT
Network of
Satellite Application
Facilities

LSA SAF
Land Surface Analysis
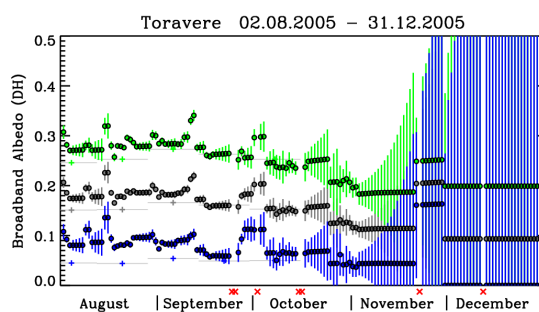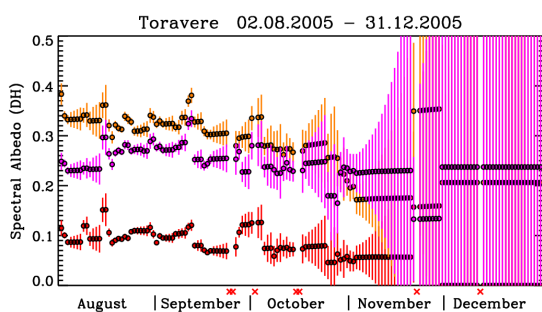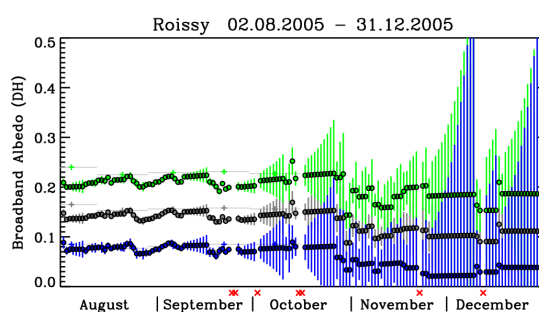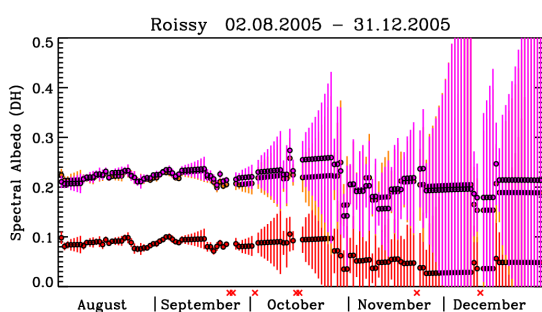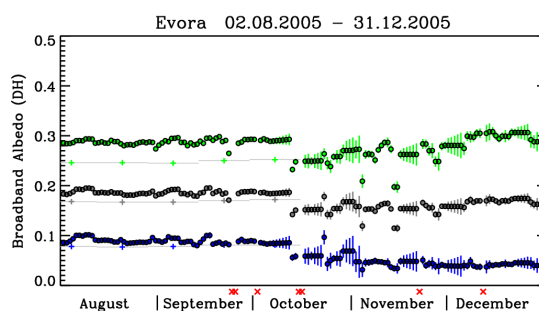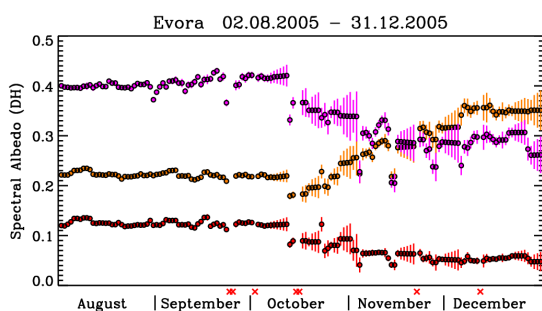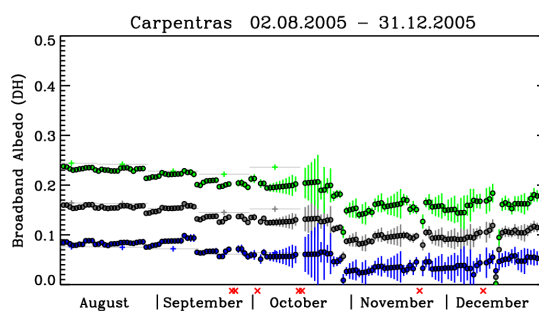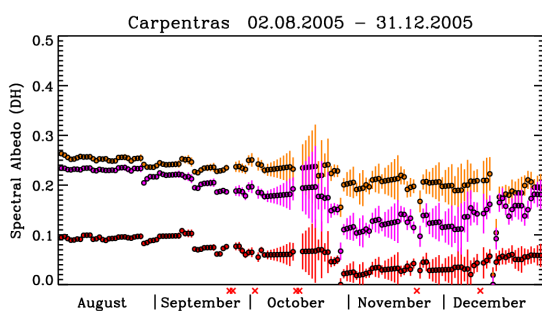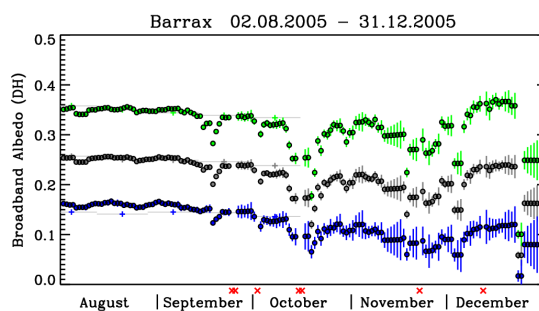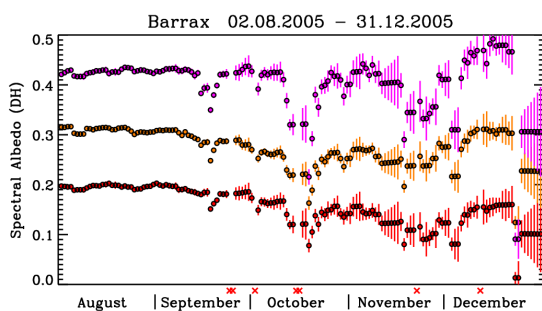
Figure 7: Time series of spectral (left) and broadband (right) directional-hemispherical albedo estimates. The information included is the same as in Figure 4 but the entire period has been reprocessed with algorithm version AL2 v5.1.

Figure 8 shows a comparison of the colour composite images obtained with the spectral albedo results from the two algorithm versions. The graphs illustrate that the spatial coherence improved as well and that some obvious dark artefacts in central Europe disappeared. [Note that the albedo estimates for Scandinavia at that time of the year are based on very few and potentially rather "old" data, which leads to large uncertainty estimates and thus a very low nominal confidence in the result. A limit on the maximal solar zenith reference angle for delivering an albedo product should probably be introduced.]
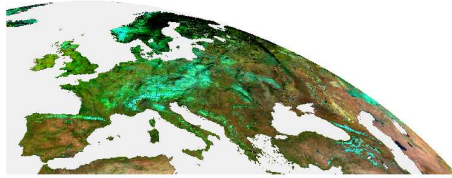
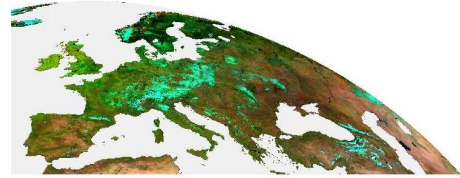**Figure 8:** Spectral albedo colour composite of the European window obtained in the operational system with version AL2 v5.0 (left) and reprocessed with version AL2 v5.1 (right).

2.4   Comparison with the MODIS Albedo Product

In this section we present a comparison of the Land-SAF results with the version 4 of the albedo product derived from observations of the MODIS instrument. The definition of the spectral limits for the broadband albedo ranges is identical for the two products. In addition, the convention for the reference illumination angle for directional-hemispherical albedo is the same (local solar noon). However, the spatial resolution and projection as well as the temporal characteristics are different and represent the main difficulties when comparing the two products. In order to investigate the sources of discrepancies in more detail the comparison is then also carried out at the level of spectral albedo and the BRDF-model parameter k0.

2.4.1   Images and elements of statistics

For the validation purposes we re-projected the higher resolution MODIS albedo product to the MSG/SEVIRI grid. For each original MODIS pixel the "closest" SEVIRI pixel was determined and afterwards the albedo estimates for all MODIS pixels assigned to the same SEVIRI pixel were averaged. For the different broadband albedo variants the resulting MODIS images in SEVIRI projection are depicted from Figure 9 to Figure 12 over Europe, and Figure 13 over Africa. The same procedure was also applied to the MODIS quality flag. Since no broadband albedo quality information was available, the flag for the spectral channel with the largest weight in the narrow- to broadband conversion was used and included in the figures. High values of the quality flag correspond to low confidence in the MODIS product.

We show MODIS results corresponding to the 16-day period from June 10 to June 25 for Europe and from July 12 to July 27 for Africa. In order to reproduce the temporal characteristics as closely as possible with the MSG data, the internal TOC-reflectance files provided by the operational system were reprocessed (at Météo-France) to generate daily albedo estimates (without iteration), which were then averaged over the relevant MODIS period. [In order to formally validate also the albedo files actually generated and distributed by the operational system, the comparison has also been performed for an example case based on the product generated on the last day of the respective MODIS reference period containing an iterative accumulation of the information of the previous days. The conclusions are qualitatively the same and small differences can be observed in the numbers for the validation statistics.]

Based on a visual inspection, albedo products derived from MSG and MODIS instruments show a very good agreement. Absolute and relative difference maps reported in the figures support such conclusion. Generally speaking, largest differences are noticed in regions for which the level of confidence on the product, based on quality flag, is low for either one or both products. As for broadband visible albedo, MSG estimates show systematically a positive bias by comparison to MODIS values. This is remarkable over Europe, even amplified over Africa with the occurrence of bright soils. Since the level of magnitude of visible signal is weak, this entails large relative differences. In addition, we show on Figure 4 time series of MSG and MODIS albedos for a representative selection of European sites. The agreement can generally be deemed satisfactory.
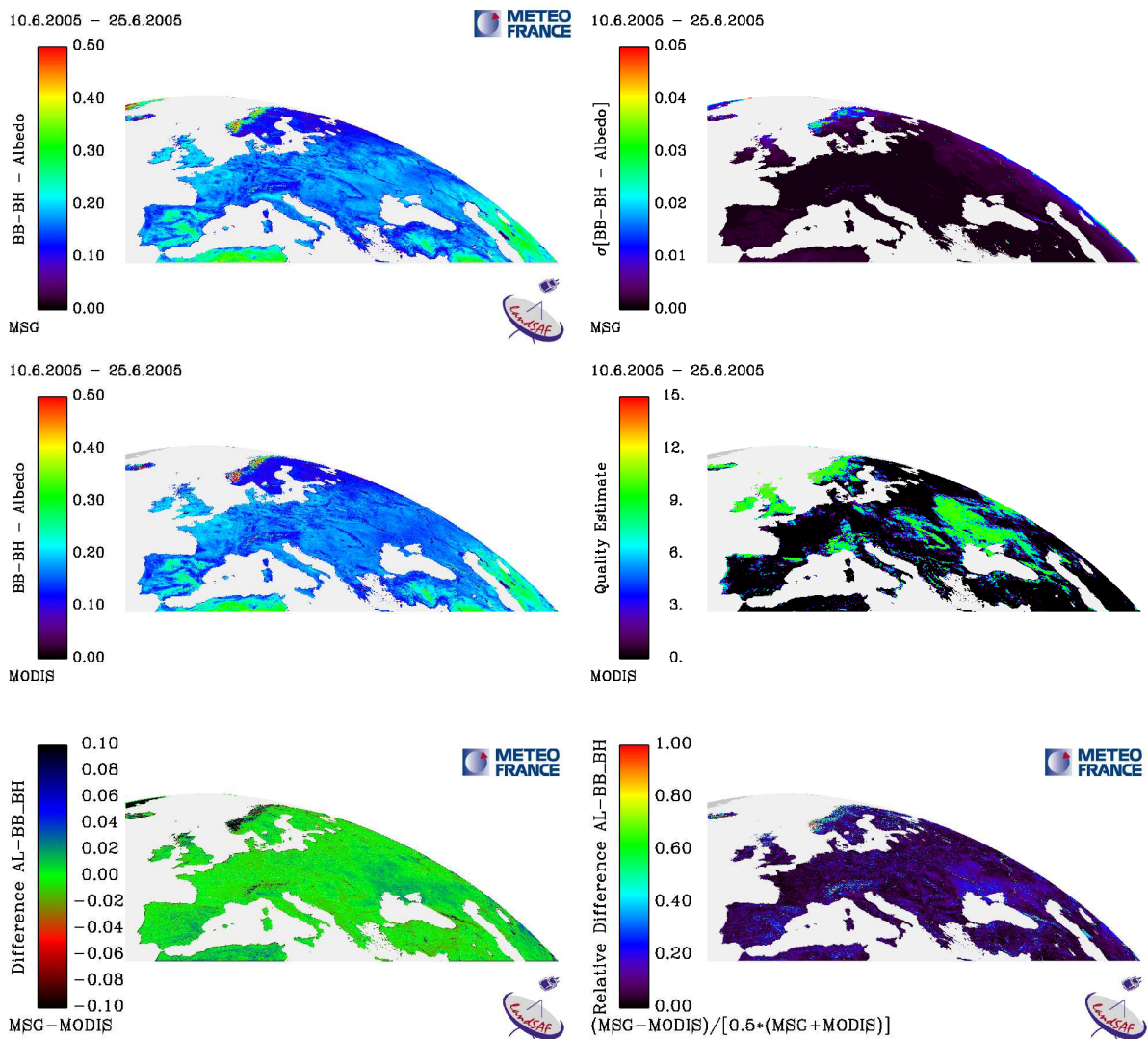

Figure 9: Comparison of bi-hemispherical total broadband albedo results. Top panels: Land-SAF albedo (left) and uncertainty estimate (right). Middle panels: MODIS albedo (left) and qualitative error estimate (right). Bottom panels: Absolute (left) and relative (right) difference between the Land-SAF and MODIS results.
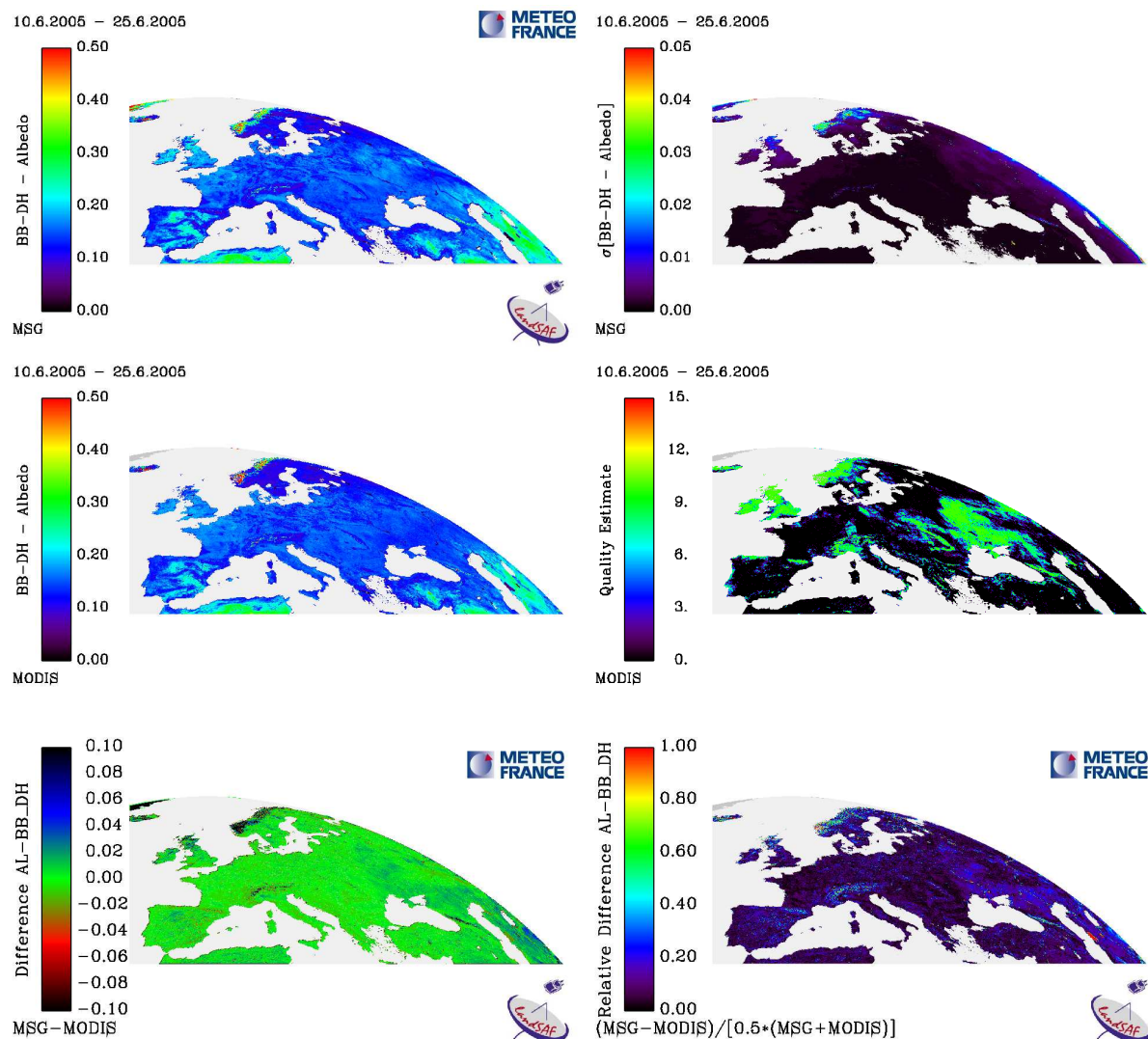
Figure 10: Comparison of directional-hemispherical total broadband albedo results. Top panels: Land-SAF albedo (left) and uncertainty estimate (right). Middle panels: MODIS albedo (left) and qualitative error estimate (right). Bottom panels: Absolute (left) and relative (right) difference between the Land-SAF and MODIS results.
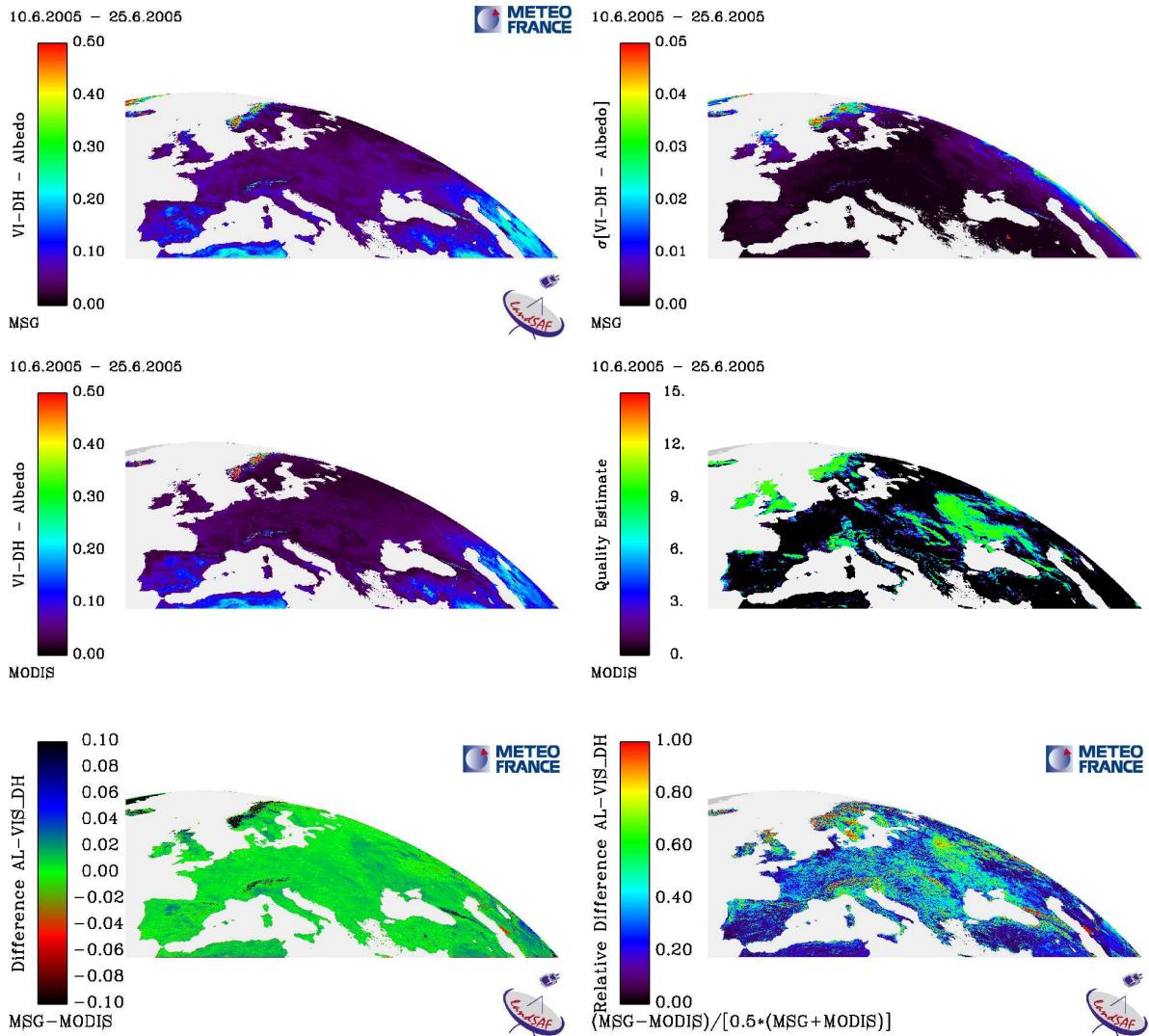
Figure 11: Comparison of directional-hemispherical visible broadband albedo results. Top panels: Land-SAF albedo (left) and uncertainty estimate (right). Middle panels: MODIS albedo (left) and qualitative error estimate (right). Bottom panels: Absolute (left) and relative (right) difference between the Land-SAF and MODIS results.
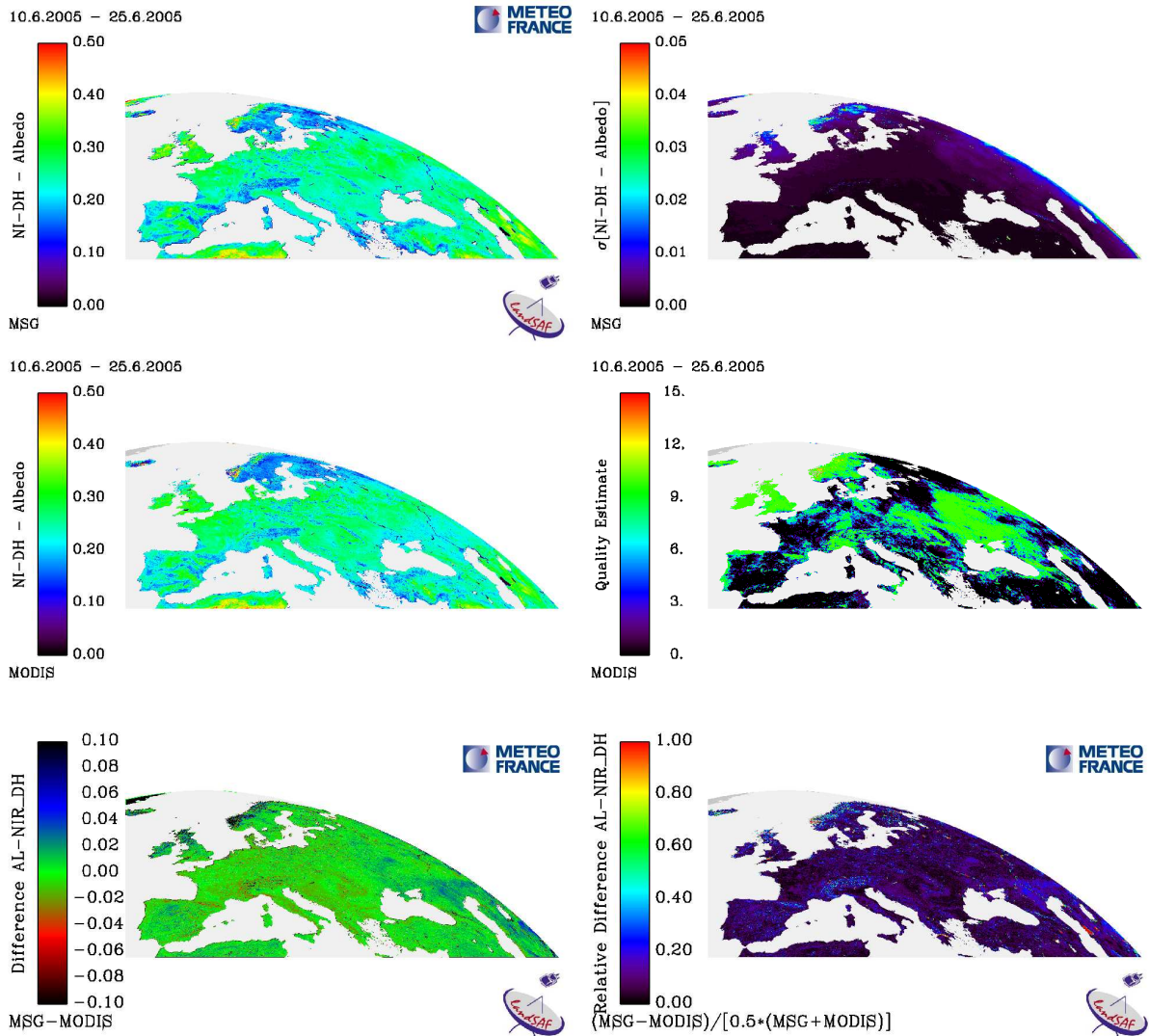
Figure 12: Comparison of directional-hemispherical near infrared broadband albedo results. Top panels: Land-SAF albedo (left) and uncertainty estimate (right). Middle panels: MODIS albedo (left) and qualitative error estimate (right). Bottom panels: Absolute (left) and relative (right) difference between the Land-SAF and MODIS results.
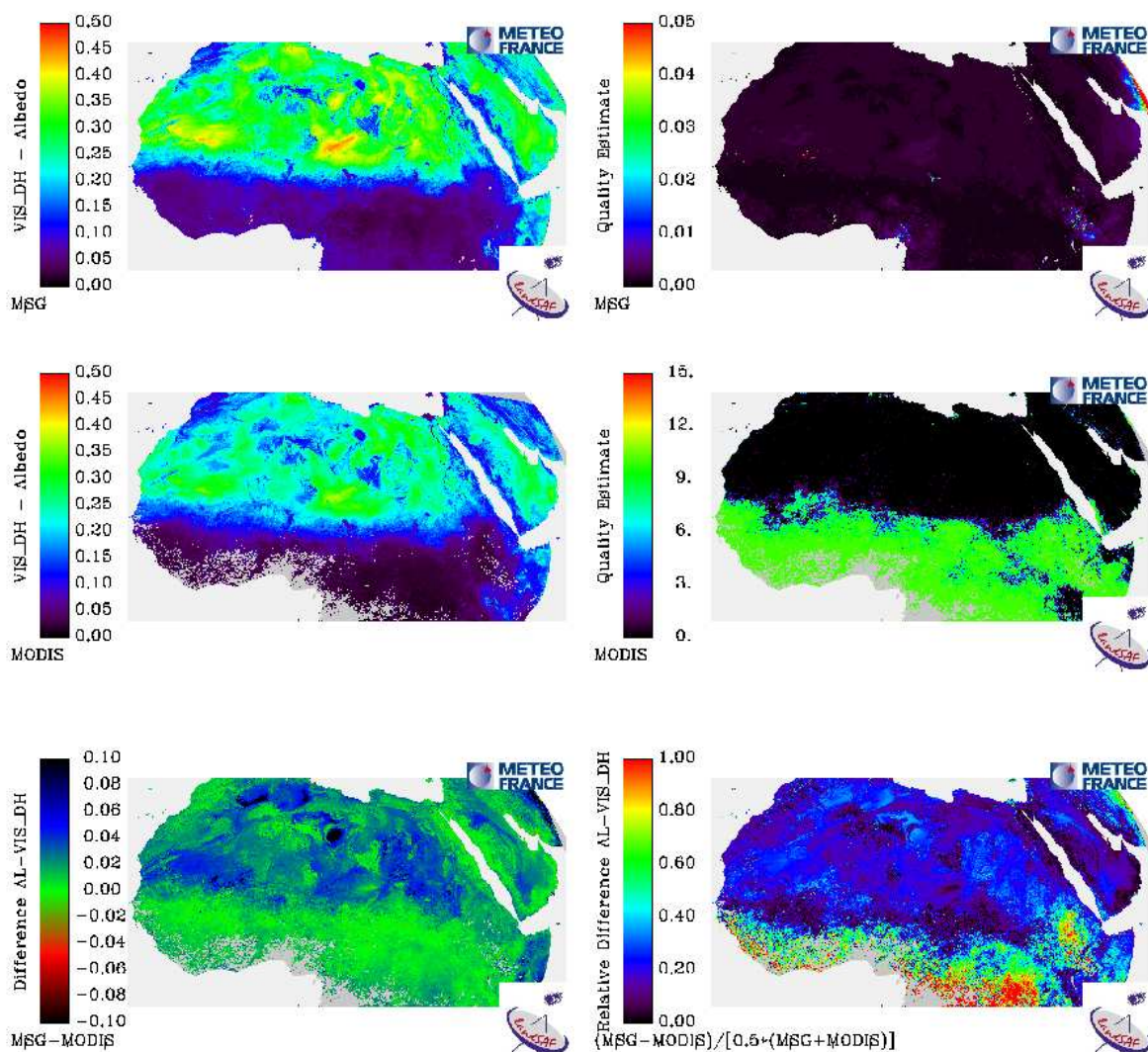
Figure 13: Comparison of directional-hemispherical visible broadband albedo products for the period 12-27 July 2006. Top panels: Land-SAF albedo (left) and uncertainty estimate (right). Middle panels: MODIS albedo (left) and qualitative error estimate (right). Bottom panels: Absolute (left) and relative (right) difference between the Land-SAF and MODIS results.

We display a quantitative analysis of the results in Figure 14 and Figure 15 for European and African continents, respectively. This includes scatter plots – or rather joint probability density plots – between the Land-SAF and MODIS albedo estimates. The respective graphs also include numerical values for the bias, i.e. the average of the difference between the two estimates, and the standard deviation (of that difference). Only pixels with MODIS quality flag equal to zero (the best value) and Land-SAF uncertainty estimate smaller than 0.1 were considered in the analysis. The obtained values for the statistical quantities confirm the qualitative conclusions reported above, i.e. a good correspondence is found for the near infrared and the total broadband ranges where there exists an evident overestimation of the visible broadband albedo for Land SAF product with respect to the MODIS product.
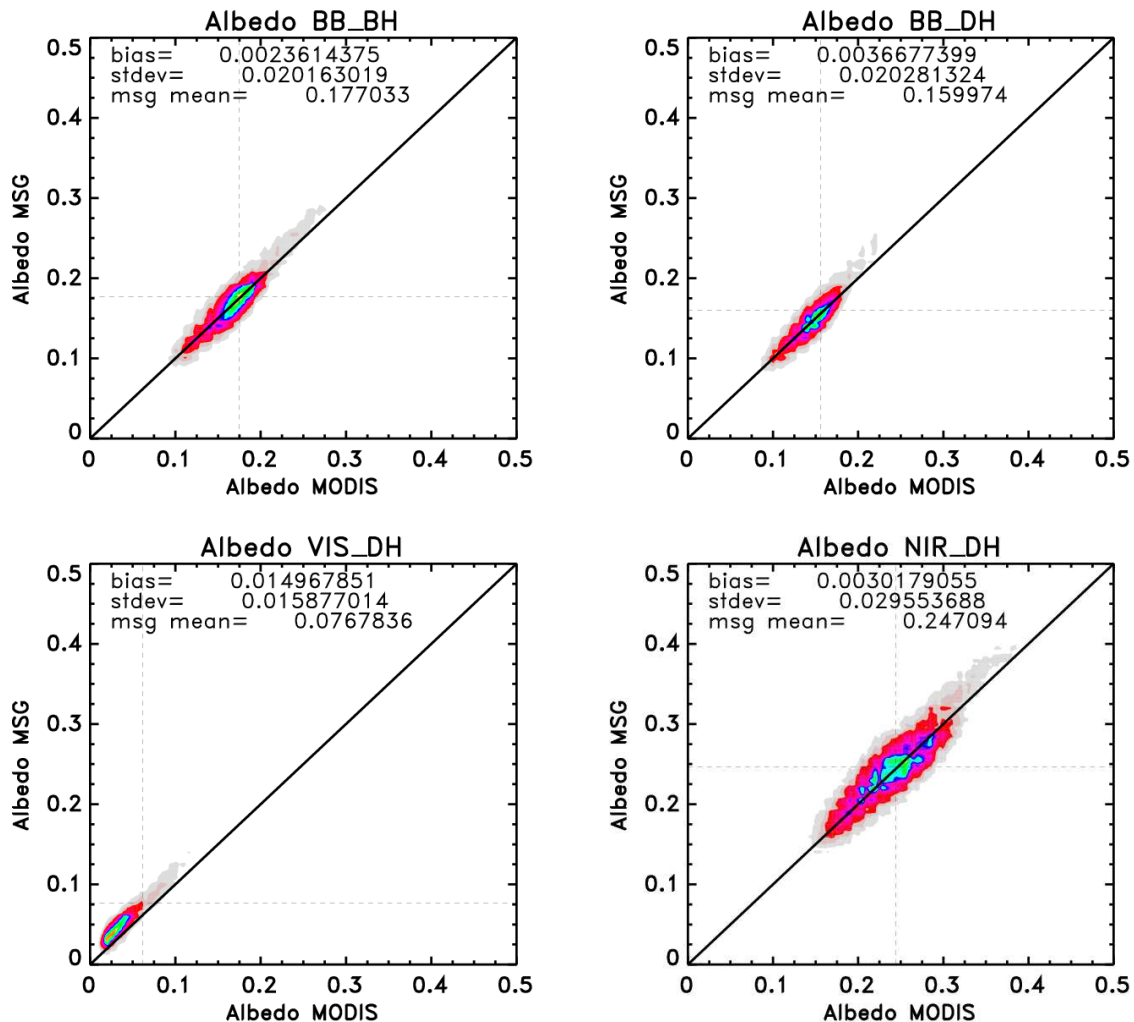

Figure 14: Scatter plots over Europe between the Land-SAF and MODIS broadband albedo products for the period June 10 to June 25 (161 MODIS period). Top Left: Total broadband bi-hemispherical. Top Right: Total broadband directional-hemispherical. Bottom Left: Visible broadband directional-hemispherical. Bottom Right: Near Infrared broadband directional-hemispherical.

Latest obtained results concern Northern African box and the 16-days MODIS periods from July 12 to September 13 of 2006. Nonetheless, only the 193 MODIS period is presented here as to be supposedly representative. Same conclusions than for Europe are stressed, i.e. there exists a good correspondence for the near infrared and the total broadband ranges, and an overestimation of the visible broadband albedo with respect to the MODIS product. However, it is worth emphasizing that the standard deviation relative to the mean albedo value is clearly reduced in comparison to those over Europe and values of albedo are usually larger than over Europe (0.27 of mean value for MSG VIS-DH albedo over North Africa against 0.08 over Europe and the 161 MODIS period).
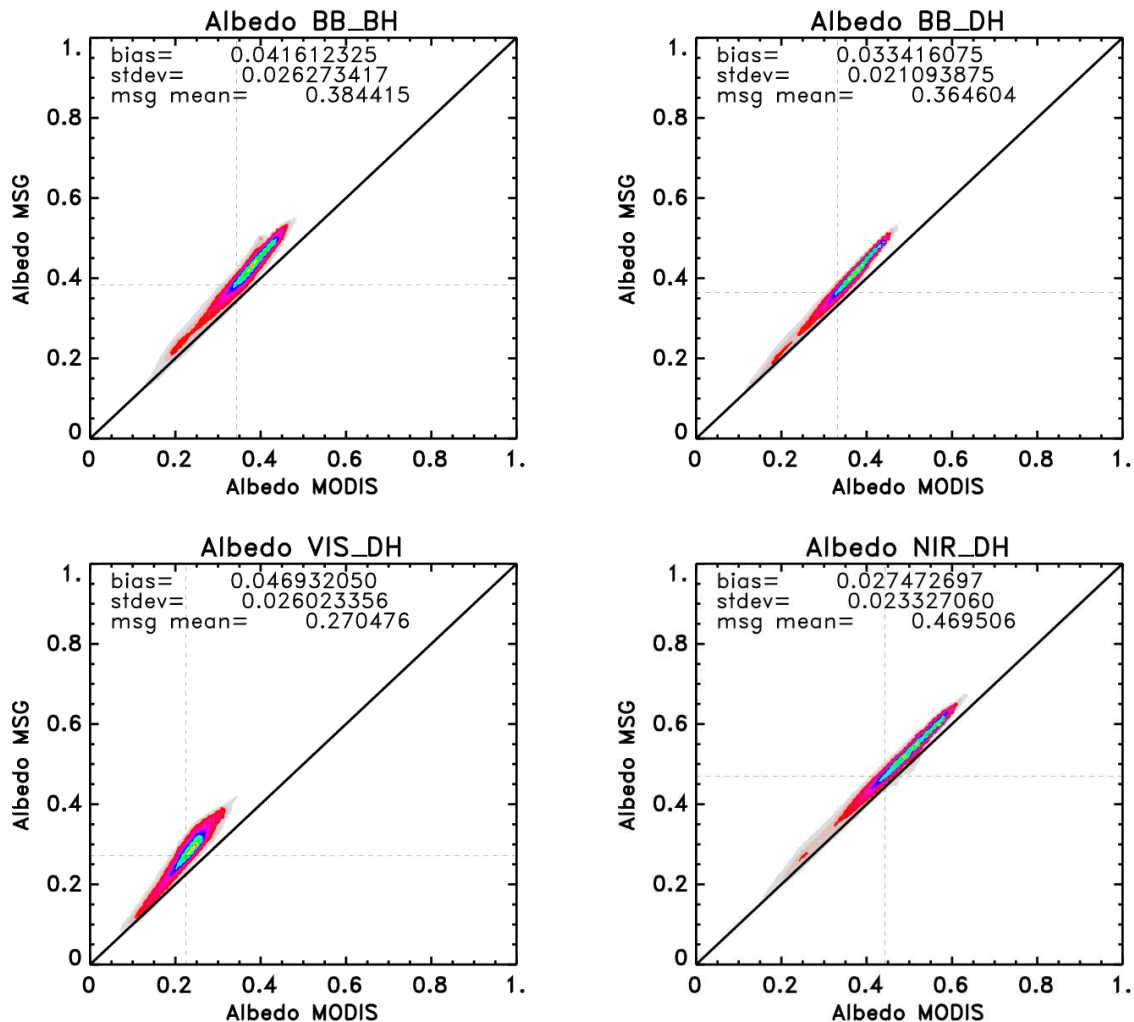

Figure 15: Scatter plots over Africa between the Land-SAF and MODIS broadband albedo products for the period July 12 to July 27 2006. Top Left: Total broadband bi-hemispherical. Top Right: Total broadband directional-hemispherical. Bottom Left: Visible broadband directional-hemispherical. Bottom Right: Near Infrared broadband directional-hemispherical.

For a deeper analysis of the cause of the bias in the visible broadband albedo, we performed the same kind of analysis for the spectral albedo estimates. The MODIS channels whose spectral properties are approximately equivalent with the MSG channels were chosen for this comparison. The results are given in Figure 17 for the bi-hemispherical and directional-hemispherical albedo variants. For the directional-hemispherical albedo the biases in the 0.6µm and 1.6µm channels are negligible, whereas the 0.8µm albedo is underestimated with respect to MODIS. On the other hand, Land-SAF bi-hemispherical albedo values are overestimated with respect to MODIS in all three channels. This stresses differences in angular integration either due to the use of different BRDF models or to a different angular sampling. Owing to some compensation in the spectral bi-hemispherical albedo, the corresponding total short-wave broadband quantity shows a good match with the MODIS result for both albedo variants (cf. top plots of Figures 14-15). In Land-SAF algorithm the same narrow-to-broadband conversion coefficients are used for the bi-hemispherical and directional-hemispherical albedo, whereas different relationships have been applied for MODIS. Figure 16 shows scatter plots between the Land-SAF and MODIS results for the BRDF model parameter k0, which matches with TOC reflectance for an illumination at zenith and an observation at nadir. Some discrepancies appear in the reflectance values measured by the two instruments due to differences in spectral sensitivity of the respective channels. Figure 17 also shows results obtained after the spectral projection of the MODIS channels in SEVIRI spectral bands. The linear transformation is the result of the best fit between the MODIS and SEVIRI channels based on numerical experiments (radiation transfer code simulations and spectral library). The impact on the obtained values for the validation statistics is however relatively small. As for the directional-hemispherical spectral albedo there is an underestimation of the 0.8µm normalised reflectances whereas the level of 0.6µm and 1.6µm reflectance values are consistent with MODIS.
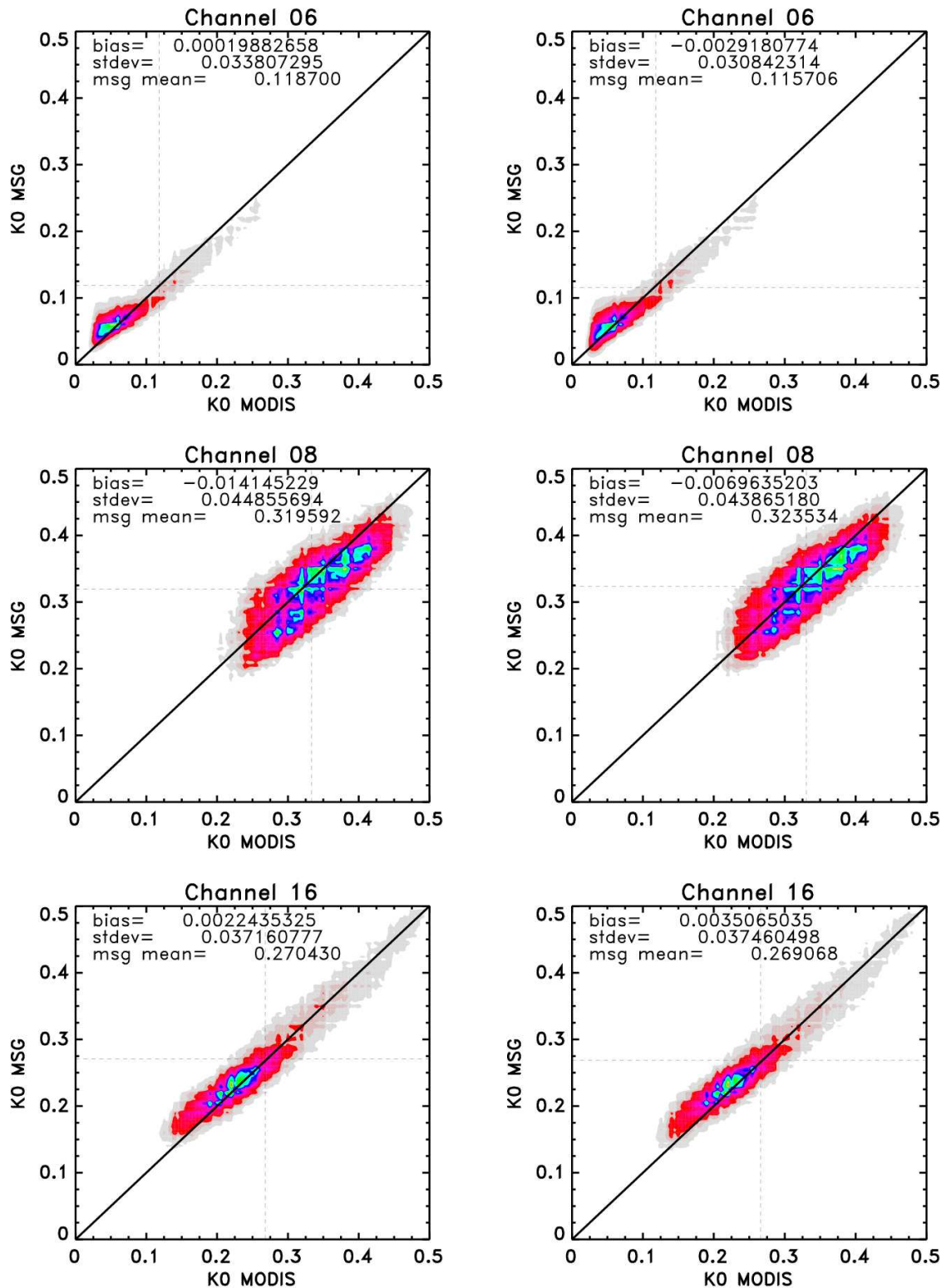
Figure 16: Scatter plots over Europe between the Land-SAF and MODIS results for the k_0 BRDF-model parameter for the period June 10 to June 25. Top: Red Channel (0.6µm). Middle: Near Infrared Channel (0.8µm). Bottom: Short-wave Infrared Channel (1.6µm). Left: Without correction. Right: After correcting for the spectral sensitivity differences of the SEVIRI and MODIS channels.
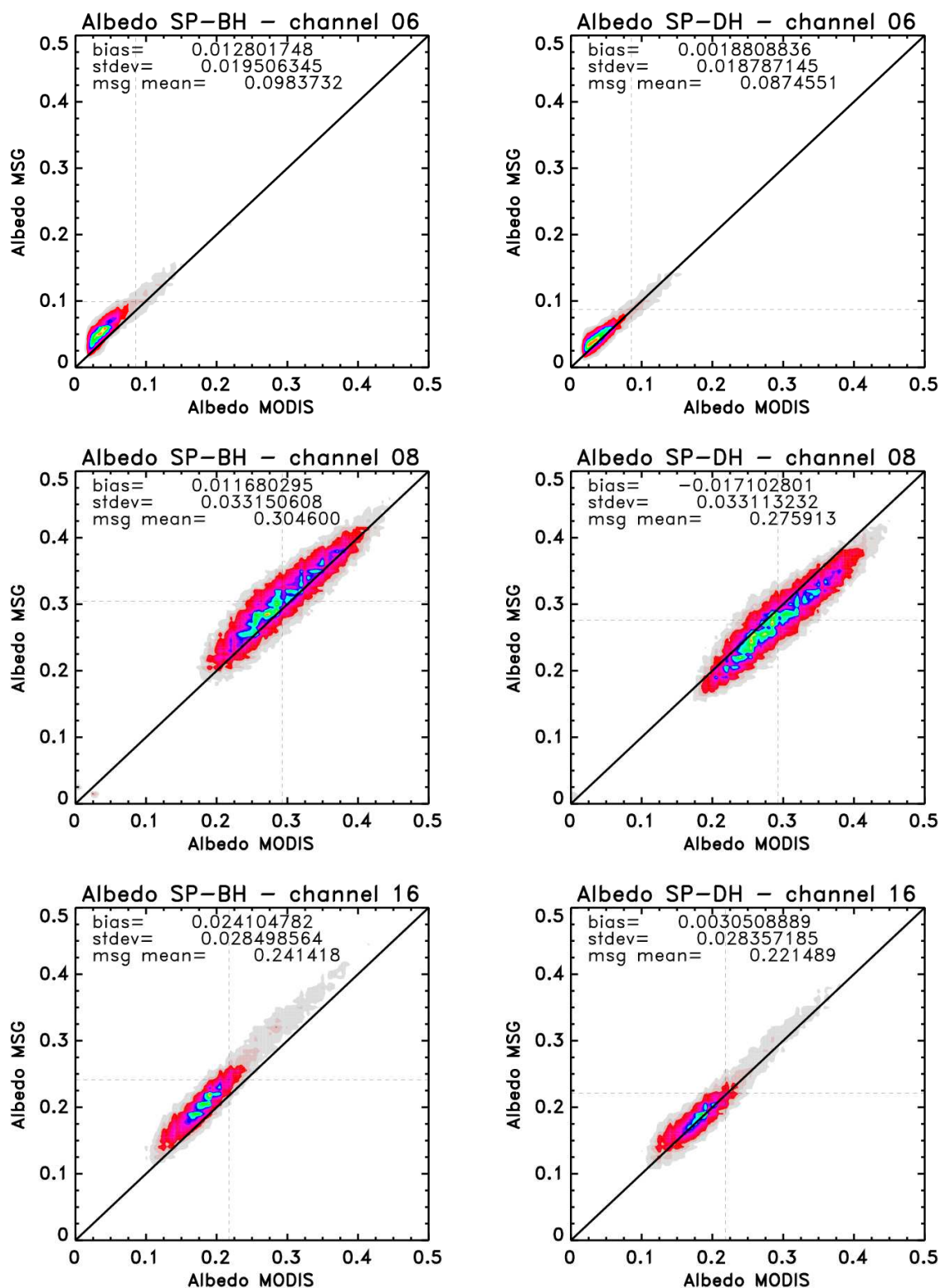
Figure 17: Scatter plots over Europe between the Land-SAF and MODIS spectral albedo results for the period June 10 to June 25. Top: Red Channel (0.6µm). Middle: Near Infrared Channel (0.8µm). Bottom: Short-wave Infrared Channel (1.6µm). Left: bi-hemispherical. Right: directional-hemispherical.

 A short-term projection of evolution of MDAL product will be to perform an aerosol correction using the MACC-II aerosol product (www.gmes-atmosphere.eu). In this regard, some evaluation was carried on for the year 2010 between AL-VI-DH and AL-BB-DH (-BH) and the corresponding MODIS albedo products. Selected results of inter-comparison are reported hereafter between the operational MDAL (OP) and the experimental MDALMC (MACC) product. Since the threshold in terms of specification was assessed to 0.15 for the albedo value, two comparisons (below and above 0.15) have been performed. This explains for instance large number of missing values over Africa and middle East (see Figure 20) in the present analysis for case of reference MDAL<0.15 for both visible and broadband albedos. Note that snow pixels were discarded from the analysis because different strategies were adopted between MODIS and LSA SAF projects. Hence, albedo values typically beyond 0.35 for the visible band were not considered here in the analysis exercise for MDAL>0.15.
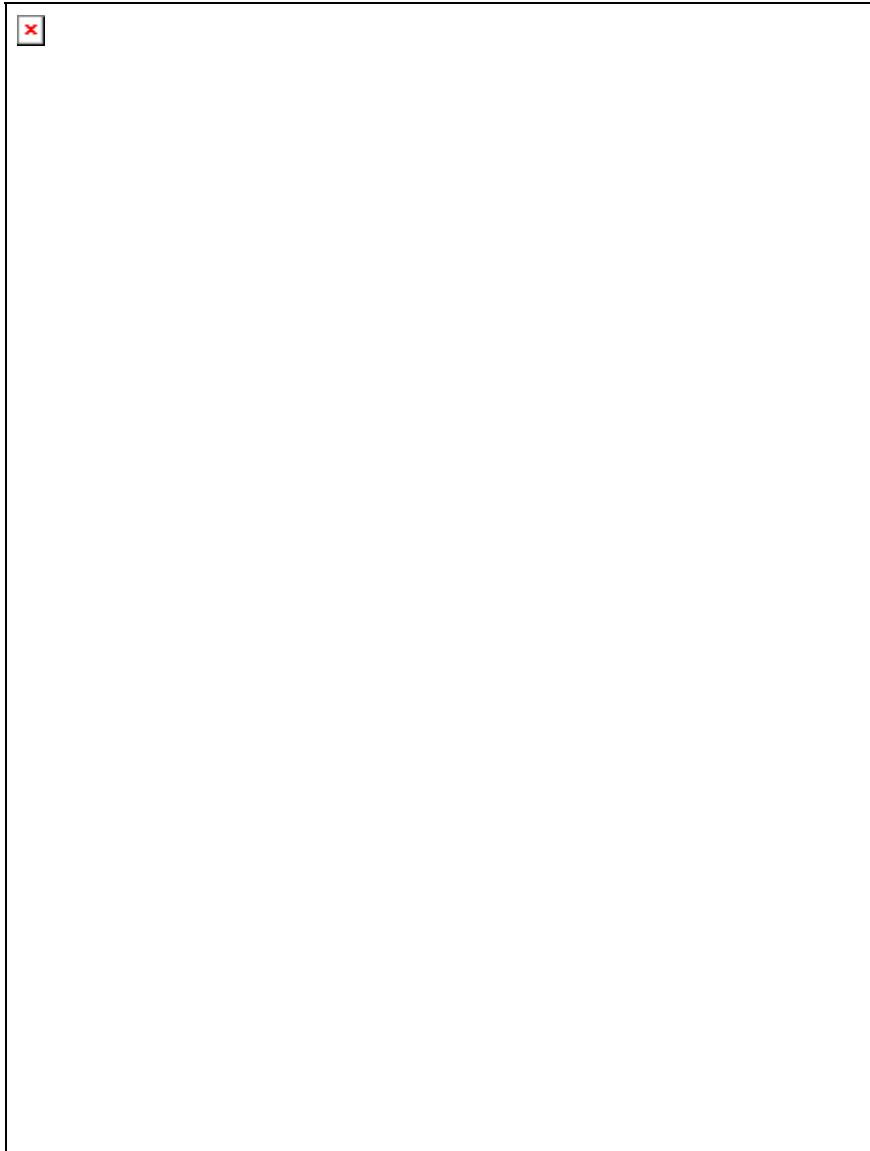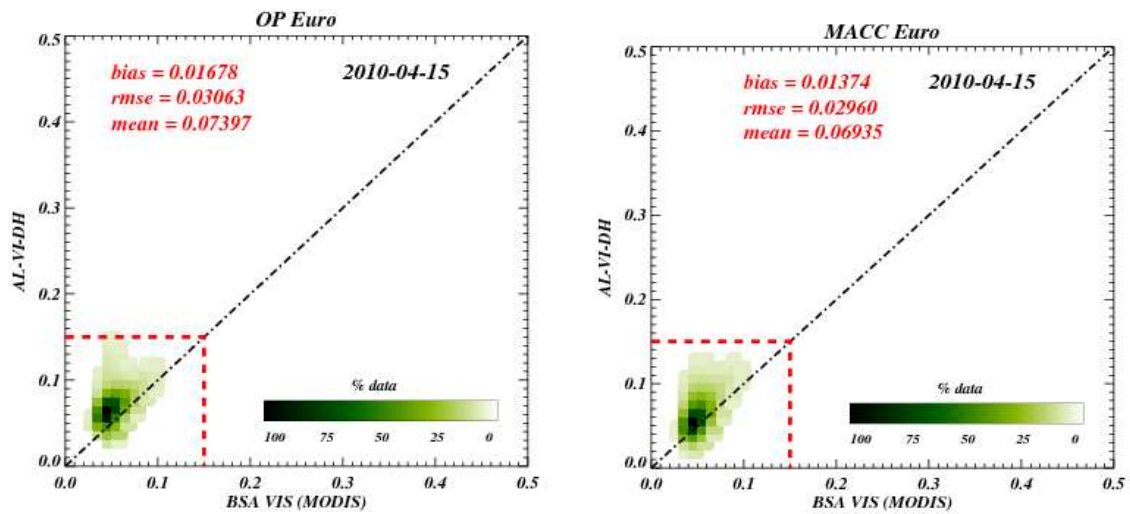
Figure 18: Comparison between MDAL (AL-VI-DH) and MODIS products on April 15, 2010.

Figure 18 shows for Europe maps of operational MDAL product below 0.15 on 2010-04-15 in the visible broadband, then these values less than MODIS, and finally MDAL based on MACC correction less than MODIS. The results are limited to the set of albedo values below the threshold of 0.15. Therefore, rmse is an absolute quantity in this case. A flag NA (Non Attributed) has been assigned to pixels that were discarded from the statistical numbers because of cloud contamination, snow occurrence, or reflectance values beyond 0.15.

The 10-day albedo product so-called MTAL derived from MDAL is also disseminated by the ground segment since 2009. Illustration of comparison between MTAL and MODIS also on April 15, 2010, is shows hereafter. Note that MTAL from MDAL corrected from MACC aerosol is not available yet. However, it is worth noticing that the accuracy assessment is improved as it could be expected for a climatologic-based product.
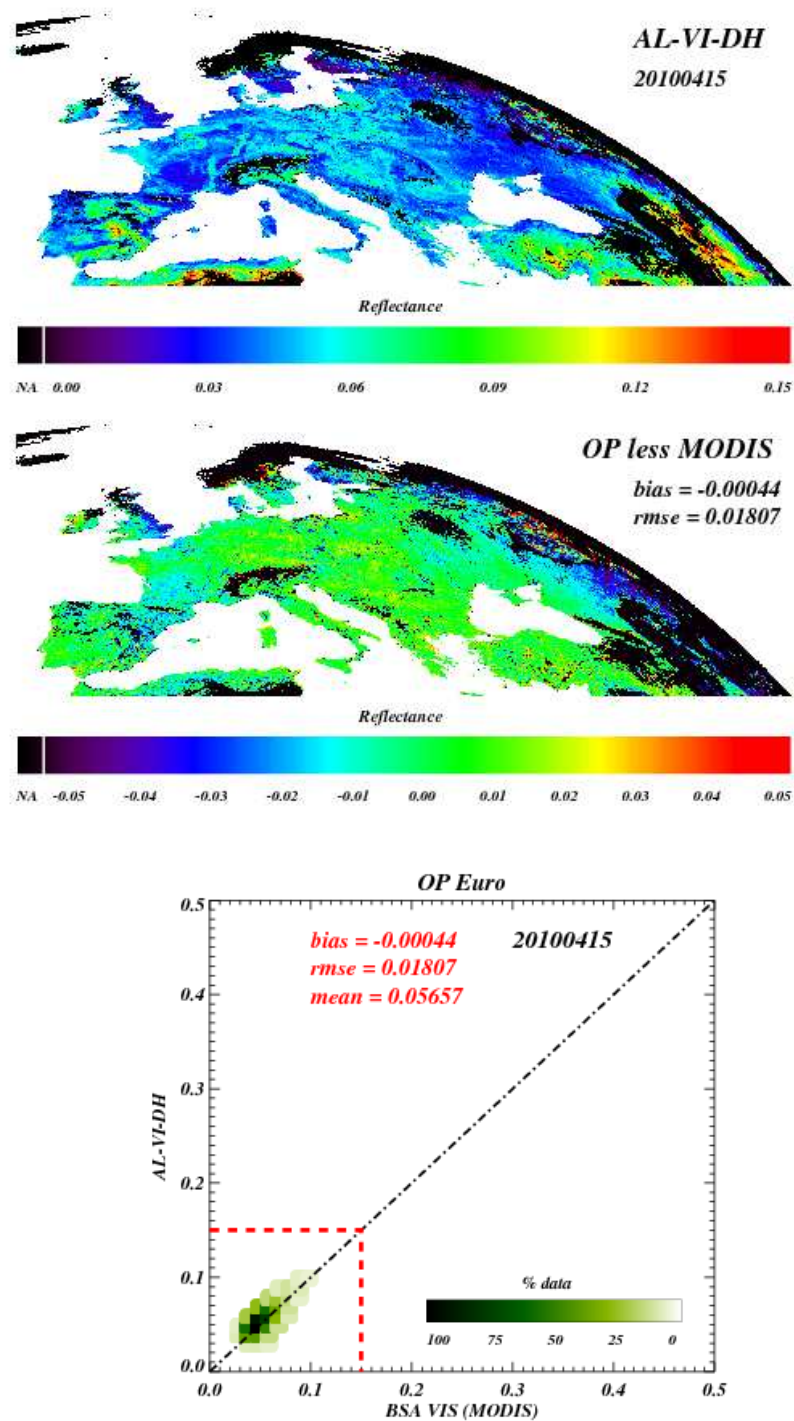
Figure 19: Comparison between MTAL (AL-VI-DH) and MODIS products on April 15, 2010.

Interestingly, Figure 20 enhances the positive effect of aerosol removal caused by the fire events that occurred in August 2010 in Russia.
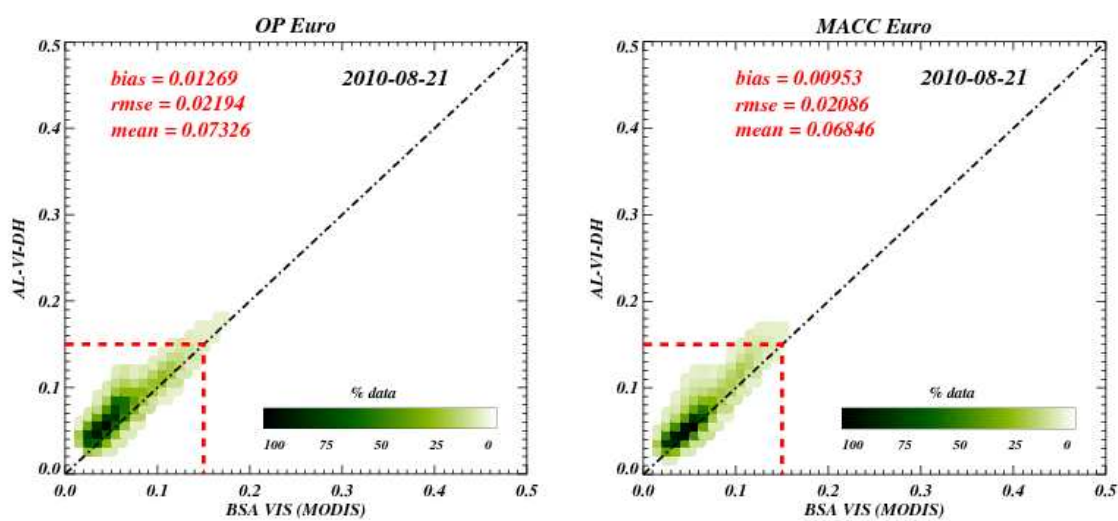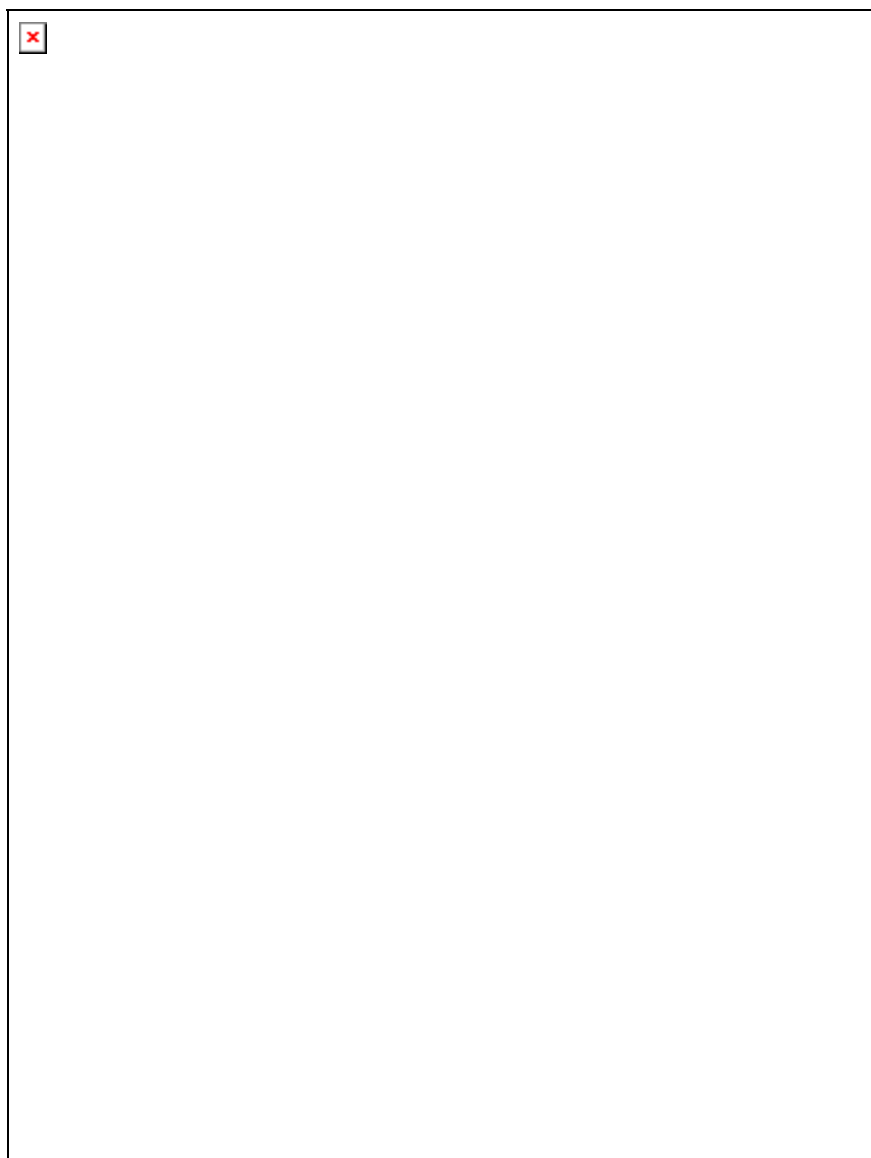
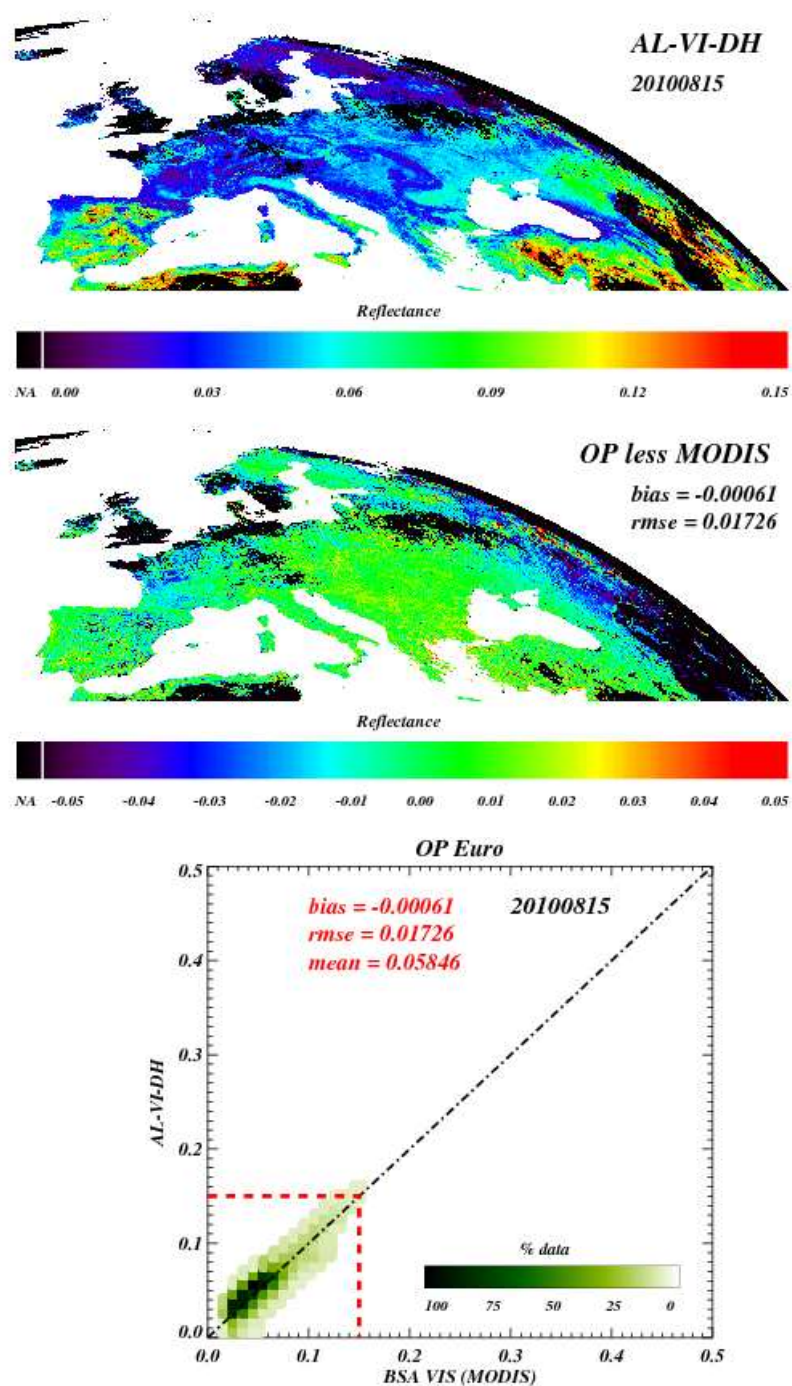Figure 20: Same as Figure 14 on August 21, 2010.

Figure 21: Same as Figure 19 on August 15, 2010.

Over North Africa (Figure 22), it is shown that the reflectance of aerosols is removed using MACC product on the edge of the zone (Somalia) since the optical pathway is therefore enhanced. The effect of the MACC correction is to reduce the value of MDAL by a few percent in absolute unit. A gain is therefore noticeable.
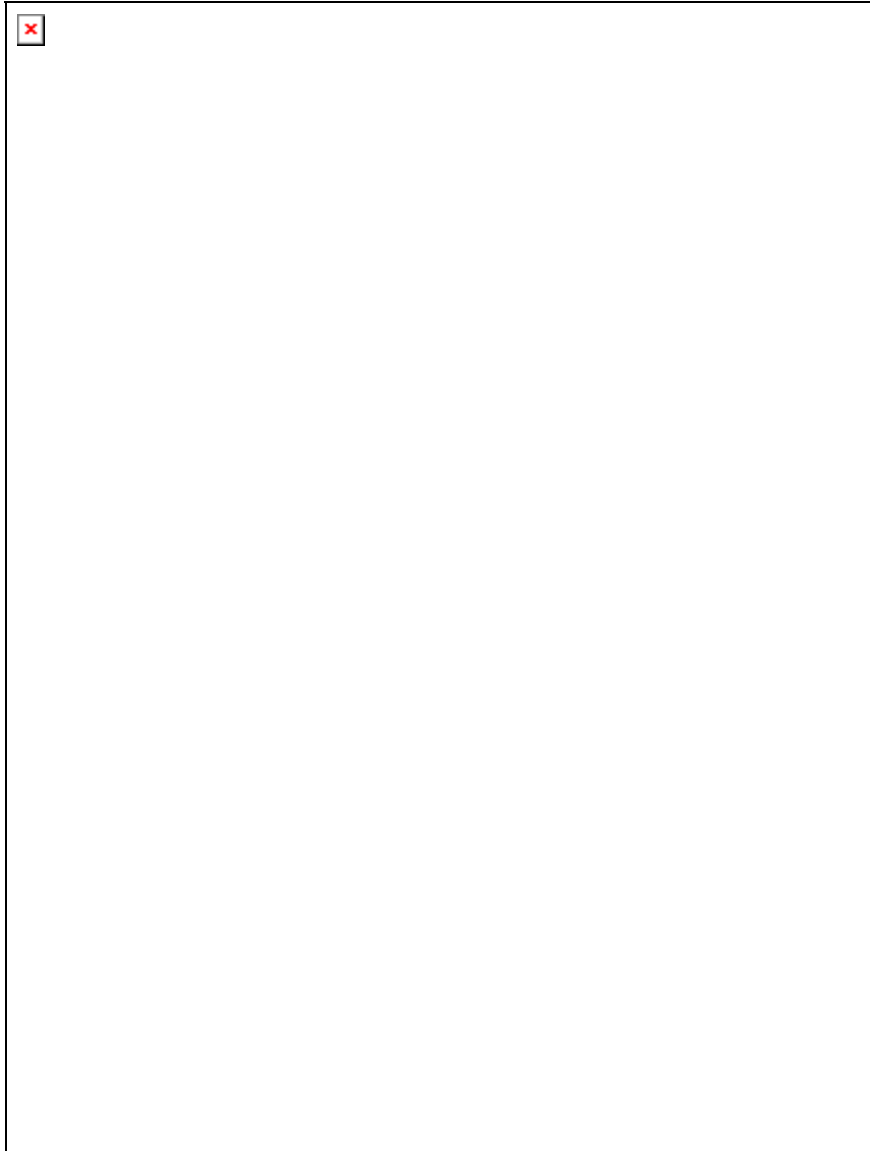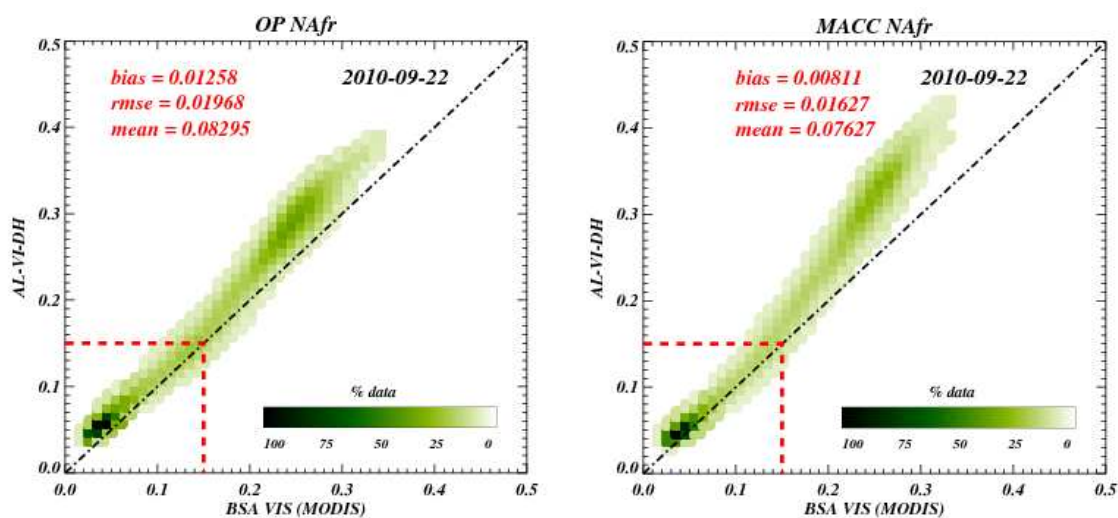
Figure 22: Comparison between MDAL (AL-VI-DH) and MODIS products on September 22, 2010.
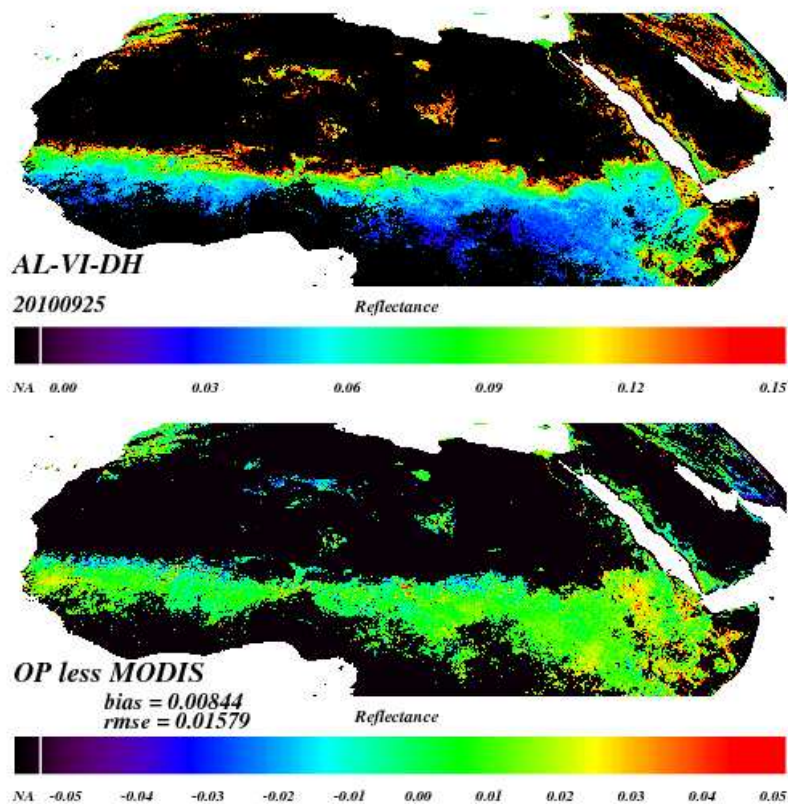
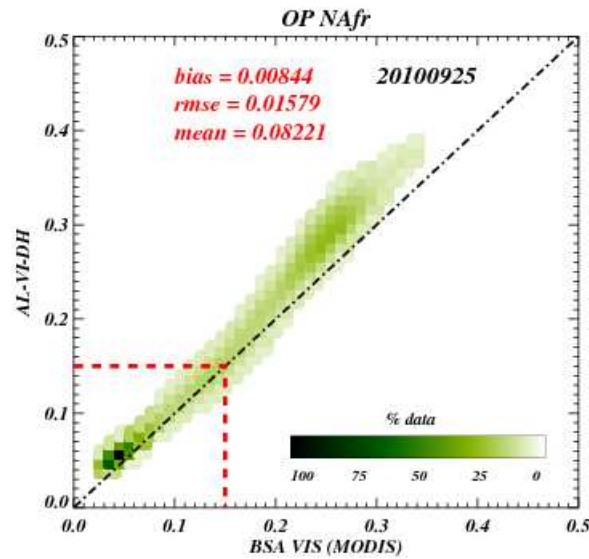Figure 23: Comparison between MTAL (AL-VI-DH) and MODIS products on September 25, 2010.

Considering now high MDAL values, desert and semi-desert targets are evidenced. In this case, it is believed MODIS would be a poor reference because it is known to fail removing properly the aerosol over bight targets. This may explain the dispersion between the two data sets is increased after MACC correction.
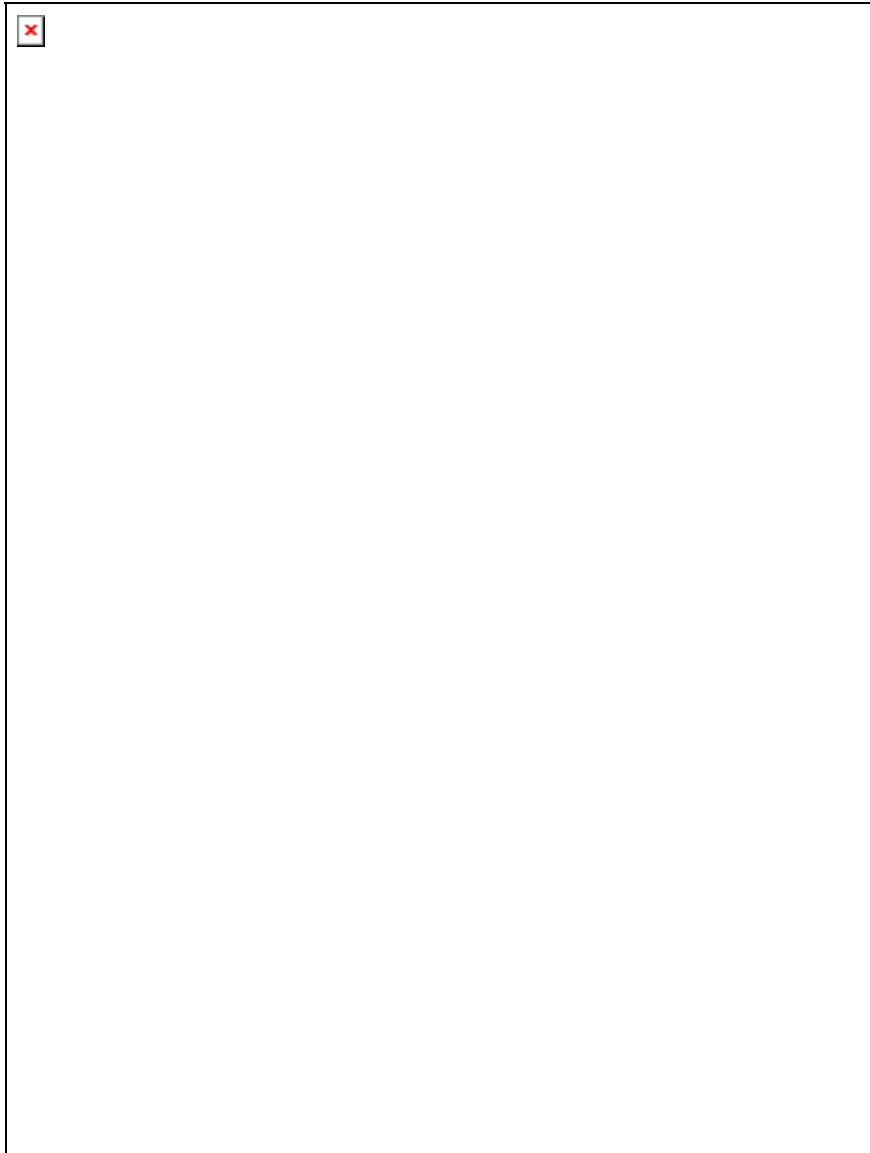
Figure 24: Same as Figure 21 for AL-VI-DH above 0.15.

It is generally observed overestimates of albedo with respect to MODIS, particularly for latest results of comparison (Figures 18 to 24). The explanation for discrepancy with MODIS is not clear although some mis-calibration of MODIS could explain such fact for the version 5 (http://mcst.gsfc.nasa.gov/index.php?section=7).

Note the the bias increases with the value of albedo, which is physically sound. In the visible, the albedo of aerosol dominates and as it removes, it can be observed a decrease of the surface albedo. In the infrared, the masking effect dominates and the surface albedo increases because it is normalized by the transmittance of aerosols, which is less than 1. The more the aerosol optical depth, the less the transmittance value. As a consequence, decontamination of aerosol during a large episode will give raise to the infrared albedo. Statistical results of comparison are slightly improved with MTAL compared to MDAL.

2.4.2 Time Series of Statistics

2.4.2.1 Statistics for operational outputs

Land-SAF output products from the operational centre in Lisbon are considered for statistical analysis. To be noticed that a local reprocessing has been achieved for cases of the operational system was not functioning.

Statistical results (bias and standard deviation) were calculated between the Land-SAF and MODIS broadband albedo estimates for a series of MODIS periods ranging from June 2005 to October 2006. Results in absolute units are shown in Figure 25.

Except for the winter season, the biases of total shortwave and near infrared broadband albedo are below 0.01 in absolute (5% in relative units over the whole time series). The standard deviation of the difference is in the order of 0.02 to 0.03. These biases increase for the last periods of 2005, especially for near infrared broadband albedo. Possible scenarios are: i) an increased cloud influence since some cloudy pixels were not efficiently eliminated by the relevant algorithm version (AL v5.0); ii) processing issues in the Land-SAF system, which led to the loss of a large number of observations available for the AL2 algorithm. The AL2 v5.1 version algorithm, which discards primarily undetected cloudy scenes, was implemented in the operational system on 20051214. For near infrared broadband albedo, statistical results are better during the following periods than before the date 20051214.

The bias for the visible broadband albedo exhibits absolute values up to 0.015, or about 20% in relative units. A For the time being, AOT is constant all along the year, being solely dependent on the latitude. The maximum of bias for the visible broadband albedo during the two summer months (July-August 2006) seems to support the role of the aerosols. The geometrical configuration is favourable in this season, thus there is no reason for having a more important bias in July than in June.

Bias and standard deviation for LSA-SAF and MODIS broadband albedo are also shown over North Africa for a series of MODIS periods between June 12 and September 13 of 2006. The results expressed in absolute units are reported in Table 3. Statistical numbers are rather stationary during such periods. A bias is still present for VIS-DH (about 20% in relative units). For other albedos, very good agreements can be noticed (usually less than 10%), with a maximum bias of 0.033 and a maximum RMSE of 0.23 for black-sky short-wave albedo (BB-DH). Jin et al. (2003) compared MODIS albedo to commonly used surface albedo data sets derived from the historical AVHRR and ERBE observations and estimated RMSE values of 0.025 and 0.047, and bias of 0.016 and –0.034 respectively for global black-sky albedo in September. Largest discrepancies were found for relative bright surfaces such as Central Asia and Northern Africa. Therefore, some conclusions can be addressed to LSA-SAF surface shortwave albedos over Northern Africa in considering their consistency whith MODIS albedo.
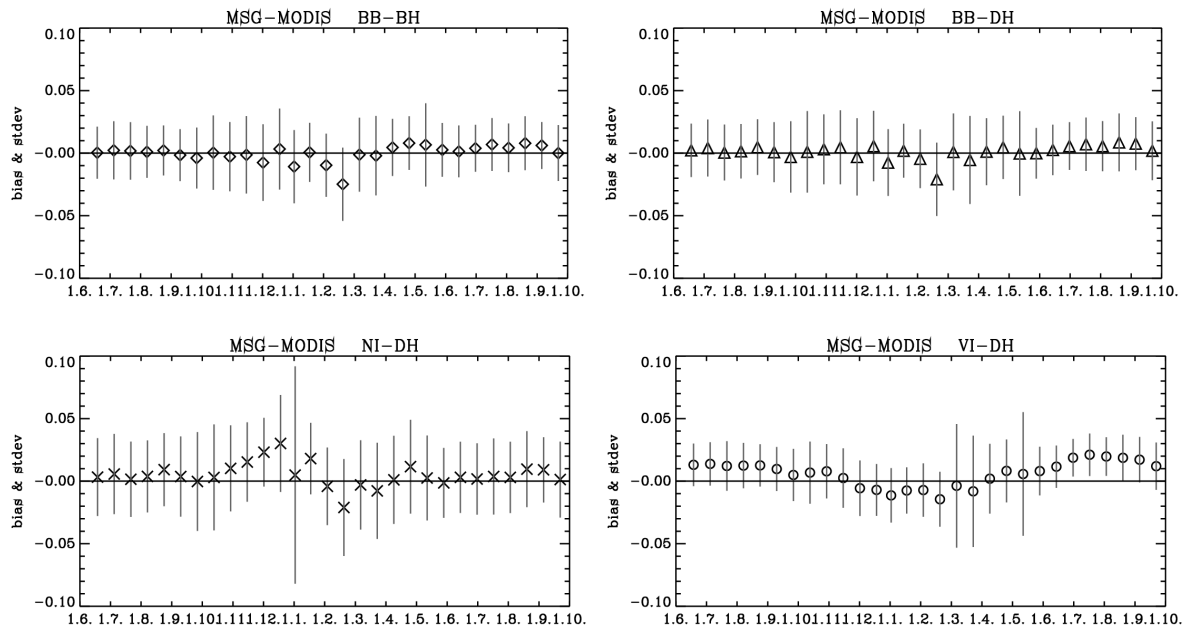
Figure 25: Temporal evolution (20050601-20060930) of the bias and standard deviation between Land-SAF and MODIS broadband albedo results. The one-sided length of the vertical bars indicates the standard deviation. Top Left (rhombus): Total shortwave bi-hemispherical. Top Right (triangle): Total shortwave directional-hemispherical. Bottom Left (cross): Near Infrared directional-hemispherical. Bottom Right (circle): Visible directional-hemispherical.

TABLE 3: BIAS AND STANDARD DEVIATION (RMSE) BETWEEN LAND-SAF AND MODIS BROADBAND ALBEDO RESULTS FOR 16 DAY PERIODS FROM JULY 12 TO SEPTEMBER 13 OF 2006 OVER NORTH AFRICA.

Albedo	Period	193 (Jul. 12–Jul. 27)	209 (Jul. 28–Aug. 12)	225 (Aug.13–Aug. 28)	241 (Aug. 29-Sept. 13)
VIS-DH	*Bias*	0,047	0,046	0,044	0,043
	RMSE	0,026	0,026	0,027	0,027
NIR-DH	*Bias*	0,027	0,026	0,024	0,020
	RMSE	0,023	0,024	0,026	0,028
BB-DH	*Bias*	0,033	0,032	0,031	0,028
	RMSE	0,021	0,021	0,023	0,023
BB-BH	*Bias*	0,042	0,039	0,039	0,034
	RMSE	0,026	0,026	0,026	0,026

Next figures show time series of statistical results coming from the comparison of MDAL with MODIS in order to assess the impact of the aerosol correction from MACC.
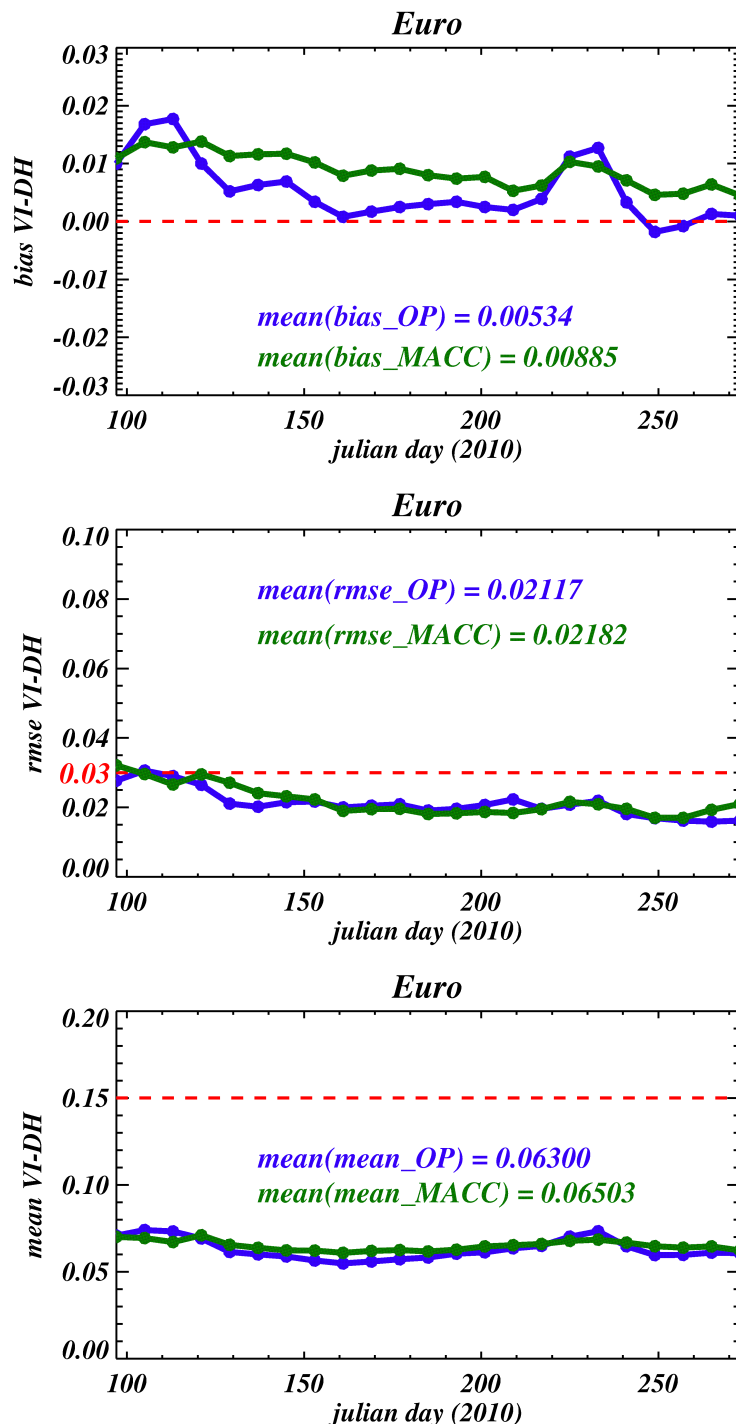

Figure 26: Times series of statistical results over the Europe area between SEVIRI (OP or MACC) and MODIS for AL-VI-DH <u>below 0.15</u>. From top to bottom: bias, rmse, and mean.
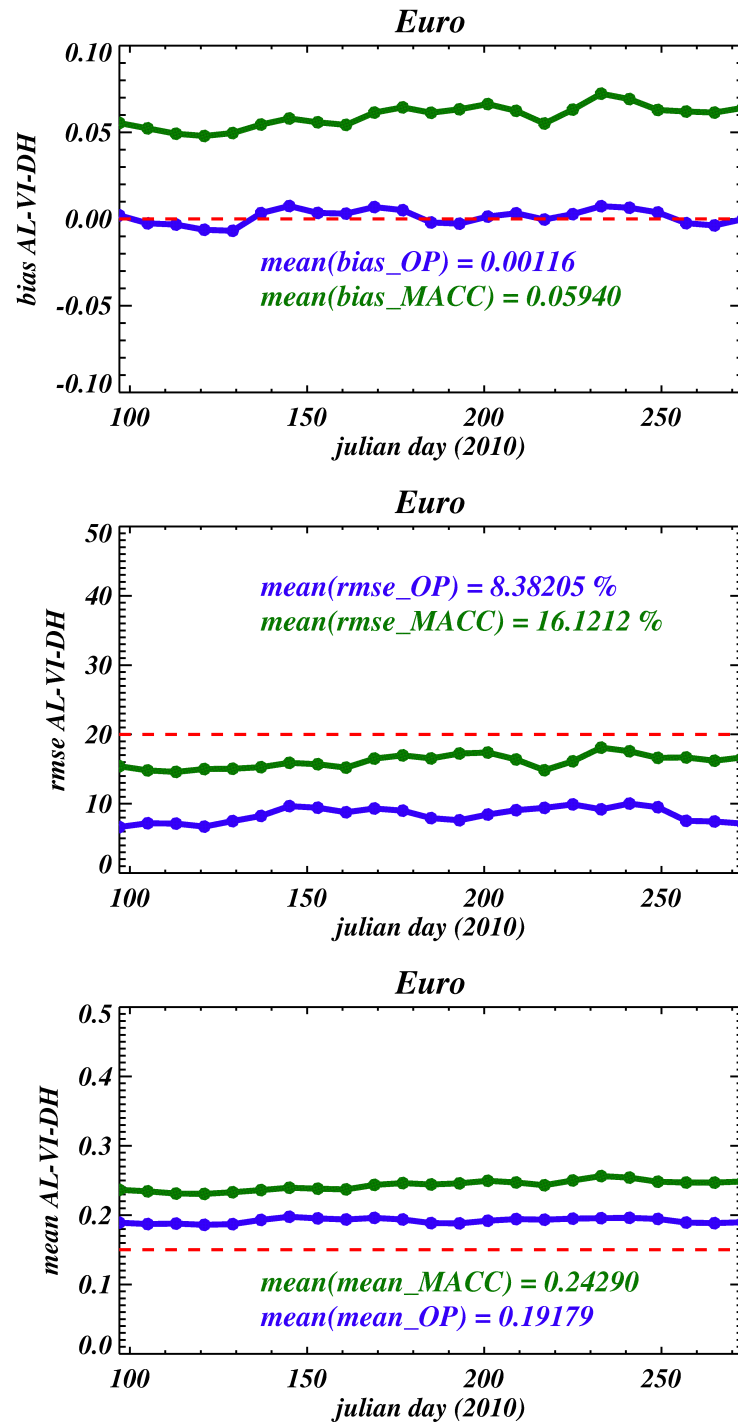
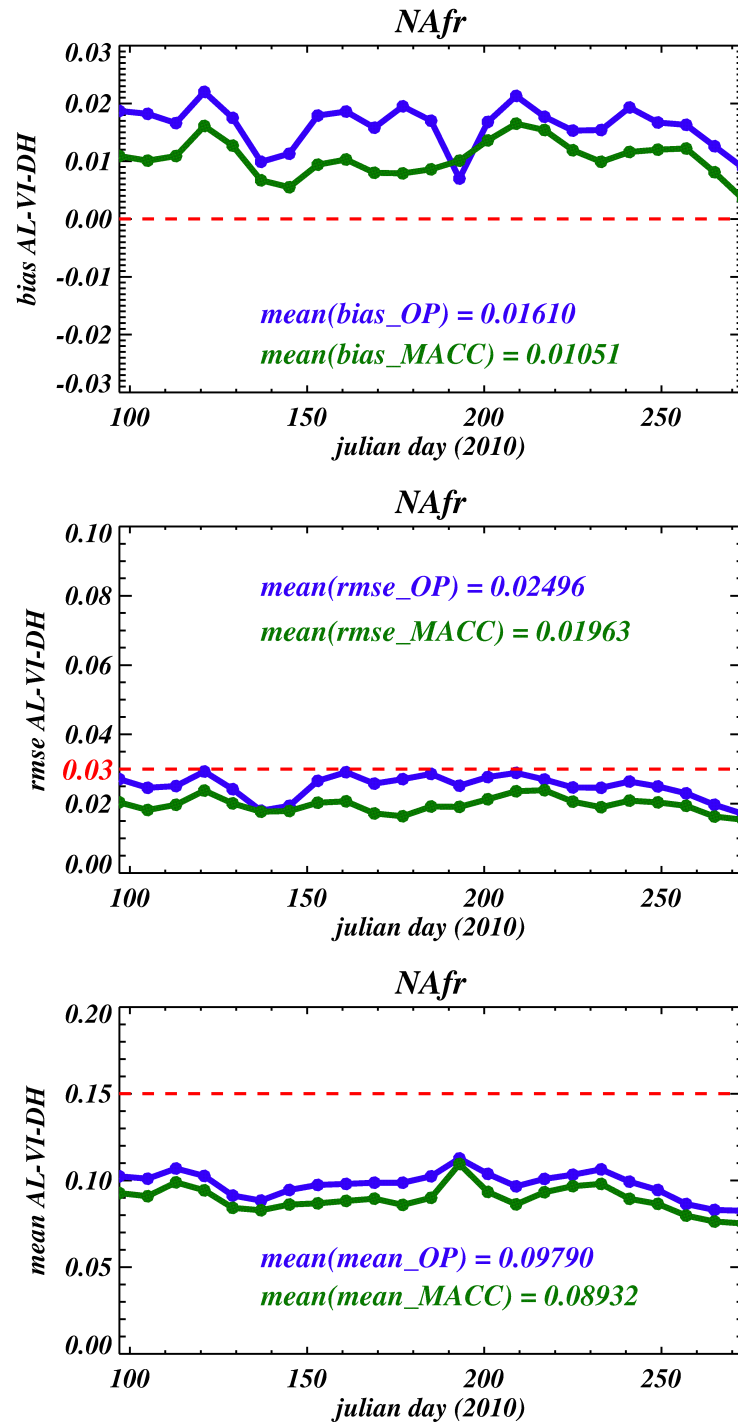Figure 27: Same as Figure 26 for AL-VI-DH <u>above 0.15</u>.

Figure 28: Times series of statistical results over the N-Africa area between SEVIRI (OP or MACC) and MODIS for AL-VI-DH <u>below 0.15</u>. From top to bottom: bias, rmse, and mean.
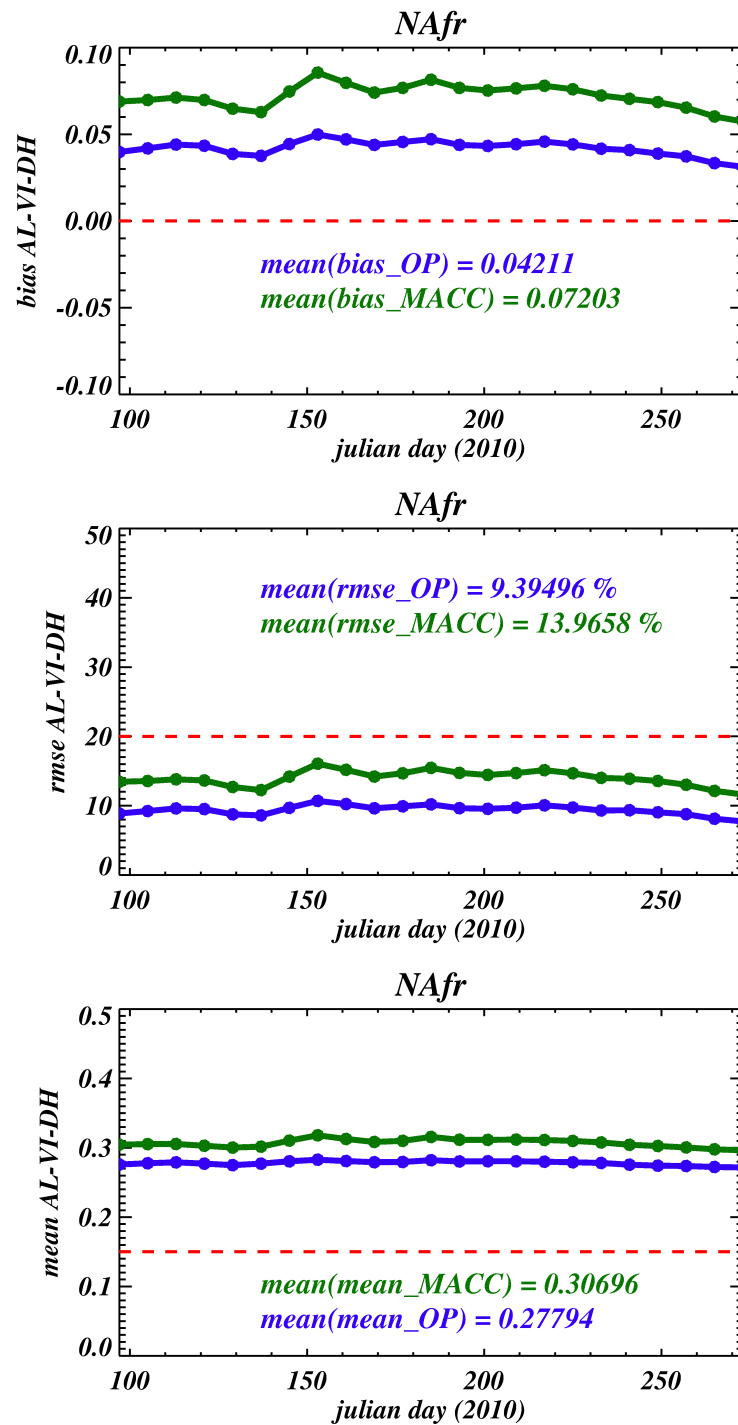
Figure 29: Same as Figure 28 for AL-VI-DH <u>above 0.15</u>.

Ref. SAF/LAND/MF/VR_AL/II_2012
Issue/II_2012
Date: 15 February 2012

The EUMETSAT Network of Satellite Application Facilities

LSA SAF
Land Surface Analysis

Numerical values are reported in Table 4 (AL-VI-DH below 0.15) and Table 5 (AL-VI-DH above 0.15). It comes out that the users requirements are satisfied in average with a low bias noticed.

TABLE 4: BIAS AND STANDARD DEVIATION (RMSE) BETWEEN MDAL AND MODIS BROADBAND ALBEDO RESULTS FOR THE PERIOD FROM APRIL TO SEPTEMBER 2010.

AL-VI-DH < 0.15

		OP Euro	*MACC Euro*	*OP NAfr*	*MACC NAfr*
AL-VIS-DH	*Bias*	0.00534	0.00885	0.01610	0.01051
	RMSE	**0.02117**	**0.02182**	**0.02496**	**0.01963**
AL-BB-DH	*Bias*	- 0.0057	0.00907	0.00637	0.01133
	RMSE	**0.02053**	**0.02565**	**0.01965**	**0.02235**
AL-BB-BH	*Bias*	0.00122	0.00299	0.01855	0.00819
	RMSE	**0.02067**	**0.02330**	**0.02957**	**0.02640**

TABLE 5: BIAS AND STANDARD DEVIATION (RMSE) BETWEEN MDAL AND MODIS BROADBAND ALBEDO RESULTS FOR THE PERIOD FROM APRIL TO SEPTEMBER 2010.

AL-VI-DH > 0.15

		OP Euro	*MACC Euro*	*OP NAfr*	*MACC NAfr*
AL-VIS-DH	*Bias*	0.00116	0.05940	0.04211	0.07203
	RMSE	**8.38205 %**	**16.1212 %**	**9.39496 %**	**13.9658 %**
AL-BB-DH	*Bias*	- 0.0003	0.07535	0.02589	0.06192
	RMSE	**5.67585 %**	**15.2634 %**	**5.03967 %**	**9.01232 %**
AL-BB-BH	*Bias*	0.01067	0.04518	0.03671	0.06396
	RMSE	**5.17971 %**	**9.82527 %**	**6.13816 %**	**9.02268 %**

TABLE 6: BIAS AND STANDARD DEVIATION (RMSE) BETWEEN MTAL AND MODIS
BROADBAND ALBEDO RESULTS FOR THE PERIOD FROM APRIL TO SEPTEMBER 2010.

AL-VI-DH < 0.15

		OP Euro	*OP NAfr*
AL-VIS-DH	*Bias*	-0.0019	0.01675
	RMSE	**0.01864**	**0.02110**
AL-BB-DH	*Bias*	- 0.0103	0.00347
	RMSE	**0.02174**	**0.01352**
AL-BB-BH	*Bias*	0.0036	0.01385
	RMSE	**0.02017**	**0.02268**

TABLE 7: BIAS AND STANDARD DEVIATION (RMSE) BETWEEN MTAL AND MODIS
BROADBAND ALBEDO RESULTS FOR THE PERIOD FROM APRIL TO SEPTEMBER 2010.

AL-VI-DH > 0.15

		OP Euro	*OP NAfr*
AL-VIS-DH	*Bias*	0.00854	0.04031
	RMSE	**9.90156 %**	**9.03892 %**
AL-BB-DH	*Bias*	- 0.00617	0.02488
	RMSE	**7.48352 %**	**4.85913 %**
AL-BB-BH	*Bias*	0.01545	0.03670
	RMSE	**6.89206 %**	**6.00649 %**

2.4.2.2 Dependence on NB to BB conversion

a./ Snow-free pixels

The conversion coefficients of *van Leeuwen and Roujean (2002)* are the operational narrow-to-broadband coefficients for snow-free pixels:

AL_BB-DH = 0.0047 + 0.5370 *C1 + 0.2805 *C2 + 0.1297 *C3

AL_VI-DH = 0.0093 + 0.9606 *C1 + 0.0497 *C2 - 0.1245 *C3

AL_NI-DH = -0.0004 + 0.1170 *C1 + 0.5100 *C2 + 0.3971 *C3

where

AL_BB-DH: Total shortwave directional-hemispherical albedo,

AL_VI-DH: Visible directional-hemispherical albedo,

AL_NI-DH: Near Infrared directional-hemispherical albedo,

C1: 0.6µm spectral albedo,

C2: 0.8µm spectral albedo,

C3: 1.6µm spectral albedo.

A statistical method (see Samain et al., IEEE, 2006) was reviewed to test new narrow-to-broadband albedo conversion coefficients as a function of surface cover:

AL_BB-DH = 0.0049 + 0.3600 *C1 + 0.3536 *C2 + 0.1495 *C3

AL_VI-DH = -0.0094 + 0.8264 *C1 + 0.0753 *C2 - 0.0868 *C3

AL_NI-DH = 0.0171 - 0.0030 *C1 + 0.5777 *C2 + 0.3515 *C3

There are these new statistics (bias and standard deviation between the Land-SAF and MODIS broadband albedo) that are used for NB/BB conversion coefficients between June 2005 and April 2006 (Figure 30). The bias for the visible broadband albedo still exhibits large values. But it turned to negative instead of being positive. Note that an absolute bias around 1% is present for the two conversion sets (Figure 26). It is comparable with the offset value of the linear regression (0.0093 according to van Leeuwen and –0.0094 for testing case). Thus, it exists potentially a gain of bias reduction in adopting a method constraining the offset value to be null.
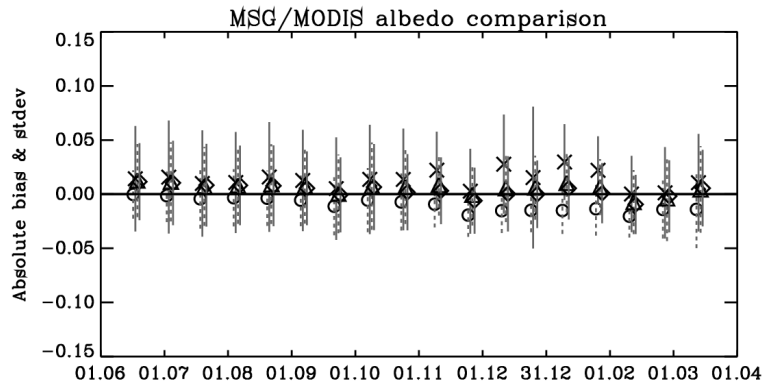
Figure 30: Temporal evolution (20050601-20060401) of the bias and standard deviation between Land-SAF and MODIS broadband albedo results over Europe. The Land-SAF broadband albedos are calculated using new coefficients for NB/BB conversion. The one-sided length of the vertical bars indicates the standard deviation. Rhombus: Total shortwave bi-hemispherical. Triangle: Total shortwave directional-hemispherical. Cross: Near Infrared directional-hemispherical. Circle: Visible directional-hemispherical.

b./ Snow-covered pixels

For snow pixels, the last version V6.1 of the code now uses a specific NB/BB conversion. The spectral properties of snow differ of spectral properties of the soil and vegetation covers, in particular because channel 1.6 of MSG is a strong absorption band for snow. Conversion coefficients for the snow pixels are:

AL_BB-DH = 0.0175+0.3890*C1+0.3989*C2-0.0141*C3

AL_VI-DH = 0.0155+0.7536*C1+0.2596*C2-0.5349*C3

AL_NI-DH = 0.0189+0.0942*C1+0.5090*C2+0.4413*C3.

Figure 31 illustrates the monthly albedo for January 2006 on Alpine Arc area. Figure 32 describes the impact of this new set of coefficients for the different kinds of albedos on this area. Albedos were usually underestimated with, however, an opposite trend for low values of visible directional-hemispherical albedo. This is probably an artefact caused by the high offset value 0.0155 (according to this new conversion coefficients) compared to 0.0093 (for the NB/BB visible conversion).

The occurrence of a snow pixels is indicated by a flag (Bit 5), which is inherited from the snow covered flag provided in the NWC-CMa product. More information can be found in PUM document (section 3.4).
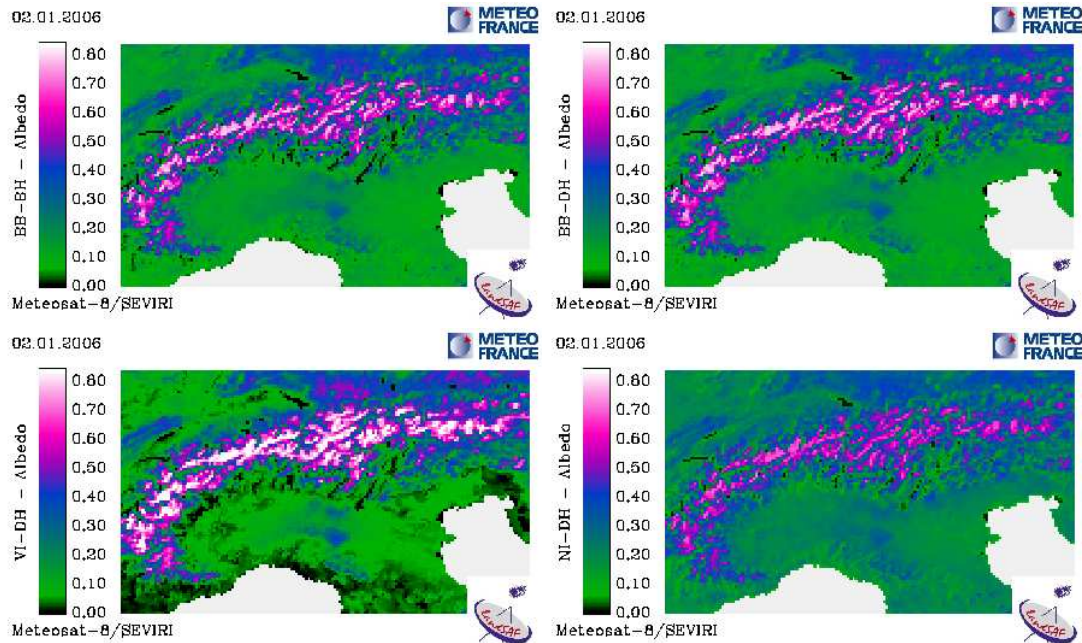
47

Figure 31: Broadband monthly albedo product images for January 2006 on Alpine Arc area. Top Left: Total short-wave bi-hemispherical. Top Right: Total shortwave directional-hemispherical. Bottom Left: Visible directional-hemispherical. Bottom Right: Near Infrared directional-hemispherical.
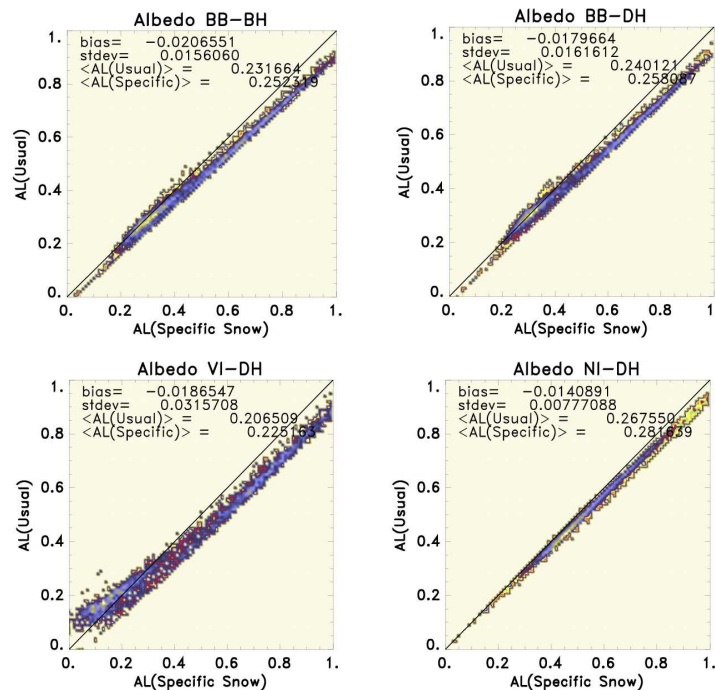

Figure 32: Scatter plots between broadband monthly albedo using the usual NB/BB conversion and broadband monthly albedo using a specific NB/BB conversion for snow pixels – for January 2006. Top Left: Total short-wave bi-hemispherical. Top Right: Total shortwave directional-hemispherical. Bottom Left: Visible directional-hemispherical. Bottom Right: Near Infrared directional-hemispherical.

2.4.2.3   Statistics for reprocessed outputs

Land-SAF products considered now are outputs from a local reprocessing using the last version of the code (version 6.1.4 of AL1 code and version 6.0 of AL2 code). Consequently, the statistics are calculated from homogeneous set of data. This last version of the code contains improvements like the residual cloud decontamination or a specific NB/BB conversion for snow-flagged pixels (cf. section 2.4.2.2).

As in section 1.4.3.1, the bias and standard deviation between the Land-SAF and MODIS broadband albedo estimates have been calculated for a series of MODIS periods between June 2005 and October 2006. The results in absolute units are shown in Figure 33. Differences between MODIS and Land-SAF albedos are lower than in Figure 25, especially during wintertime. The reason seems then an improvement of the residual cloud decontamination (ref section 1.4.2).
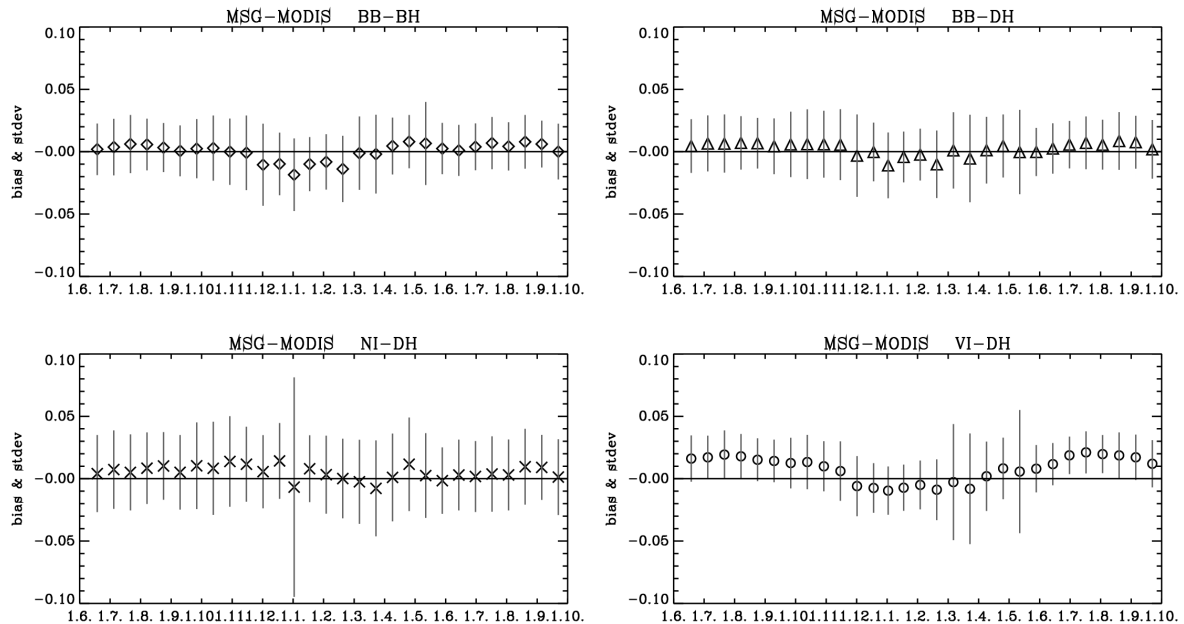

Figure 33: Temporal evolution (20050601-20060930) of the bias and standard deviation between Land-SAF reprocessed and MODIS broadband albedo results over Europe. The one-sided length of the vertical bars indicates the standard deviation. Top Left (rhombus): Total shortwave bi-hemispherical. Top Right (triangle): Total shortwave directional-hemispherical. Bottom Left (cross): Near Infrared directional-hemispherical. Bottom Right (circle): Visible directional-hemispherical.

2.4.3   Using MODIS BRDF model

In this section, Land-SAF albedo is calculated with the BRDF model of LiRoss, the one for MODIS. Deviations are slightly reduced between SEVIRI and MODIS (Figure 34). Hence, it is likely that previously annotated discrepancies between the two albedo products could be attributed to the use of different BRDF models. Nonetheless, no conclusion can be raised about the respective model performances.
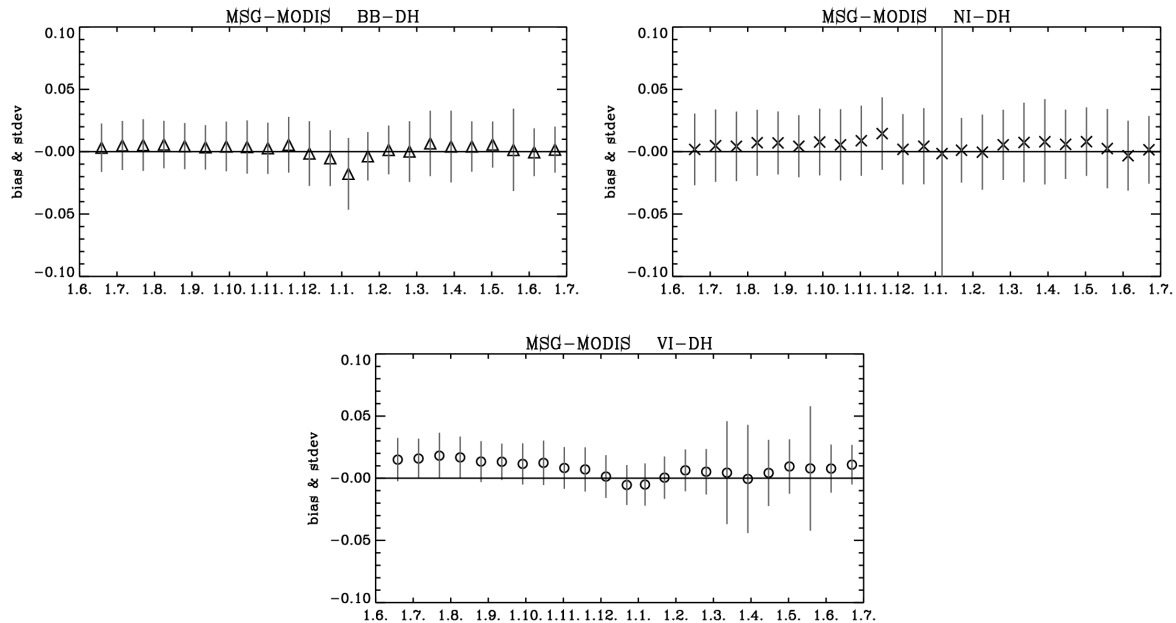

Figure 34: Temporal evolution (20050601-20060930) of the bias and standard deviation between Land-SAF reprocessed with Li-Ross BRDF model and MODIS broadband albedo results over Europe. The one-sided length of the vertical bars indicates the standard deviation. Top Left (rhombus): Total shortwave bi-hemispherical. Top Right (triangle): Total shortwave directional-hemspherical. Bottom Left (cross): Near Infrared directional-hemspherical. Bottom Right (circle): Visible directional-hemspherical.

2.4.4   Dependence on Surface Type

The statistical quantities were also investigated as a function of the surface type based on a re-projected on the SEVIRI grid of the GLC2000 land cover classification. As a remind, the generation of the albedo product itself relies entirely on the satellite observations and no a priori database is used. In order to avoid heterogeneity and geo-location problems, only those pixels are considered whose neighbours belong to the same class and which respect a certain purity criterion. Figure 35 shows the results obtained for four land cover classes based on the data period from June 10 to June 25.
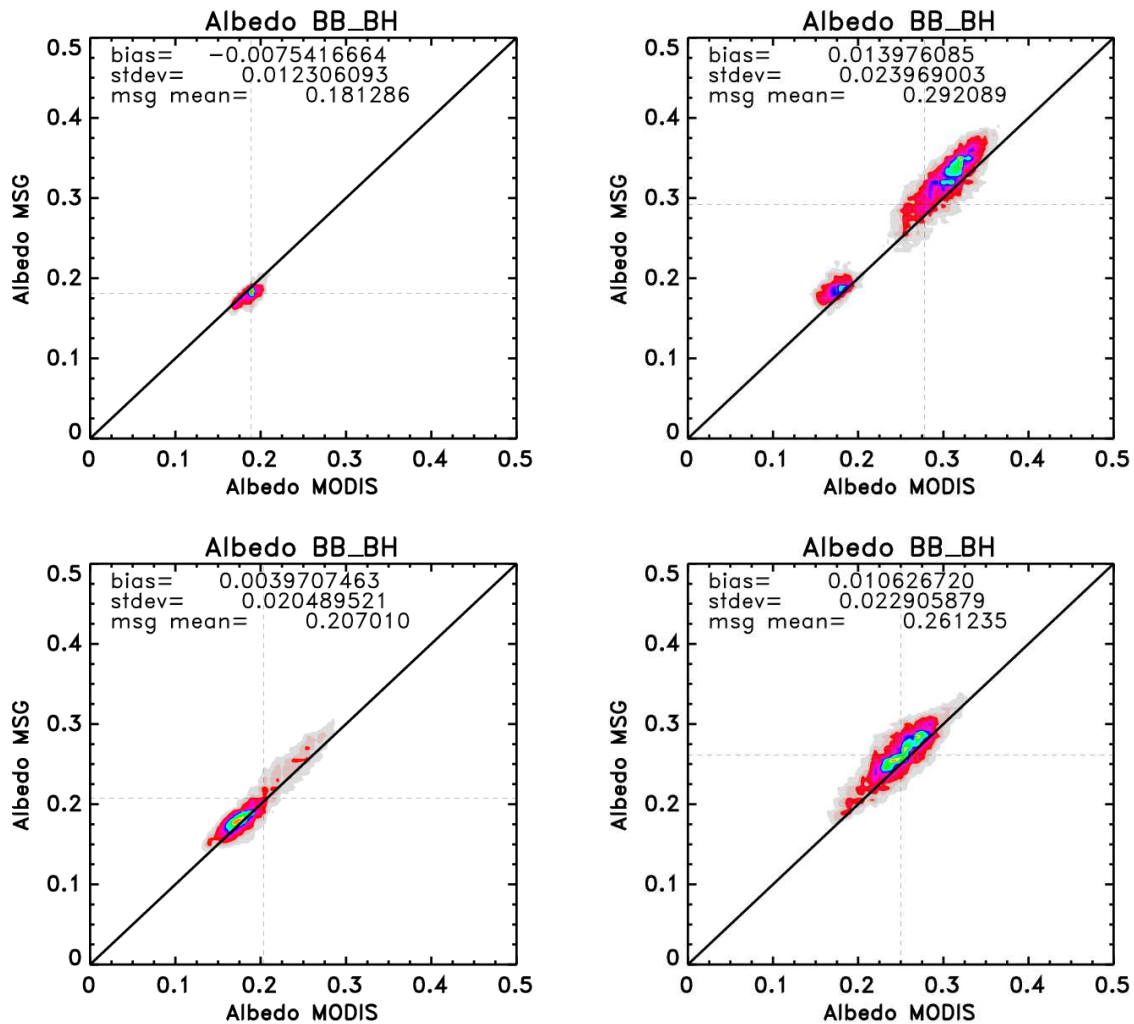
Figure 35: Scatter plots between the Land-SAF and MODIS broadband albedo results for different land cover classes. Top Left: Herbaceous Cover. Top Right: Sparse herbaceous or sparse shrub cover. Bottom Left: Cultivated and managed areas. Bottom Right: Bare areas.

2.5   Comparison with the POLDER Albedo Product

As for MODIS, an exercise of inter-comparison has been performed with POLDER for the same period of time, that is between April and September 2010. The specific design of POLDER makes suitable to sample the BRDF and is first class sensor for delivering an albedo product. This product is disseminated on days 5, 15 and 25 of each month and the procedure is quite similar to MTAL. Therefore, the comparisons is limited here to MTAL.
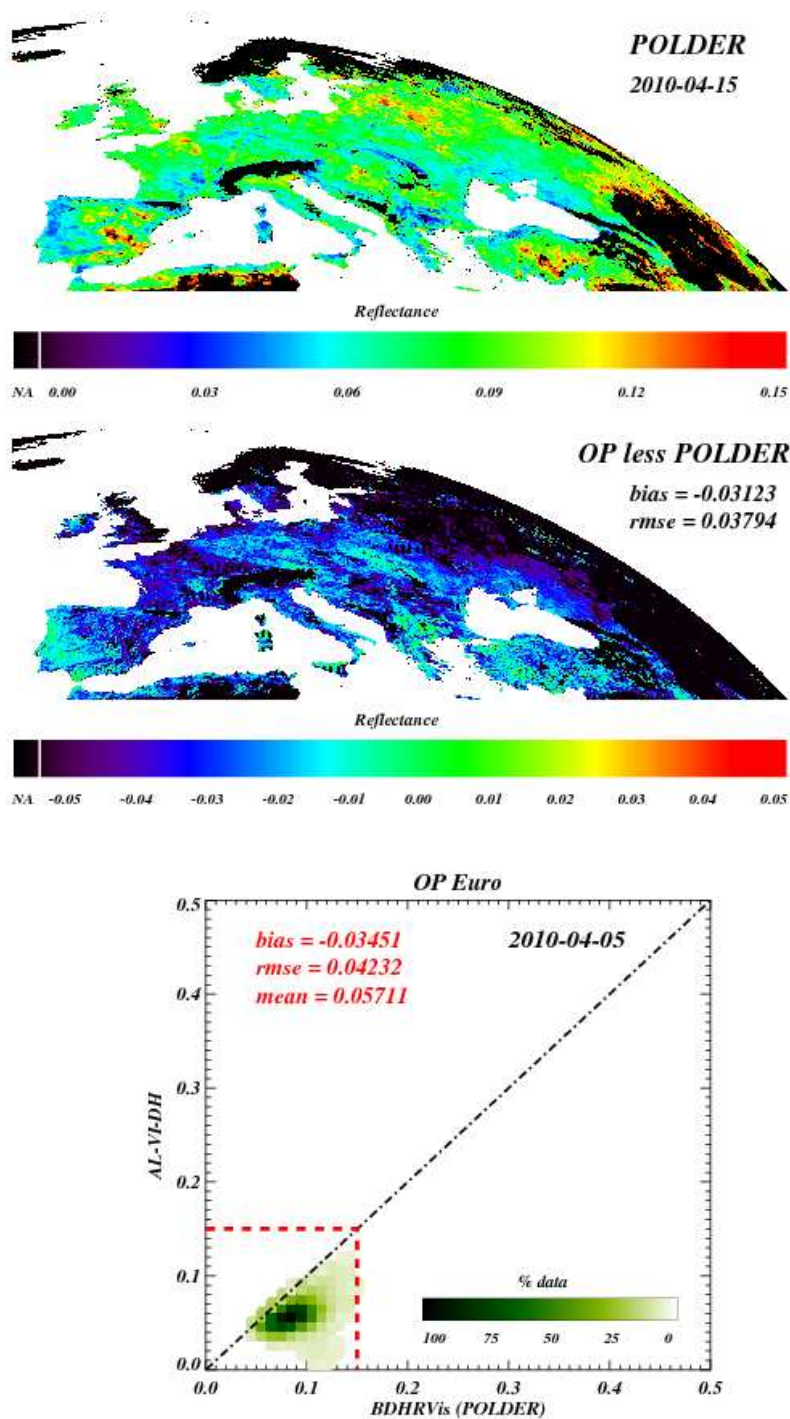
The EUMETSAT
Network of
Satellite Application
Facilities

LSA SAF
Land Surface Analysis

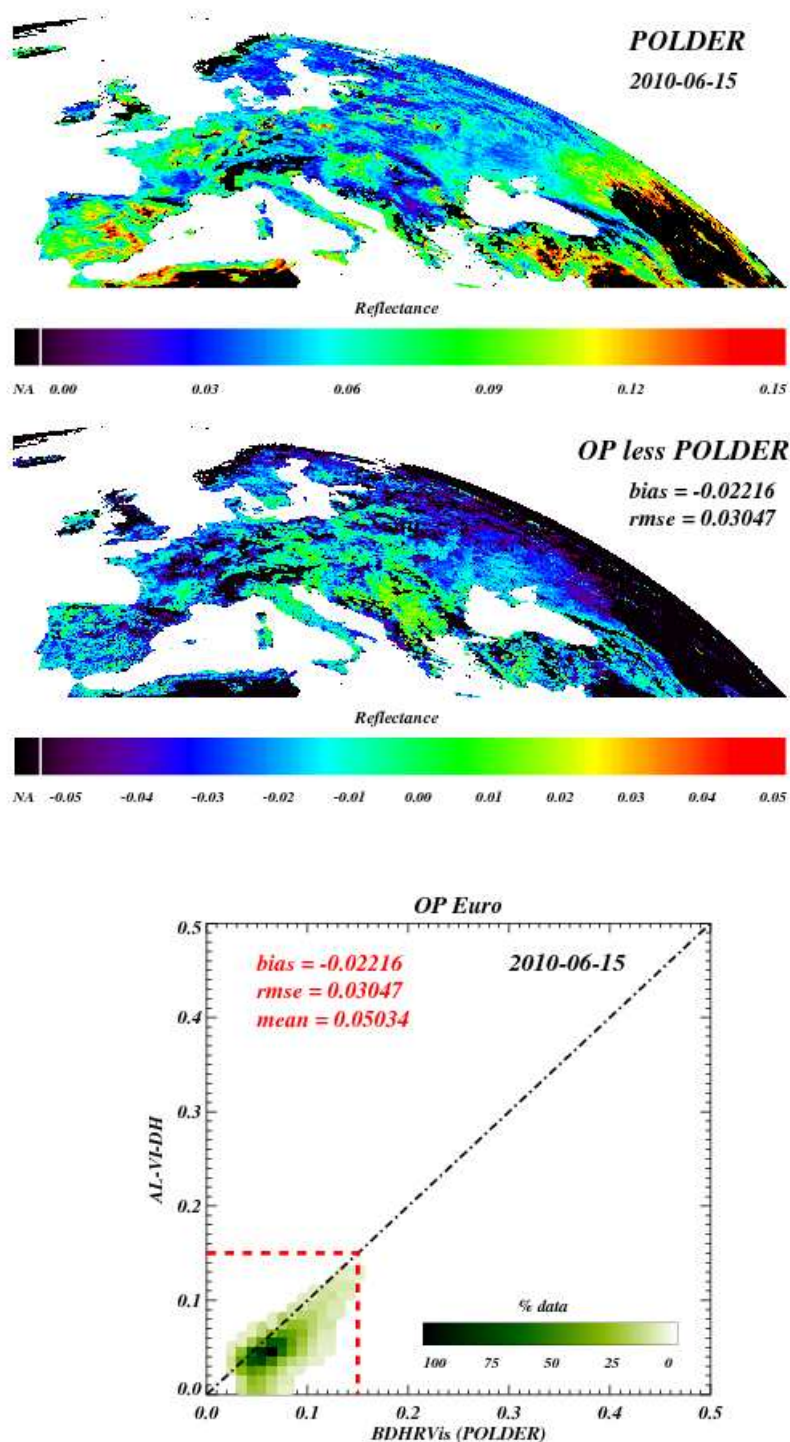**Figure 36: Comparison between MTAL (AL-VI-DH) and POLDER VIS on April 15, 2010.**

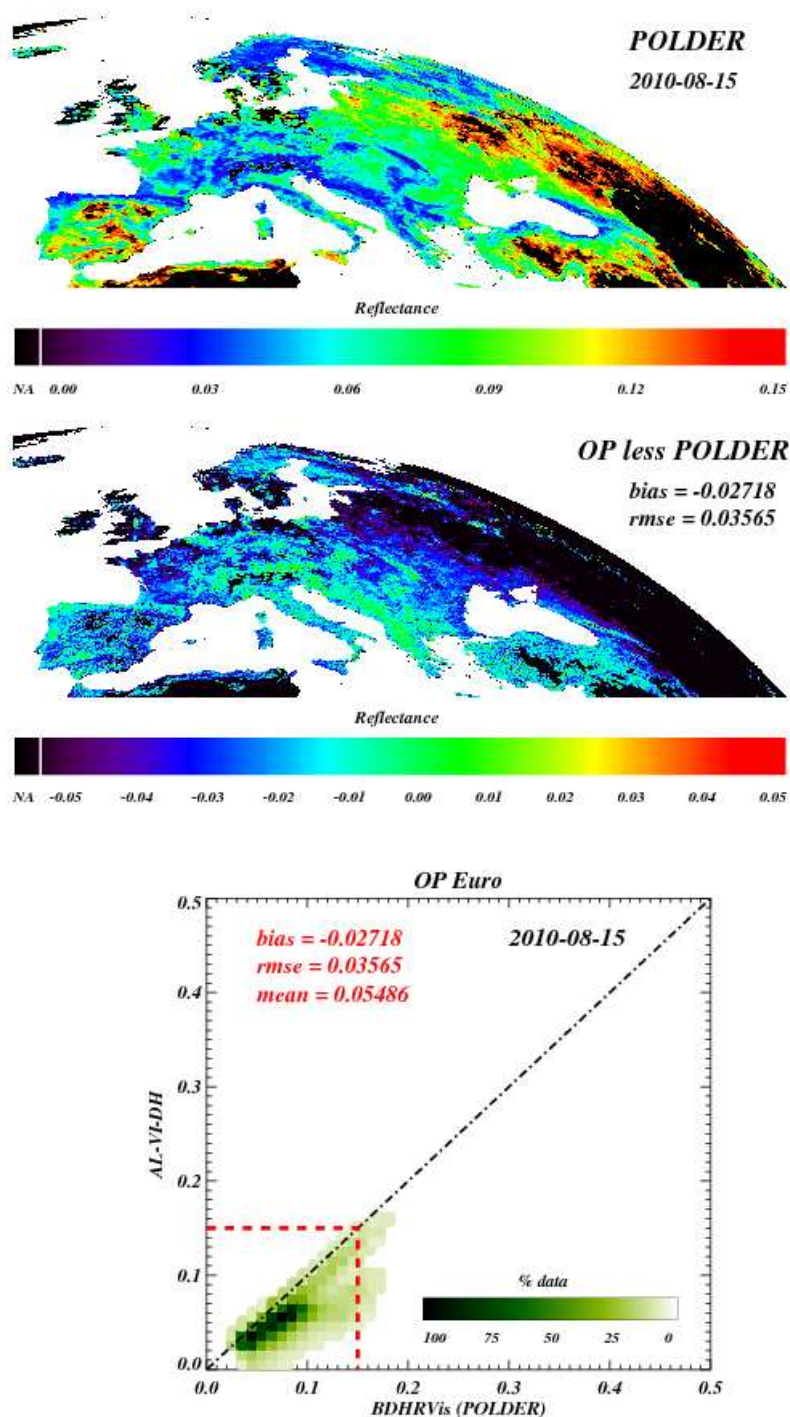**Figure 37: Comparison between MTAL (AL-VI-DH) and POLDER VIS on June 15, 2010.**

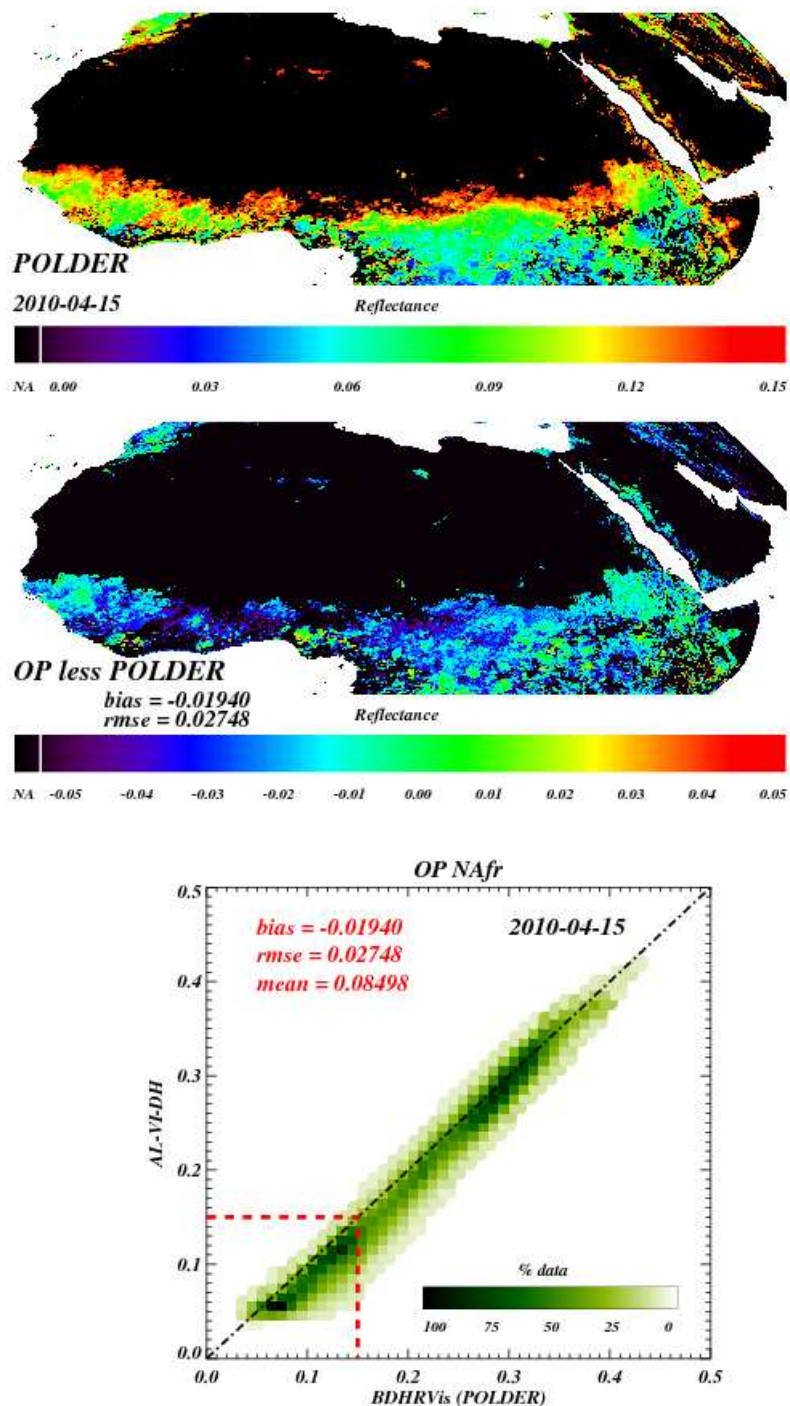**Figure 38: Comparison between MTAL (AL-VI-DH) and POLDER VIS on August 15, 2010.**

Figure 39: Comparison between MTAL (AL-VI-DH < 0.15) and POLDER VIS on April 15, 2010.
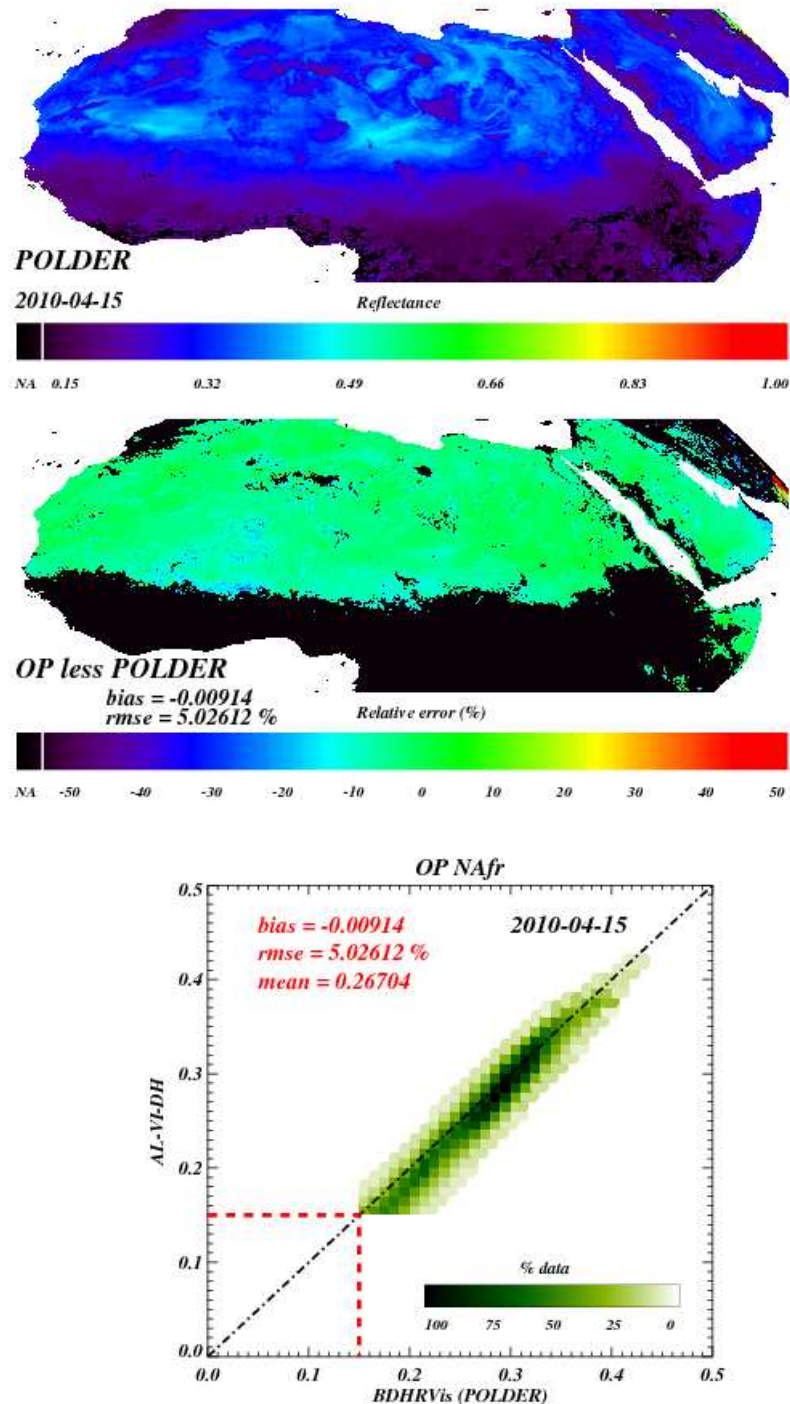
Figure 40: Comparison between MTAL (<u>AL-VI-DH > 0.15</u>) and POLDER VIS on April 15, 2010.
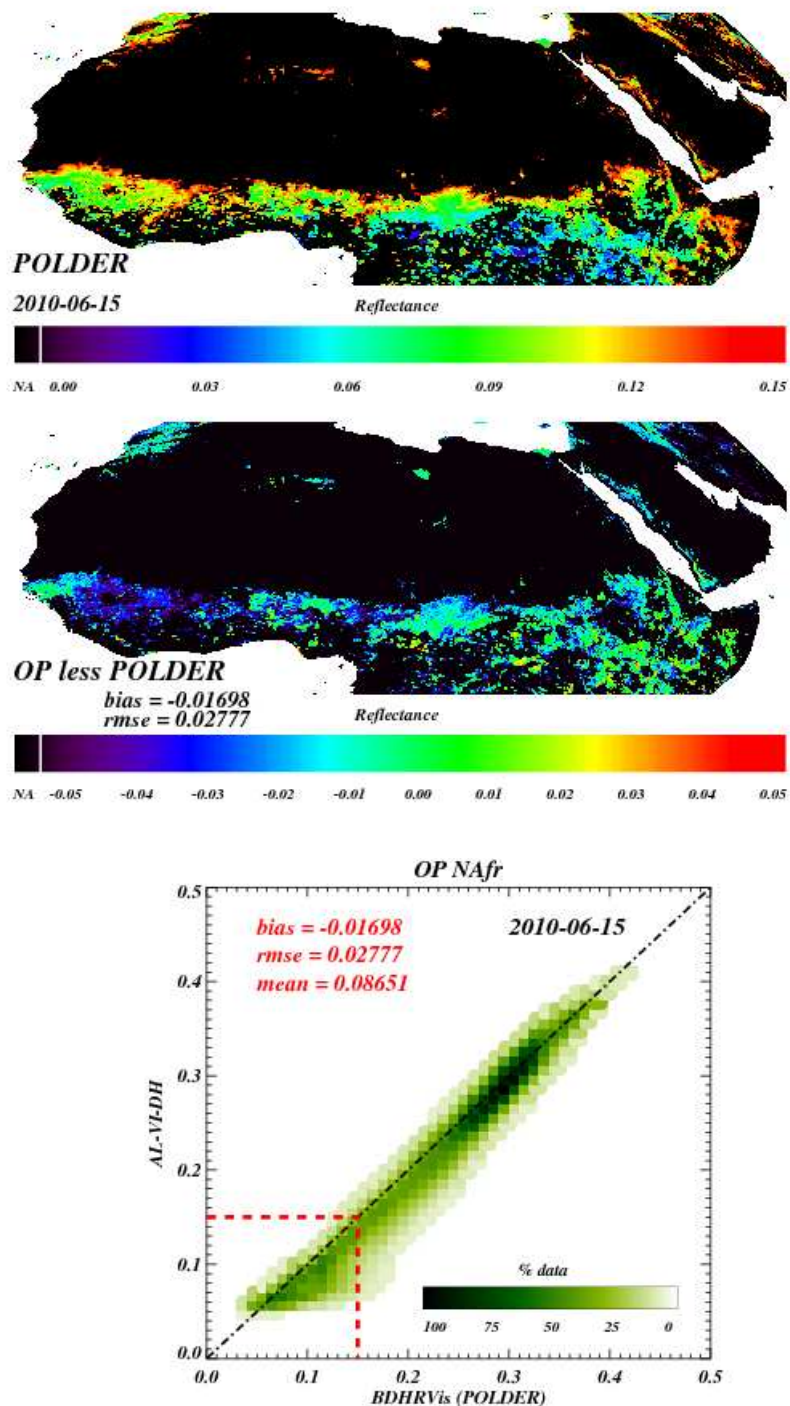
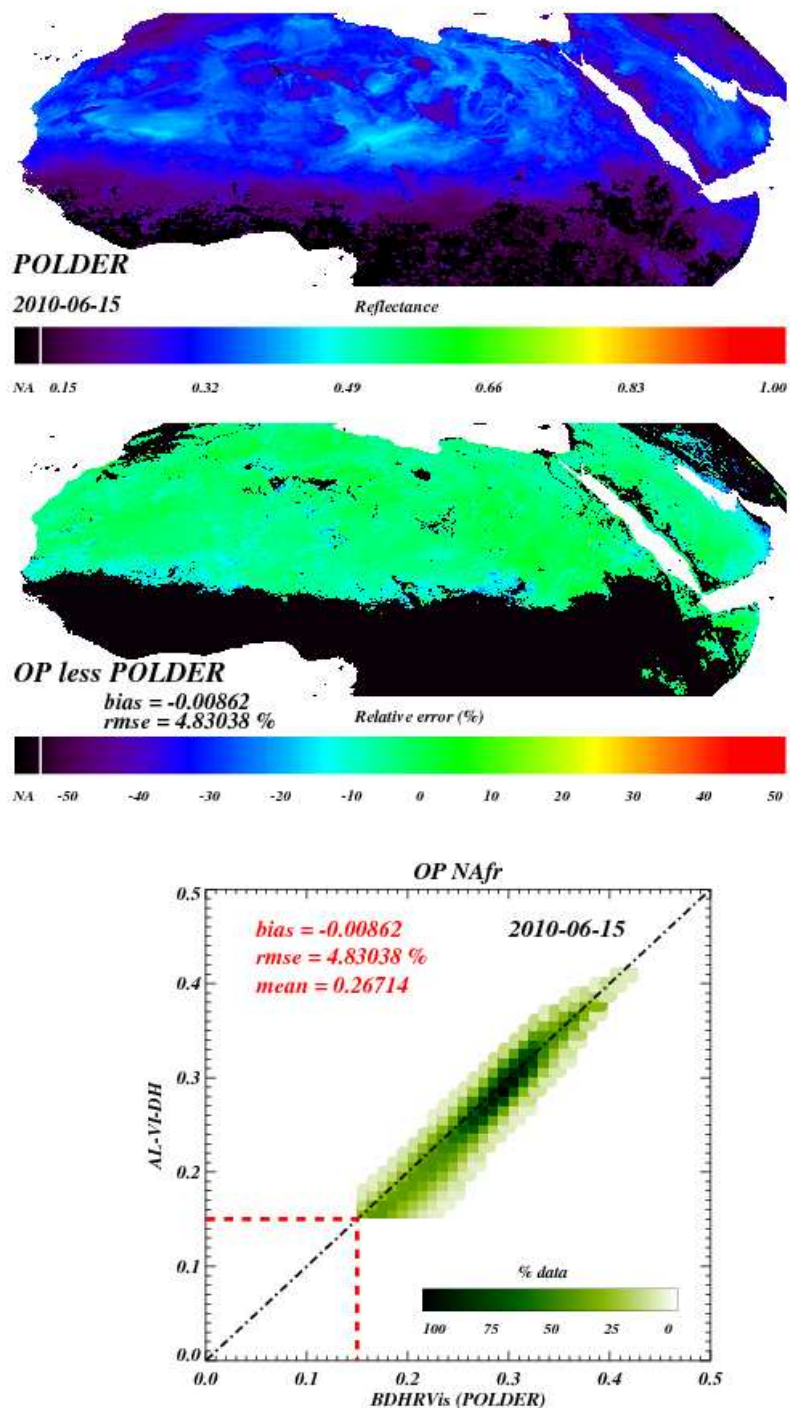**Figure 41: Comparison between MTAL (<u>AL-VI-DH < 0.15</u>) and POLDER VIS on June 15, 2010.**

Figure 42: Comparison between MTAL (AL-VI-DH > 0.15) and POLDER VIS on June 15, 2010.
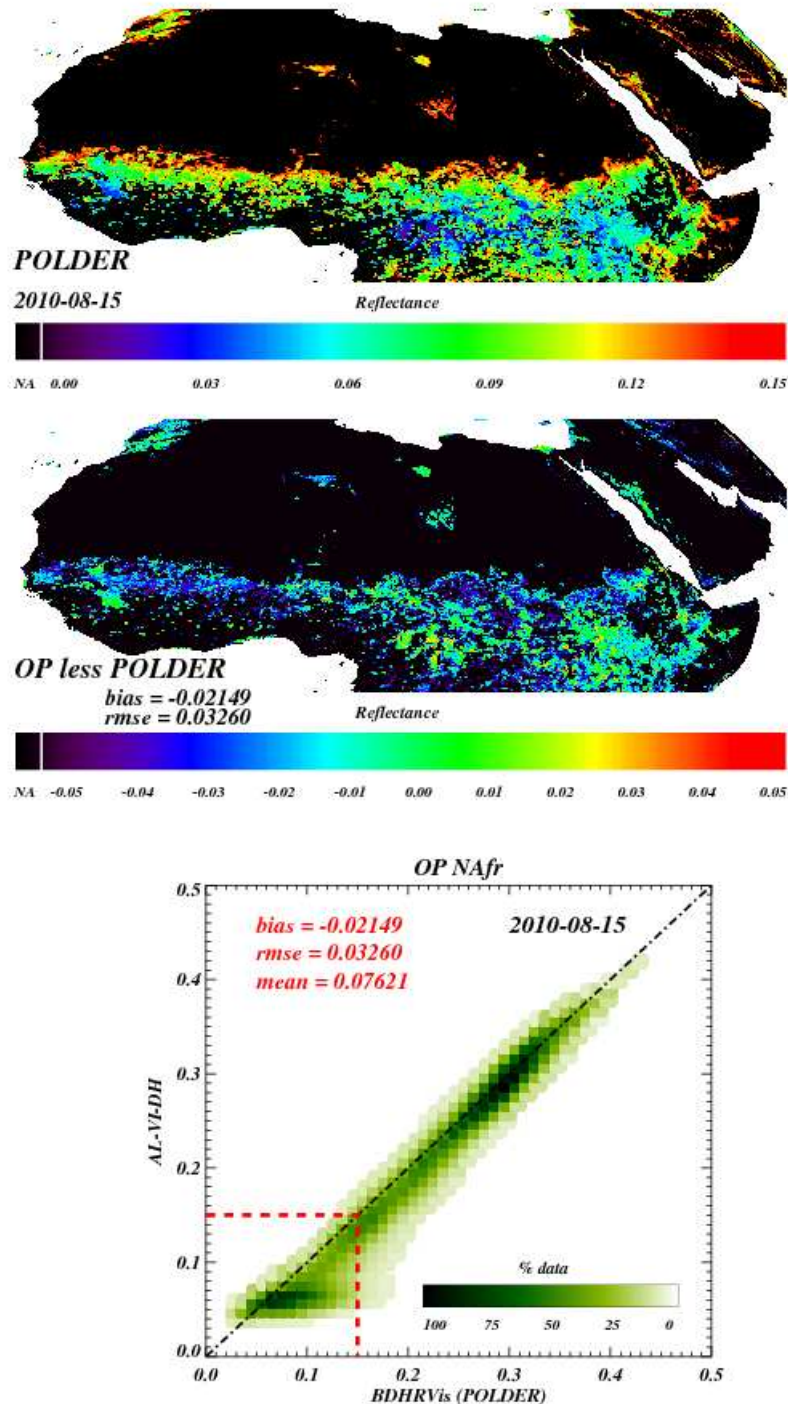
Figure 43: Comparison between MTAL (AL-VI-DH < 0.15) and POLDER VIS on August 15, 2010.

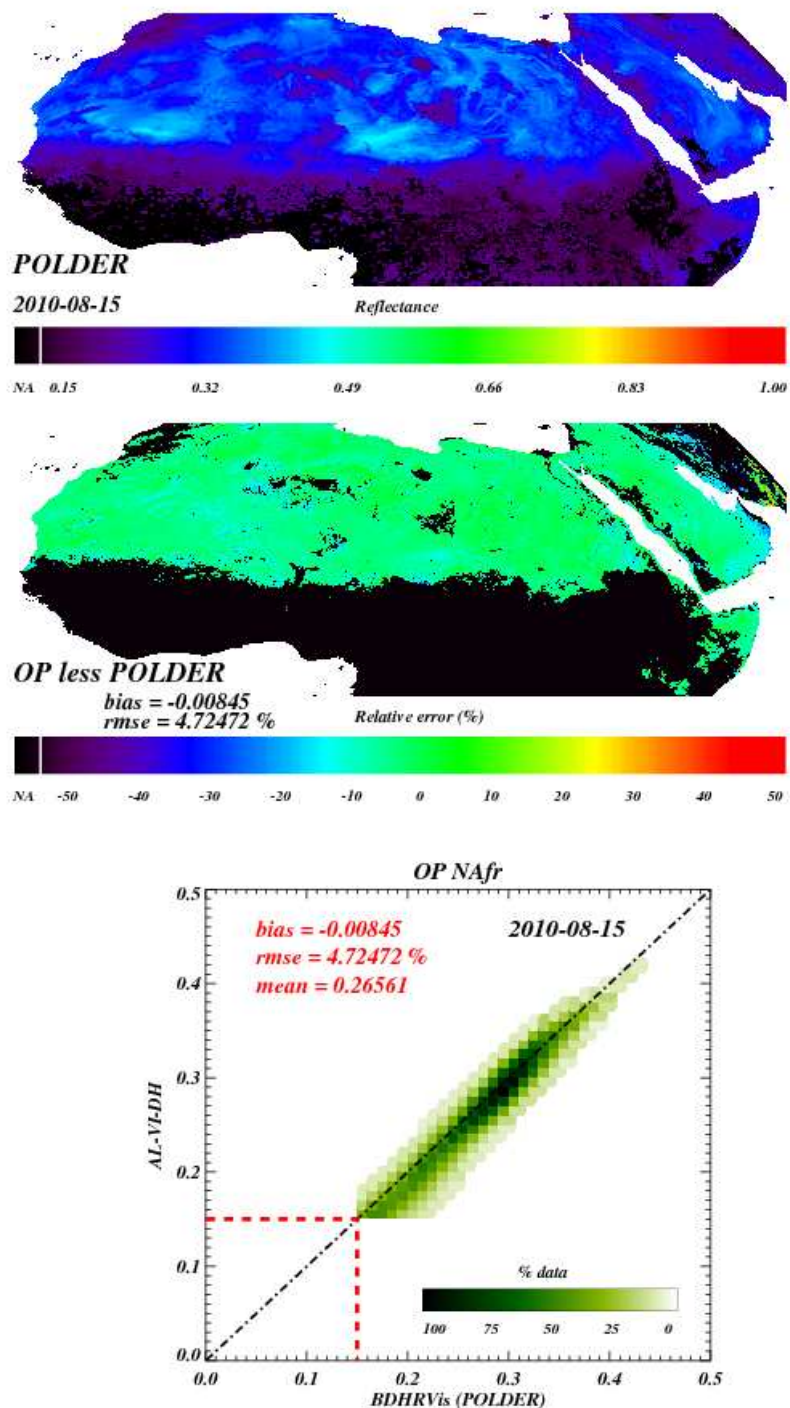**Figure 44: Comparison between MTAL (<u>AL-VI-DH >0.15</u>) and POLDER VIS on August 15, 2010.**
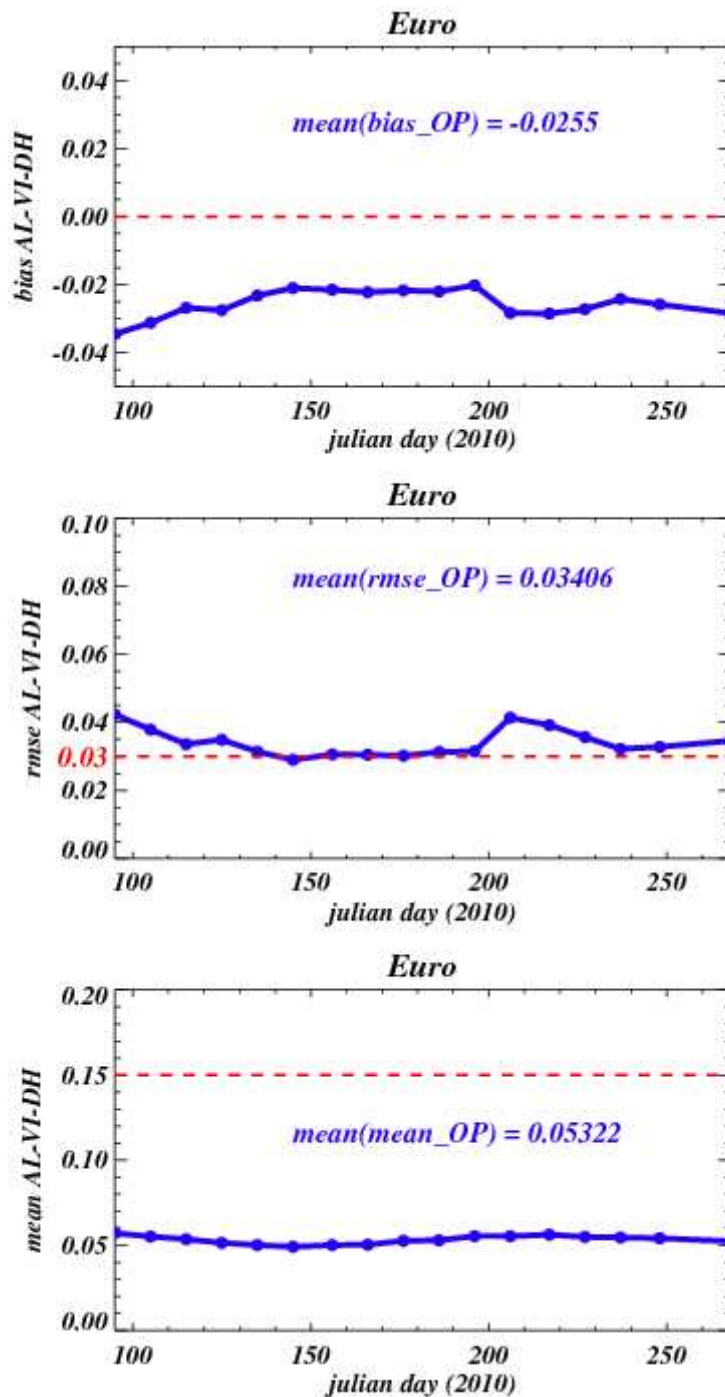
Figure 45: Times series of statistical results over the Europe area between MTAL and POLDER for AL-VI-DH < 0.15. From top to bottom: bias, rmse, and mean.

Figure 46: Times series of statistical results over the Europe area between MTAL and POLDER for AL-BB-DH < 0.15. From top to bottom: bias, rmse, and mean.
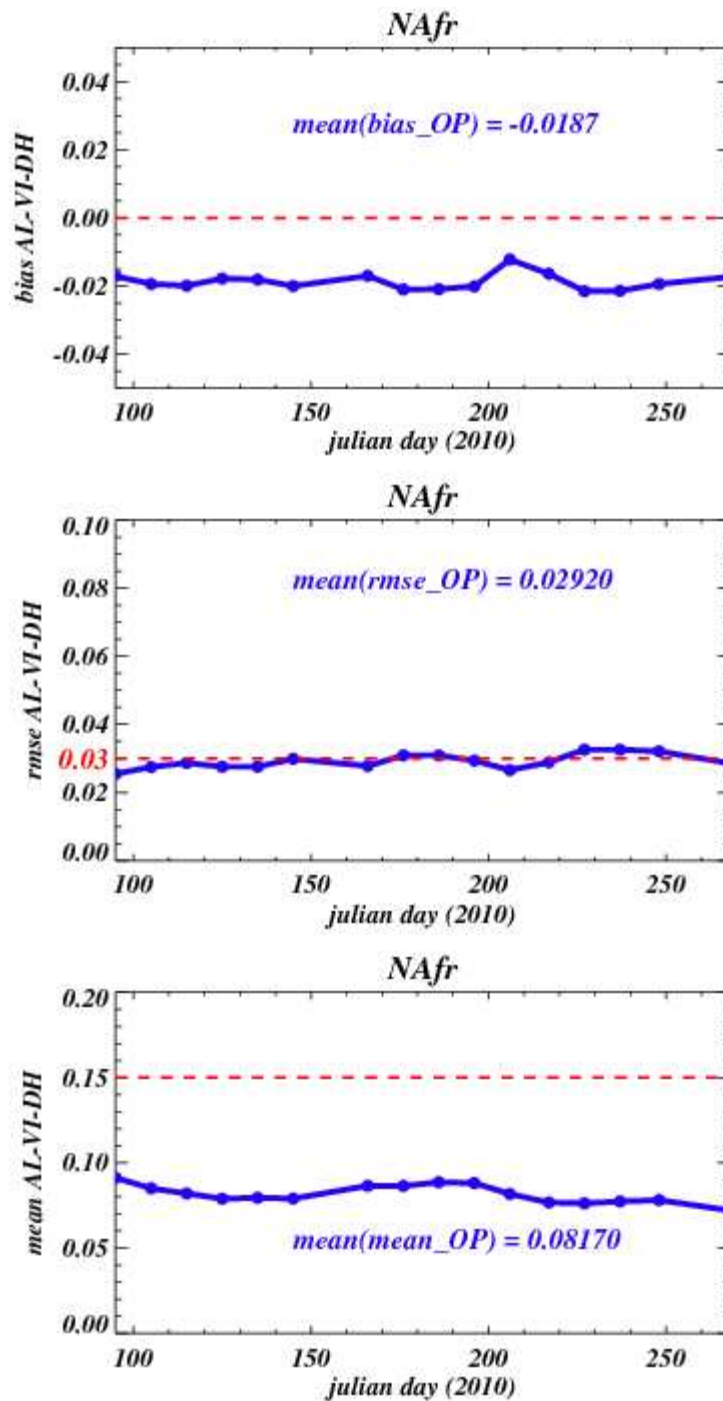
Figure 47:Times series of statistical results over the NAfr area between MTAL and POLDER for <u>AL-VI-DH < 0.15</u>. From top to bottom: bias, rmse, and mean.

Figure 48: Times series of statistical results over the NAfr area between MTAL and POLDER for AL-BB-DH < 0.15. From top to bottom: bias, rmse, and mean.

Figure 49: Times series of statistical results over the NAfr area between MTAL and POLDER for <u>AL-VI-DH > 0.15</u>. From top to bottom: bias, rmse, and mean.
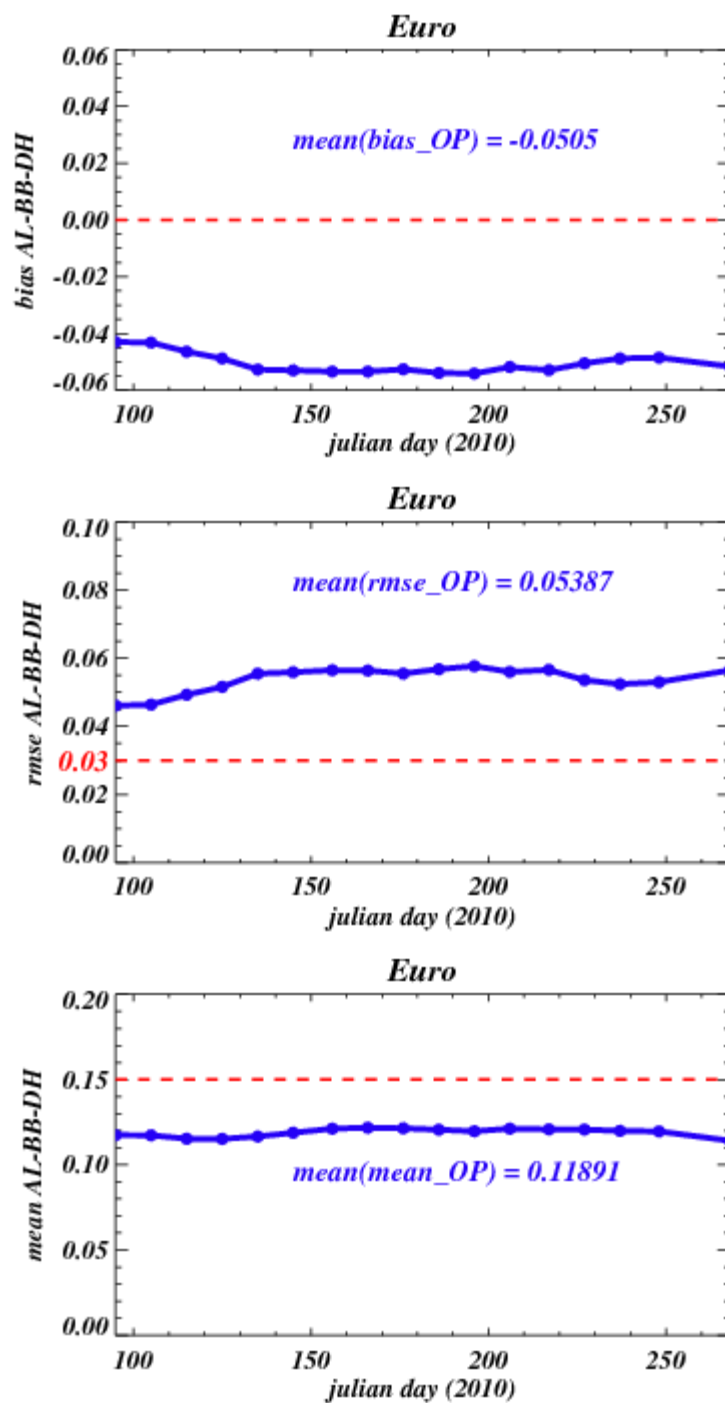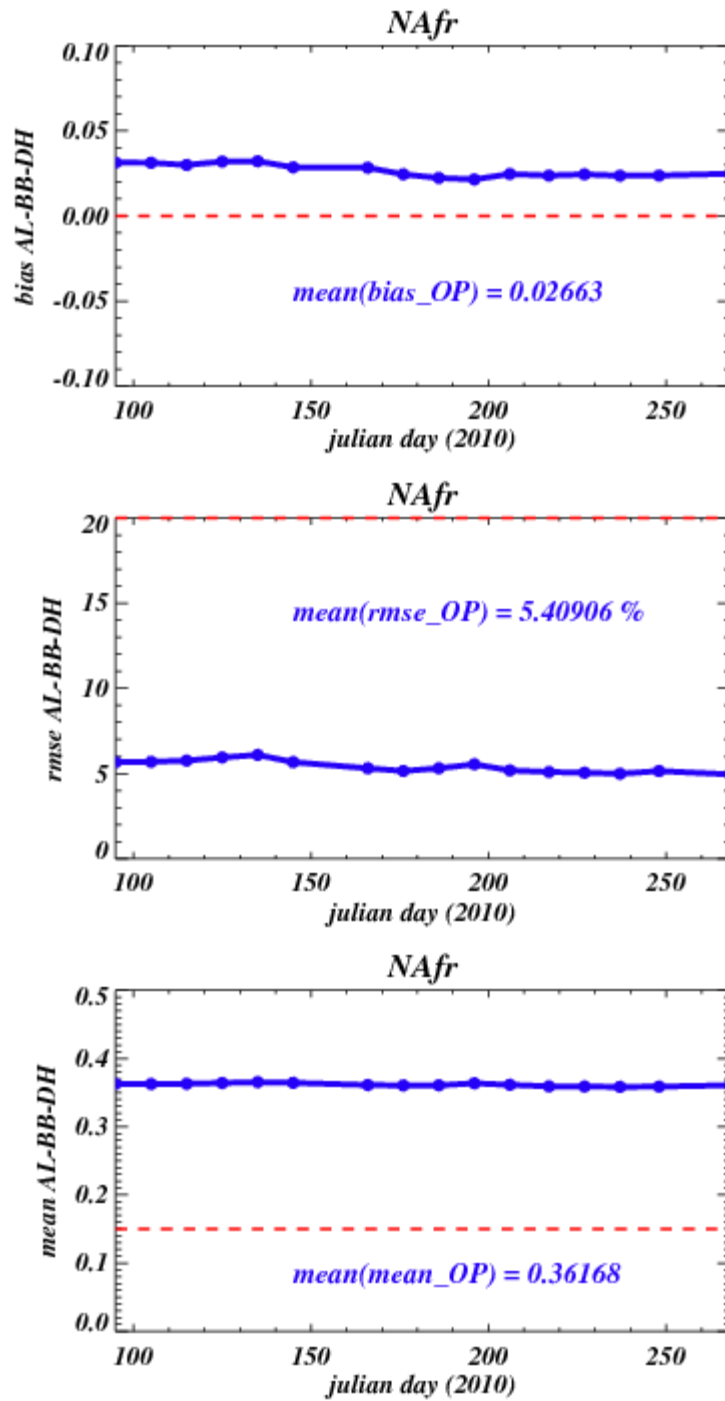
Figure 50: Times series of statistical results over the NAfr area between MTAL and POLDER for AL-BB-DH > 0.15. From top to bottom: bias, rmse, and mean.
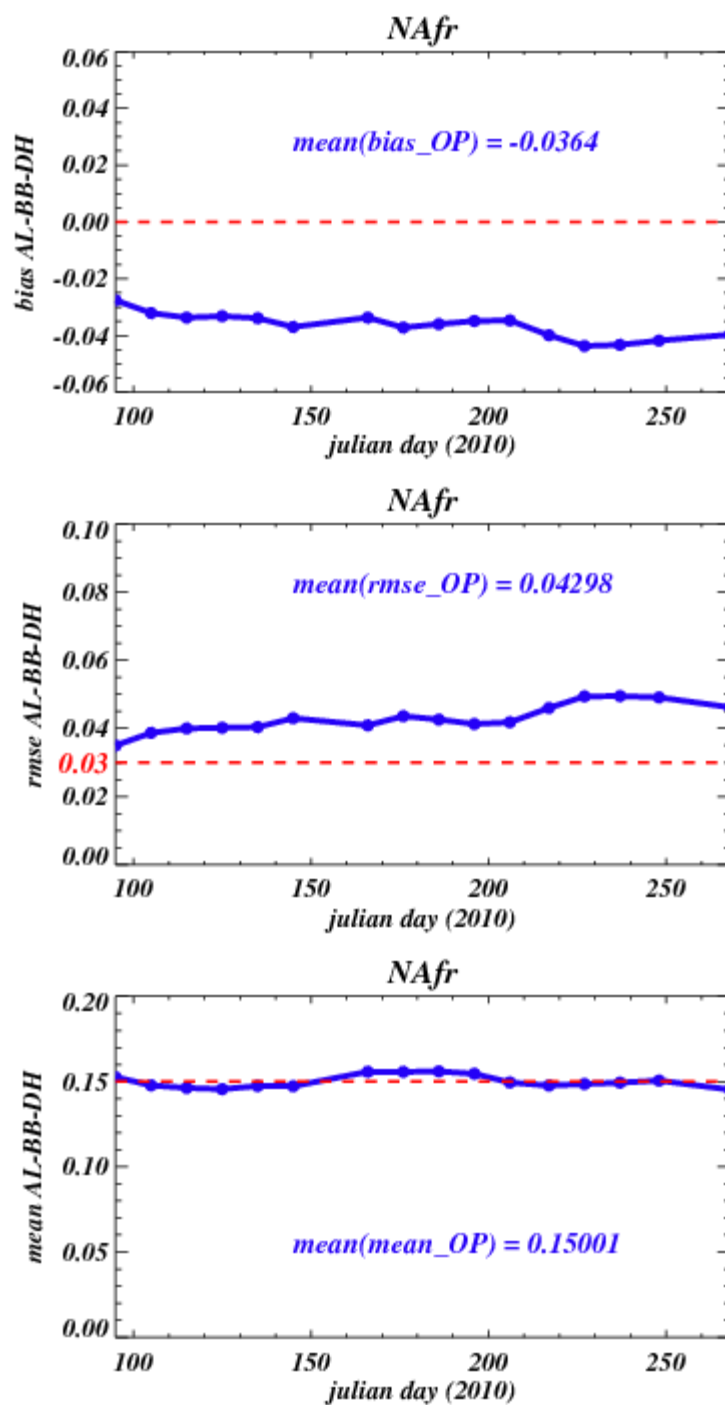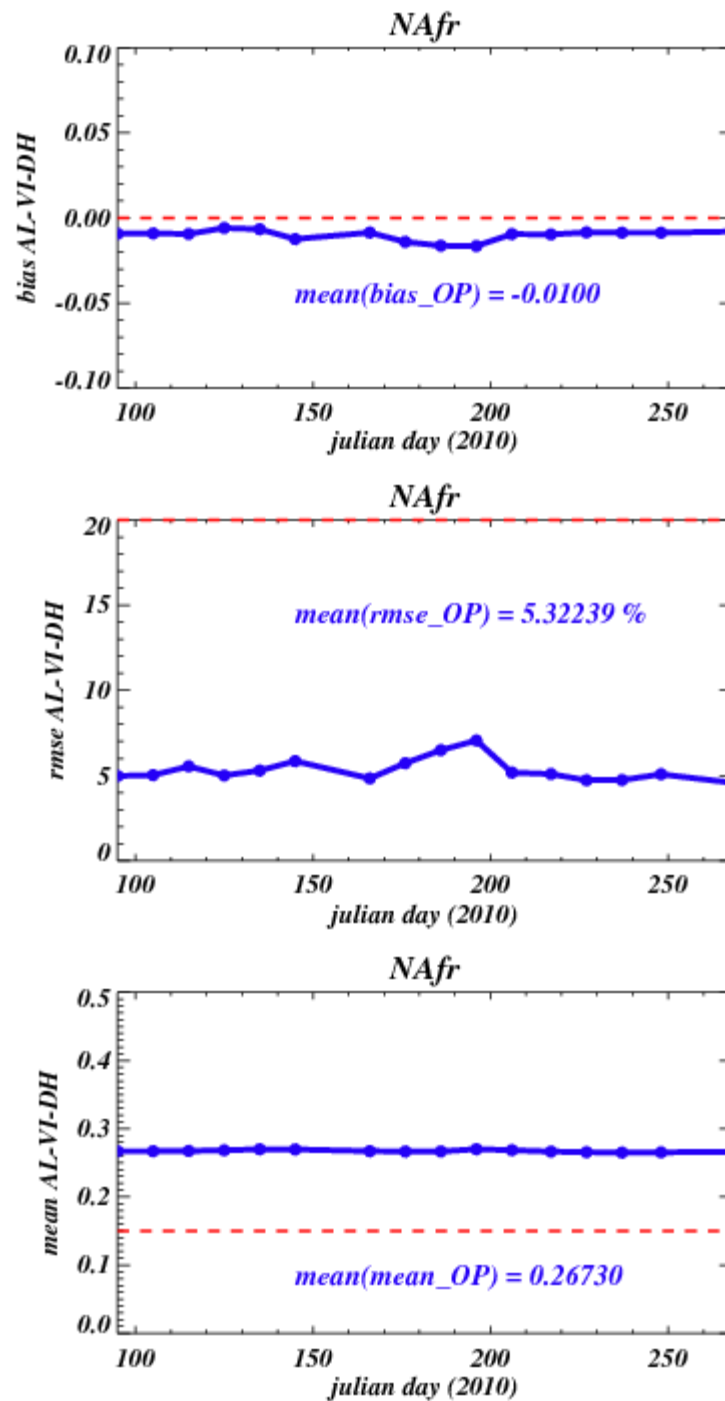
TABLE 8: BIAS AND STANDARD DEVIATION (RMSE) BETWEEN MTAL AND POLDER BROADBAND ALBEDO RESULTS FOR THE PERIOD FROM APRIL TO SEPTEMBER 2010.

AL-VI-DH < 0.15

		OP Euro	*OP NAfr*
AL-VIS-DH	*Bias*	-0.0256	-0.0187
	RMSE	**0.03417**	**0.02920**
AL-BB-DH	*Bias*	-0.0448	-0.0364
	RMSE	**0.04960**	**0.04298**
AL-BB-BH	*Bias*	-0.0428	-0.0367
	RMSE	**0.04872**	**0.04895**

TABLE 9: BIAS AND STANDARD DEVIATION (RMSE) BETWEEN MTAL AND POLDER BROADBAND ALBEDO RESULTS FOR THE PERIOD FROM APRIL TO SEPTEMBER 2010.

AL-VI-DH > 0.15

		OP Euro	*OP NAfr*
AL-VIS-DH	*Bias*	-0.0304	-0.0100
	RMSE	**11.8026 %**	**5.32302 %**
AL-BB-DH	*Bias*	-0.0056	0.02663
	RMSE	**8.05389 %**	**5.40886 %**
AL-BB-BH	*Bias*	0.00078	0.02869
	RMSE	**7.60139 %**	**5.48015 %**

2.6   Sensitivity to Aerosols

For the atmospheric correction of the observed reflectance factor values the concentration of aerosols represents the most important quantity. Although aerosols are highly variable in space and time, they are described for the time being with a very simple dependence on latitude. The aerosol information is provided to the algorithm in the form of input files containing estimates of the aerosol optical thickness at 550nm for each image pixel. The aerosol information can therefore easily be updated by replacing these files when improved climatologies or preferably when a dynamic aerosol product is becoming available.

2.6.1   Sensitivity study

This study quantifies the impact of aerosols on the quality of the albedo product. Two configurations were tested for August 30 2005 with respectively zero and 0.5 of aerosol optical thicknesses at 550nm. Figures 51 to 54 show the consequences of aerosol optical thickness uncertainties on the albedo variants. As could be expected, the impact depends on the wavelength ; it is critical for 0.6µm channel, significant for 0.8µm channel and low for 1.6µm channel.
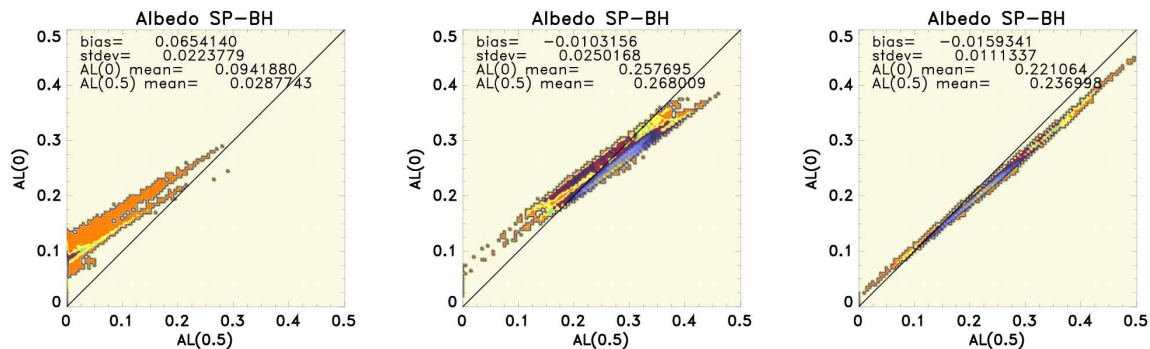

Figure 51: Comparison between spectral (bi-hemispherical) albedo products for the 30st of August 2005 with respectively zero and 0.5 of aerosol optical thicknesses at 550nm. Left: Red Channel (0.6µm). Middle : Near Infrared Channel (0.8µm). Right: Short-wave Infrared Channel (1.6µm).

Figure 52: Comparison between spectral (directional-hemispherical) albedo products for the 30st of August 2005 with respectively 0. and 0.5 of aerosol optical thicknesses at 550nm. Left: Red Channel (0.6µm). Middle : Near Infrared Channel (0.8µm). Right: Short-wave Infrared Channel (1.6µm).

Figure 53: Comparison between broadband (directional-hemispherical) albedo products for the 30st of August 2005 with respectively 0. and 0.5 of aerosol optical thicknesses at 550nm. Left: BB-DH. Middle : NI-DH. Right: VI-DH.

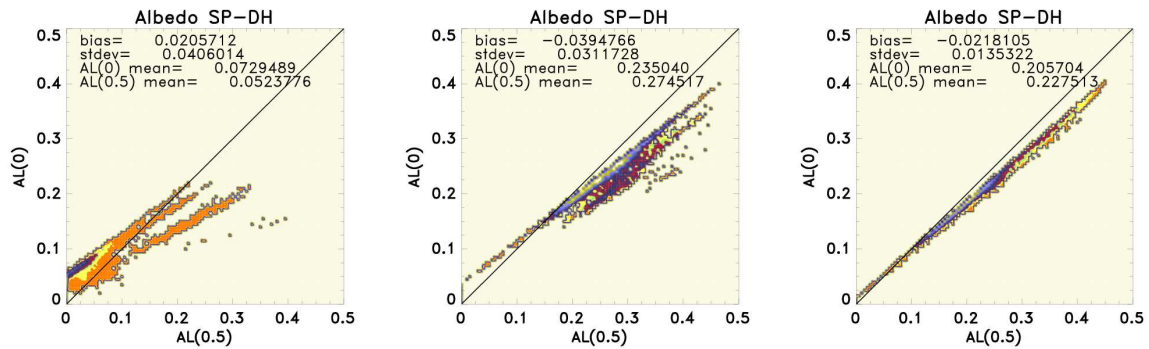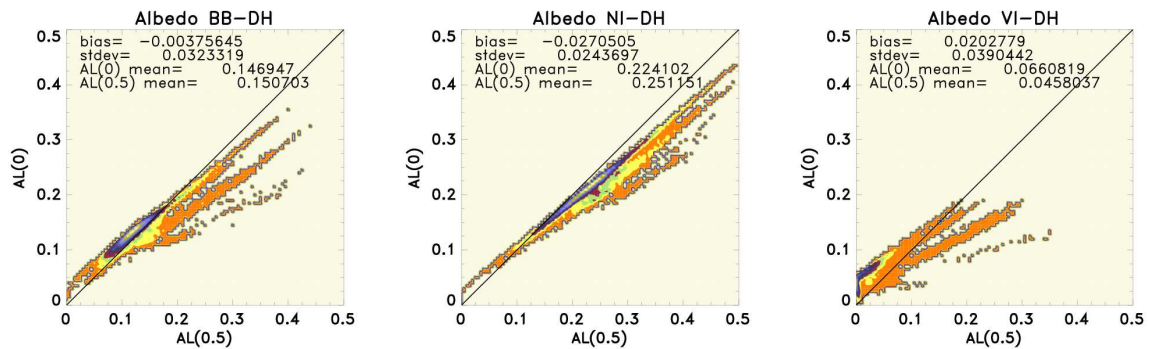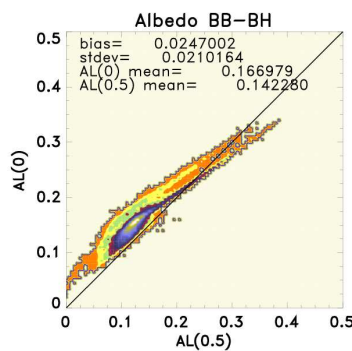**Figure 54:** Comparison between broadband (bi-hemispherical) albedo products for the 30st of August 2005 with respectively 0. and 0.5 of aerosol optical thicknesses at 550nm.

Ref. SAF/LAND/MF/VR_AL/II_2012
Issue/II_2012
Date: 15 February 2012

The EUMETSAT
Network of
Satellite Application
Facilities

LSA SAF
Land Surface Analysis

2.6.2 Observed impact of aerosols

Figure 55 shows albedo time series for two sites for which ground measurements of the aerosol optical thickness are available from the AERONET project. A correlation of the obtained surface albedo estimates with the optical thickness can be perceived, which suggests that aerosols are responsible for a part of the (spurious) temporal variability remaining in the time series. These variations tend to be smoothed out by the temporal composition scheme. However, a potential bias remains if the averaged optical thickness does not correspond to the climatologic value specified.

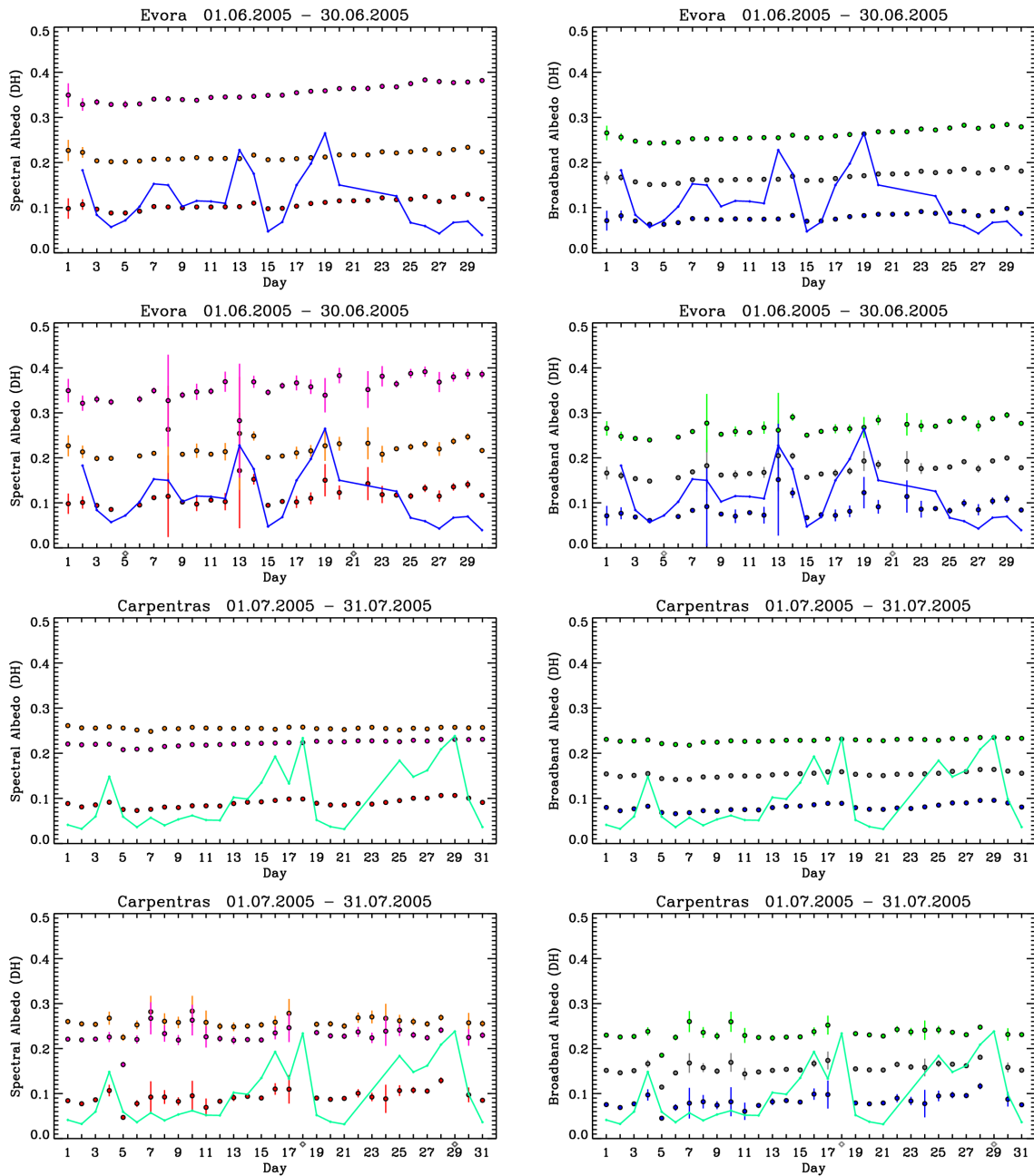**Figure 55:** Spectral (left) and broadband (right) MDAL for Evora in June 2005 and Carpentras in July 2005 reprocessed with algorithm version AL2 v5.1. The solid lines in the graphs show daily averaged Aeronet measurements of the aerosol optical thickness at 440nm (Evora) and 500nm (Carpentras). The results are shown with (top) and without (bottom) iterative temporal composition of the daily estimates.

2.7 Comparison with In-Situ Measurements

Recent in-situ data including measurements of the down- and up-welling short-wave radiation are available for the BSRN-station of Toravere (Estonia) and for a site located at Agoufou (Mali) from the AMMA project. Figure 56 depicts examples of the time series obtained at the Toravere station during clear and cloudy days. On clear days the direct down-welling flux dominates and the illumination conditions approximate the conditions required in the definition of the directional-hemispherical albedo. In this case the in-situ albedo at local solar noon may be compared with the directional-hemispherical total short-wave broadband albedo product. For cloudy days the diffuse illumination conditions may rather resemble those of the bi-hemispherical albedo variant. For the comparison we therefore consider different averaging periods of the in-situ albedo measurements depending on a simple criterion for distinguishing clear and cloudy days. For clear days an interval of one hour centred at local solar noon is taken, whereas for cloudy days the whole diurnal series is considered (with a cut-off at a solar zenith angle of 80°).
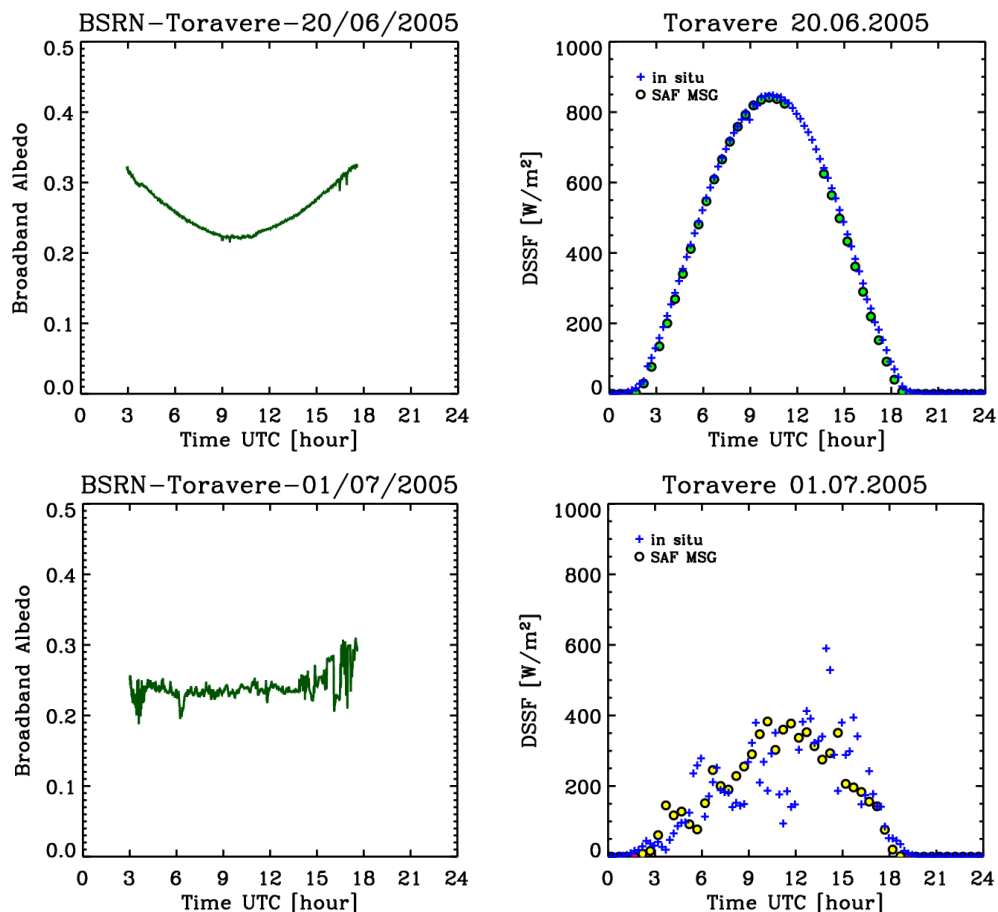

Figure 56: BSRN-measurements of albedo (left) and down-welling short-wave radiation (right) for examples of a clear (top) and a cloudy (bottom) day at Toravere. The plots on the right also include the Land-SAF down-welling short-wave radiation estimates.

Figure 57 shows graphs for Toravere with time series spanning the period for which both Land-SAF products and ground measurements are available. Satellite estimates are lower during the first half of the period and consistent during the second half. Figure 43 shows results for AMMA sites. The apparent outlier, which can be seen for Toravere at the end of June in the bi-hemispherical albedo time series was caused by a bug related to the missing initialisation of a variable in the AL2 code. This problem occurred very rarely, but in a deterministic way. It was solved in version AL2 v5.1.
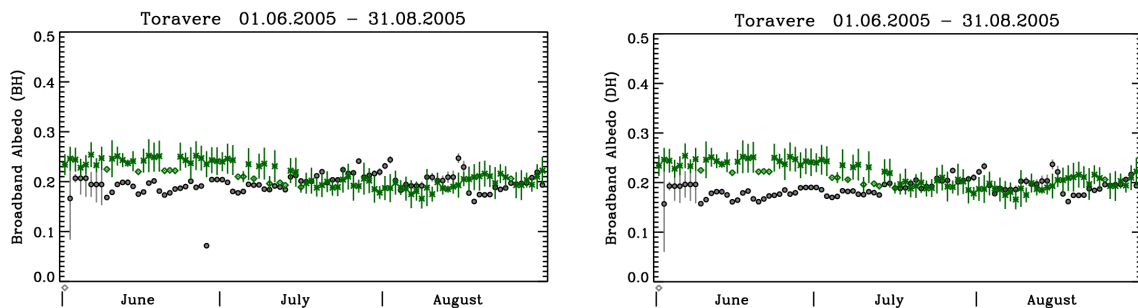

Figure 57: Comparison of the Land-SAF albedo estimates with ground measurements for Toravere, Left plot shows the Land-SAF bi-hemispherical broadband albedo results, and right plot the directional-hemispherical estimate. The ground measurement data points marked in dark green colour are the same in the two cases. Crosses indicate days classified as cloudy and the rhombuses indicate clear days. The error bars of the in-situ data points correspond to the observed standard deviation during the averaging period.

For Agoufou the Land-SAF product overestimates slightly the albedo with respect to the ground measurements during the whole period. At the end of May, a rapid decrease of LAND-SAF albedo is caused by an aerosol episode, however not evidenced by ground measurements. Further in the season, in August, the lack of available products explains by the occurrence of rainfall events. Two sites, in Banizoumbou and Niamey, were equipped from instruments of an ARM Mobile Station (Radagast project). For Banizoumbou, Land-SAF albedo is positively biased compared to ground measurements, probably because in situ sensor sampled more vegetation. As for Niamey, the matching between Land-SAF and ground-measured albedo is particularly remarkable. General information from a comparison with AMMA sites is the excellent correlation, in particular during aerosol and rainfall events (Figure 58).

However, in the light of the considerable geo-location uncertainties and the questionable representativeness of the local ground measurements for the rather large SEVIRI pixel size (especially for Toravere) the pertinence of these results remains somewhat questionable and could then probably be improved in the future.
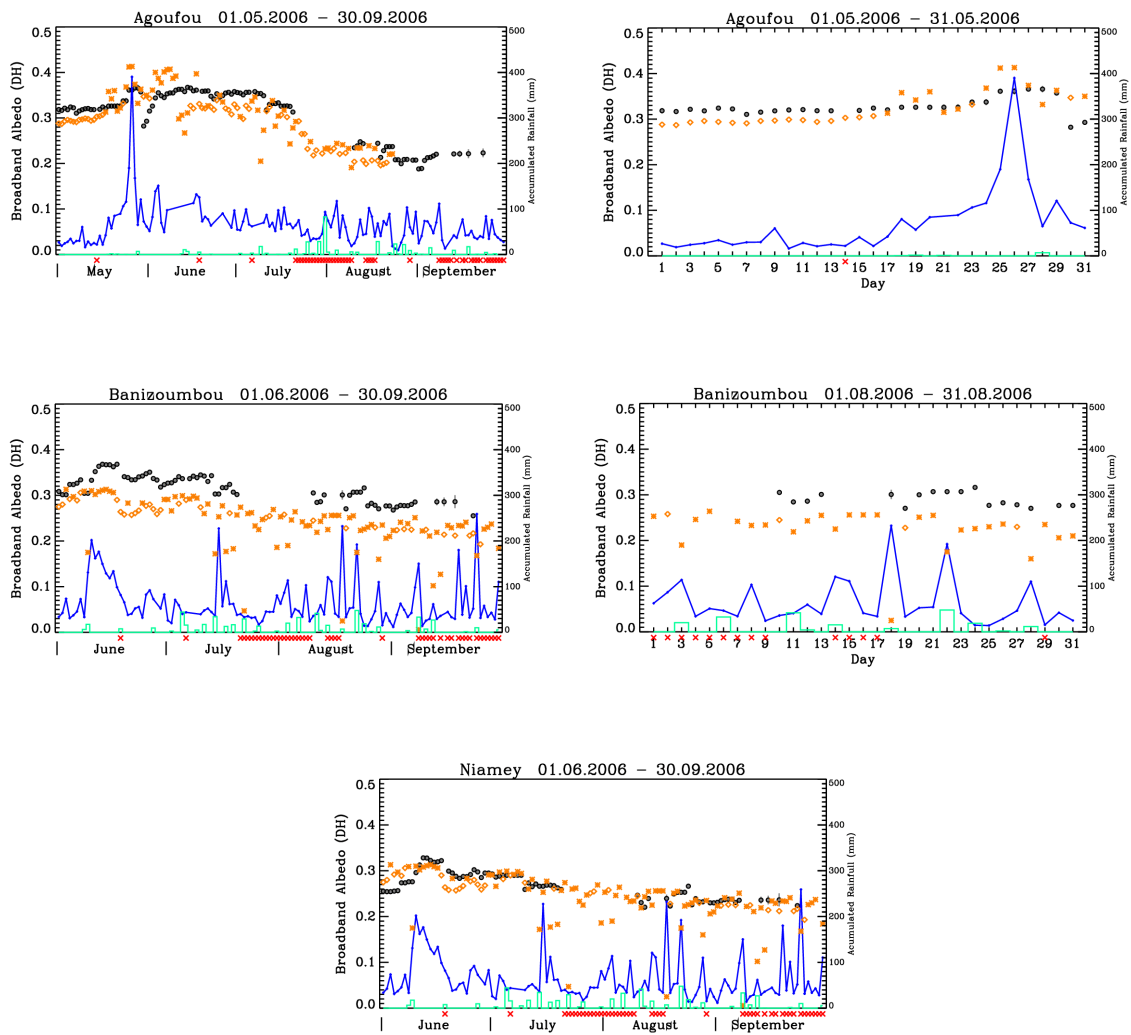
Figure 58: Comparison of the Land-SAF albedo (directional-hemispherical) estimates AMMA ground measurements. From top to bottom: Agoufou, Banizoumbou, Niamey. Ground measurement and Land SAF albedo data dots are shown in orange and black, respectively. Crosses indicate days classified as cloudy and the rhombuses indicate clear days. The error bars on the in-situ data points correspond to the observed standard deviation during the averaging period. Daily averaged aerosol optical thickness values at 440nm measured by the respective Aeronet station are included as blue lines. The numerical values shown on the y-axis need to be multiplied by 10 to obtain the correct optical thickness.). Rainfall estimates (in mm) from TRMM satellite are indicated in green colour as an histogram representation.

For the station of Carpentras (Figure 59), the distance of AL-BB-BH to MODIS is still large compared to the differences between OP and MACC MDAL products. This would suppose an over correction with MODIS. The AOD values remain relatively low for this station (less than 0.1 in general). Interestingly, it may be noticed a significant reduction of MACC AL-BB-BH at the end of April, consistently with an aerosol event evidenced by MACC in using the correct forecast. Note that the OP product is not reactive to this aerosol episode. No ground reference was available for Carpentras.
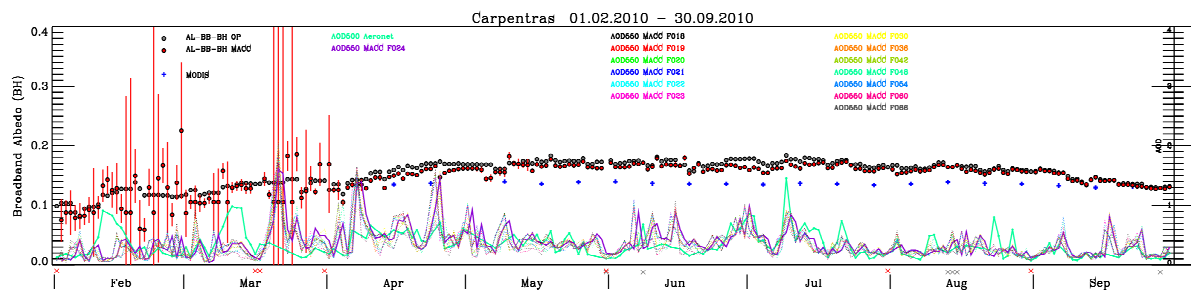

Figure 59: Times series for the station of Carpentras of AL-BB-BH (OP and MACC), and MODIS (blue). AERONET and MACC forecast for optical depth are also reported.

For AL-BB-BH in Evora (Figure 60), it is worth noticing that the signal is more scattered with MACC compared to OP. The region of Evora is attractive for depicting aerosol events and the large variability observed (a good correlation exists between AERONET and MACC aerosol chronology) confirms this statement. Finally, the impact of the MACC aerosol correction is weak compared to the distance to MODIS (above) or ground truth (below).
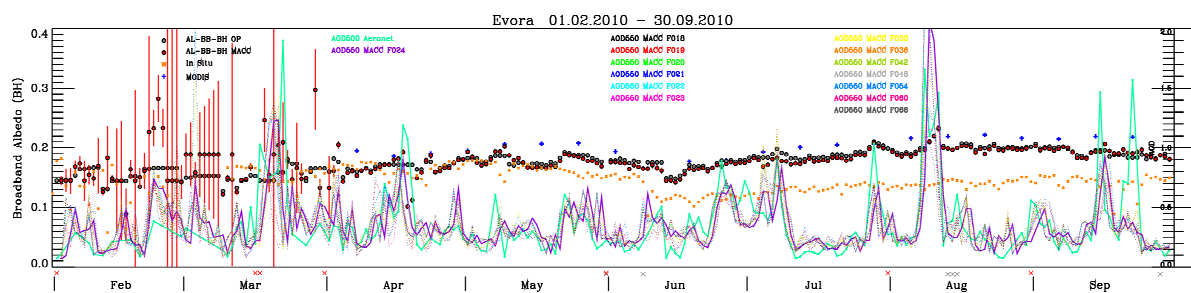

Figure 60: Times series for the station of Evora of AL-BB-BH (OP and MACC), and MODIS (blue). AERONET and MACC forecast for optical depth are also reported. Ground measurements are indicated (orange color).

This site of Hesse (Figure 61) located near Nancy (France) is marked by snowfall episodes, with full ablation occurring in April. This site is a forest of ~4.5 km². The in situ PAR albedo measurements locate slightly above MODIS and below MDAL (Al-VI-DH). The effects of the MACC correction seems to increase the quality of the comparison. At least, it reveals that it yields an impact. For AL-BB-DH, it is very difficult to conclude on any improvement whereas MODIS data match well with in situ BB albedo.
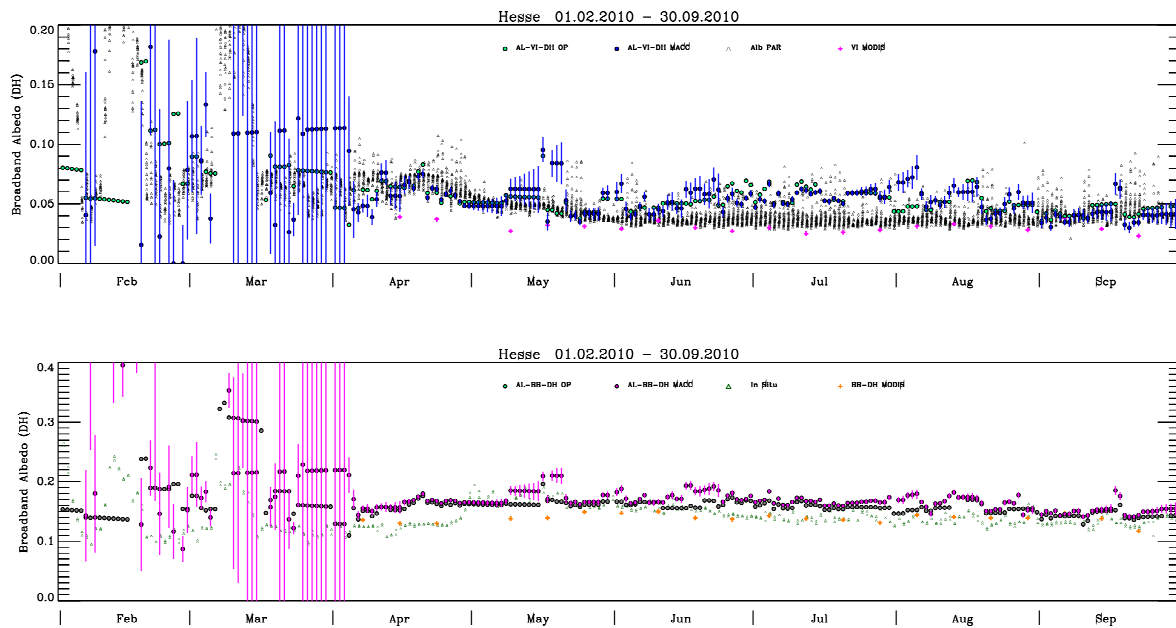

Figure 61: Times series for the station of Hesse of MDAL (OP and MACC), and MODIS (blue). AERONET and MACC forecast for optical depth are also reported. Ground measurements are indicated (black color). Top: AL-VI-DH. Bottom: AL-BB-DH.

The station of Tamanrasset (Figure 62) site is marked by the occurrence of large aerosol load according to AERONET whereas MACC fails to reproduce such intensity. Clearly, there is a better reactivity of the signal after MACC correction. At any wavelength, it is shown an increase, which outlines the impact of the aerosol scattering transmittance. In comparison, MODIS remains low. This may suppose an underestimate of the aerosol correction due to the weakness to depict correctly aerosol over bright targets in the case of MODIS.
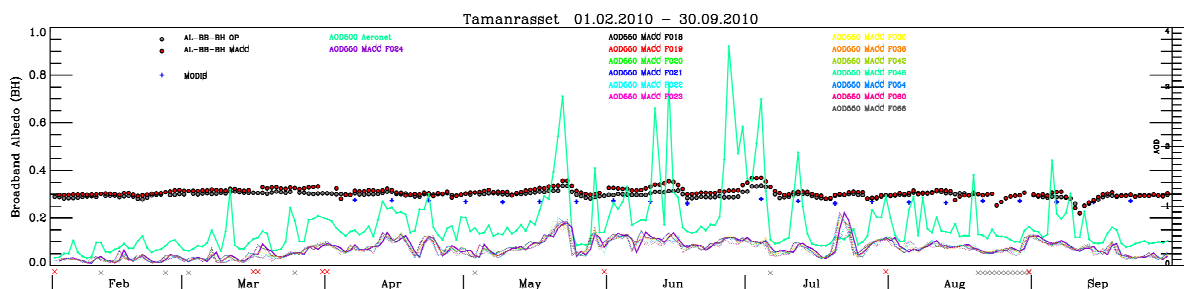

Figure 62: Times series for the station of Tamanrasset of AL-BB-BH (OP and MACC), and MODIS (blue). AERONET and MACC forecast for optical depth are also reported.

2.8   Comparison with ECMWF Albedo product

Finally, we performed a preliminary comparison of the Land-SAF and MODIS albedo products with the albedo map of the ECMWF model (Figure 63). For this purpose the daily Land-SAF and ECMWF estimates were averaged over a 16-day MODIS period in November 2005. The ECMWF and MODIS results were re-projected to the SEVIRI grid. The visual impression suggests that ECMWF overestimates albedo in snow-free regions with respect to the satellite products.
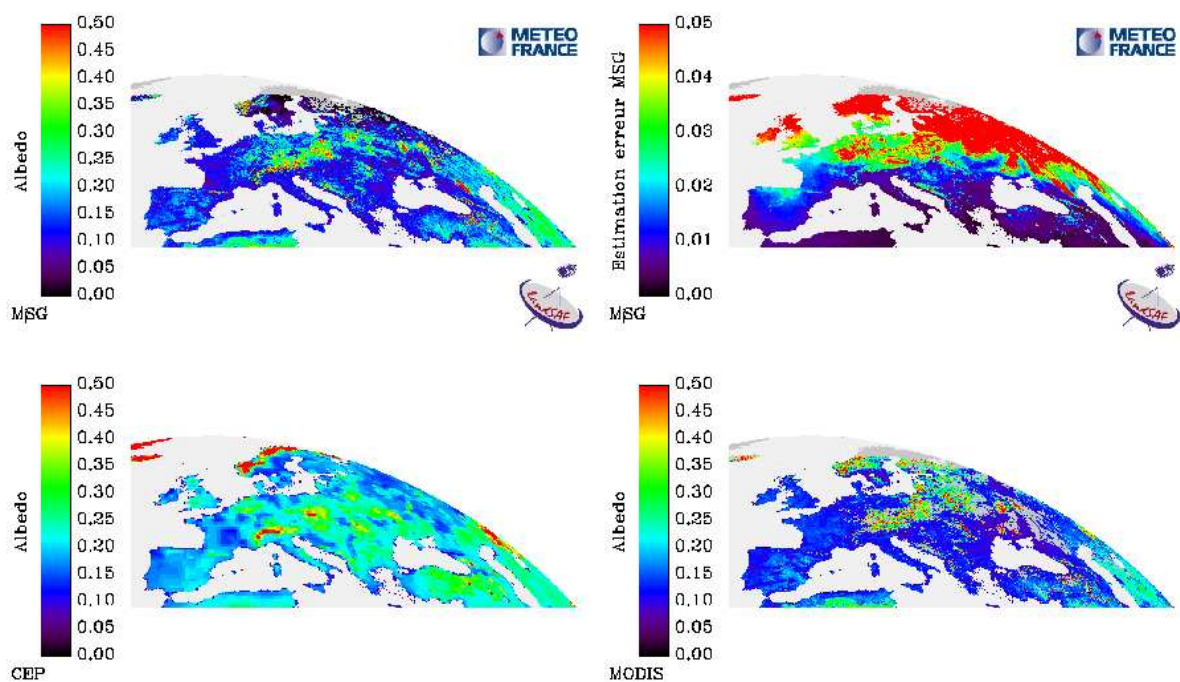

Figure 63: Comparison of total short-wave broadband albedo estimates for the period from November 17 to December 2. Top left: Land-SAF albedo product. Top right: Uncertainty estimate for the Land-SAF albedo product. Bottom Left: ECMWF albedo map: Bottom Right: MODIS albedo product. (Note that the Land-SAF uncertainty estimates are very high at Northern latitudes due to the unfavourable angular conditions at that time of the year.)

2.9   Comparison between D01 and D10 products

The D10 is a composite product expanding over a typical 30-day and which is derived from the daily (D01) albedo products. The D10 product is produced every 10 days. The reliability of this climatologic product is verified through a comparison with the daily (D01) product over 2 contrasted sites located in Namibia (Gobabeb) and Estonia (Toravere). The validation is supported by the availability of time series of tower flux measurements of broadband albedo collected over these 2 sampled sites in 2009 (Figure 64).
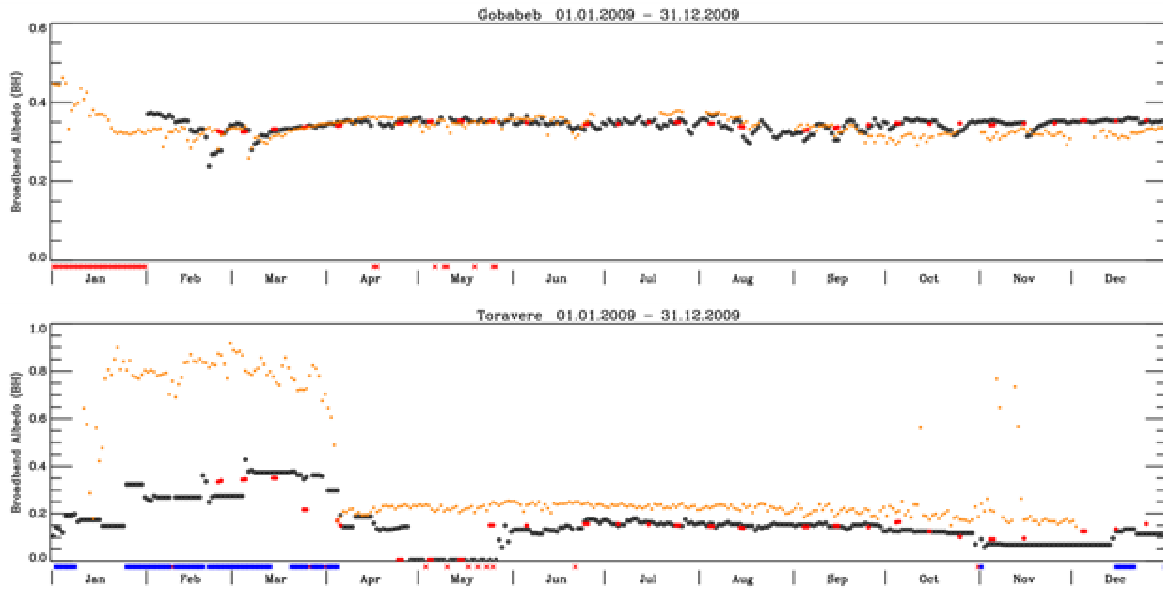
Figure 64: Time series of broadband albedo acquired in 2009 over 2 confident sites (Top: Gobabeb; Bottom: Toravere). Ground measurements (orange). MDAL (black). MTAL (red). Red/blue dots on the X-axis indicate missing data.

2.10 Foreseen activities

The continuation plan will consist before all to collect extended times series of ground measurements over more reference sites in order to strengthen the independent comparison. However, it is recognized that ground measurements fail to be representative of the content of the pixel of a moderate resolution sensor like SEVIRI. The impact will be the definition of a snow albedo algorithm with possible addition of a specific kernel for snow. This will take benefit of the implementation of the SNORTEX (Snow Reflectance Transition Experiment) project that took place in spring 2009 and 2010. SNORTEX was dedicated to explore the seasonal trend of the snow albedo of the boreal forests. The strategy in implementing SNORTEX is to first obtaining stratification in terms of land cover of the studied area sized roughly as 30 km by 30 km. Then, ground snow measurements were routinely operated over various landscape units (different forests, marsh, lake, bare soil, artificial) that are dominant within the area. Ground albedo measurements, snow properties, and modelling efforts serve to estimate an albedo for each land cover type. Then, based on the land cover classification, a snow albedo is reconstituted for the region, which further serves to validate the LSA SAF albedo. Actually, airborne instrument OSIRIS (AirPOLDER) acquired BRDF measurements of a few meters resolution. This allows extension of the 'local' BRDF once calibrated against snow measurements. Inter-comparison between AirPOLDER and POLDER data will be shown for matching period, and further between POLDER and ETAL (when available) for concomitant periods of time. This will serve to sustain an indirect validation of snow albedo from ETAL over boreal ecosystem.

2.11 Conclusions

This document resumes the efforts of the project to maintain the Land SAF albedo products (MDAL, MTAL, and forthcoming ETAL) at a level of precision that could answer to the needs of the users community. The core of the validation relies on a comparison with widely used albedo products from sensors like MODIS and POLDER. A major source of discrepancy still today seems to be the aerosol correction, with a clear difficulty above bright targets. Therefore, a recent investigation aimed at replacing in the LSA SAF atmospheric correction procedure the climatologic-based AOD (aerosol optical depth) with the operational AOD issued from GEMS/MACC project and disseminated routinely by ECMWF from 2010.

The specification of the albedo product expressed in the Product Requirements Table (PRT) states an accuracy objective (relative to the respective albedo level) of 0.03 for MDAL below 0.15 and 20% for MDAL above 0.15. This turns to be 0.015 for MTAL below 0.15 and 10% for MTAL above 0.15.

The comparative studies with the corresponding MODIS albedo product show a good consistency for both AL-VI-DH and AL-BB-DH (-BH). If MODIS is considered as a valid (unbiased) reference, the bias requirements can be considered as fulfilled for the series of MDAL products. Interpreting such information as standard deviation (rmse) of the difference between the estimate and the supposed reference value (MODIS mostly, ground truth when it exists) - the results can be deemed satisfactory in respect to the specifications. If VI clearly contains more piece of information in regard to the aerosol correction, however the improvement on BB can also be judged significant. This means that the narrow-to-broadband conversion is correct and not the source of uncertainty. By comparison with MODIS albedo, the statistics are slightly improved with MTAL compared to MDAL. But since the specifications are two times more stringent, it cannot clearly meet the requirements of 0.015 for absolute accuracy while the 10% of relative accuracy is reached.

The exercise of comparison with POLDER reveals the existence of a bias particularly for low albedo values. For this reason, values of MTAL below 0.015 cannot satisfy to requirements and even a value of 0.03 could not be advised. Further investigation is needed to better understand such bias like a possible improved inter-calibration of the sensors (aerosol signal cannot hardly explain such bias).

This study confirms that MDAL product already fell within the specifications in fact. Considering that the only (relevant) criteria is the impact of MACC aerosol correction consistently with an aerosol event well depicted by AERONET, the results can be deemed promising. As a result, the new MDAL products will show more time variations, as it could be somewhat expected. In fact, it seems to be particularly the case when an aerosol event is lasting over several days because the a priori information keeps memory of this event.

Finally, it is worth stressing that this exercise is pioneer for handling an aerosol correction based on the information issued from a transport model for atmospheric particles in the frame of a satellite data processing chain.

The validation studies presented here need to be pursued and the results investigated in more detail as a function of geographic location, surface type, snow cover, precipitation, and atmospheric conditions. For suitable sites, validation studies at the level of directional reflectance values after atmospheric correction may also be considered.

2.12 List of references

Barnsley M.J., Strahler A.H., Morris K.P. and J.P. Muller, 1994, *Sampling the surface bidirectional reflectance distribution function (BRDF): Evaluation of current and future satellite sensors*, Remote Sens. Rev., 8, 271-311.

Hu B., Lucht W., Li X. and A.H. Strahler, 1997, *Validation of kernel-driven models for global modeling of bidirectional reflectance*. Rem. Sens. Env., 62, 201-214.

Jin, Y., C. B. Schaaf, F. Gao, X. Li, A. H. Strahler, W. Lucht, and S. Liang, Consistency of MODIS surface bidirectional reflectance distribution function and albedo retrievals: 1. Algorithm performance, J. Geophys. Res., 108, doi:10.1029/2002JD002803, 2003.

van Leeuwen, W. and J.-L. Roujean, Land Surface Albedo from the Synergistic use of Polar (EPS) and Geo-Stationary (MSG) Observing Systems: an Assessment of Physical Uncertainties, *Remote Sensing of Environment*, 81, 1-17, 2002.

Lucht W. and J.L. Roujean, 2000, *Considerations in the parametric modeling of BRDF and albedo from multiangular satellite sensor observations*, Remote Sens. Rev., 18, 343-379.

Product Requirement Document (PRD) (available from landsaf.meteo.pt).

Product User Manual (PUM) on Surface Albedo (available from landsaf.meteo.pt).

Roujean J.-L., M. Leroy and P.-Y. Deschamps, 1992, *A bidirectional reflectance model of the Earth's surface for the correction of remote sensing data*, J. Geophys. Res., 97(D18), 20455-20468.

Samain, O, B. Geiger, and J.-L. Roujean, Spectral normalization and fusion of optical sensors for the retrieval of BRDF and albedo: Application to VEGETATION, MODIS and MERIS data sets, *IEEE Transactions on Geoscience and Remote Sensing*, Vol. 44, 11, Part 1, 3166-3179, 2006.

Strahler, A.H., 1994, *Vegetation canopy reflectance modeling - Recent developments and remote sensing perspectives,* Proceedings of 6th Int. Symp. Phys. Meas. Sign., p. 593-600.

Wanner, W., Li, X. and A.H. Strahler, 1995, *On the derivation of kernels for kernel-driven models of bidirectional reflectance*, J. Geophys. Res., vol. 100, p. 21077-21090.